## NOTICE

The quality of this microform is heavily dependent upon the quality of the original thesis submitted for microfilming. Every effort has been made to ensure the highest quality of reproduction possible.

If pages are missing, contact the university which granted the degree.

Some pages may have indistinct print especially if the original pages were typed with a poor typewriter ribbon or if the university sent us an inferior photocopy.

Reproduction in full or in part of this microform is governed by the Canadian Copyright Act, R.S.C. 1970, c. C-30, and subsequent amendments.

## AVIS

La qualité de cette microforme dépend grandement de la qualité de la thèse soumise au microfilmage. Nous avons tout fait pour assurer une qualité supérieure de reproduction.

S'il manque des pages, veuillez communiquer avec l'université qui a conféré le grade.

La qualité d'impression de certaines pages peut laisser à désirer, surtout si les pages originales ont été dactylographiées à l'aide d'un ruban usé ou si l'université nous a fait parvenir une photocopie de qualité inférieure.

La reproduction, même partielle, de cette microforme est soumise à la Loi canadienne sur le droit d'auteur, SRC 1970, c. C-30, et ses amendements subséquents.

# A THREE DIMENSIONAL KINEMATIC ANALYSIS OF AN ELITE SQUASH FOREHAND STROKE

by

Helen Woo

B.Sc. (Honours), Simon Fraser University, 1988

THESIS SUBMITTED IN PARTIAL FULFILLMENT OF

THE REQUIREMENTS FOR THE DEGREE OF

MASTER OF SCIENCE

in the School

of

Kinesiology



SIMON FRASER UNIVERSITY

September 1993

ISBN 0-315-91094-1

# PARTIAL COPYRIGHT LICENSE

I hereby grant to Simon Fraser University the right to lend my thesis, project or extended essay (the title of which is shown below) to users of the Simon Fraser University Library, and to make partial or single copies only for such users or in response to a request from the library of any other university, or other educational institution, on its own behalf or for one of its users. I further agree that permission for multiple copying of this work for scholarly purposes may be granted by me or the Dean of Graduate Studies. It is understood that copying or publication of this work for financial gain shall not be allowed without my written permission.

**Title of Thesis/Project/Extended Essay**

A Three Dimensional Kinematic Analysis of an Elite Squash Forehand Stroke

**Author:**

(signature)

HELEN WU

(name)

Sept 16/93

(date)

**APPROVAL**

Name: Helen Woo

Degree: Master of Science in Kinesiology

Title of Thesis: **A Three Dimensional Kinematic Analysis of an Elite Squash Forehand Stroke**

Examining Committee:

Chair: Dr. John Dickinson

Dr. Arthur E. Chapman
Professor
Senior Supervisor

Dr. David J. Sanderson
Associate Professor
School of Human Kinetics
University of British Columbia

Dr. Igor B. Mekjavic
Professor

Dr. Thomas W. Calvert
Professor, Schools of Computing Science, Kinesiology and Engineering Science
External Examiner

Date approved: 14 September 1993

# Abstract

General movement patterns are commonly used criteria to assess and understand human movement. Proper coordination of the body segments is essential to successful performance. A proximal to distal (PD) pattern of segmental motion has been observed in a variety of multisegmental sporting skills, such as throwing, kicking and striking, where sometimes the objective is to generate high endpoint velocities. It was the intention in this thesis to investigate the 3D kinematics of the upper body of an elite squash forehand stroke and to determine the extent to which this stroke follows or departs from this sequential pattern.

Past biomechanical studies analyzing the segmental coordination of a sporting skill have employed various kinematic measures to quantify movement. Human movement is a combination of linear and angular motion. The measures commonly used to describe the temporal coordination of body segments have been peak resultant linear velocities of the segmental endpoints, 3D resultant joint angular velocities and anatomical joint angular velocities. It was unknown as to how these various measures would compare in describing the temporal coordination of the same complex movement.

An elite squash forehand stroke was analyzed using high-speed cinematographical techniques. The direct linear transformation (DLT) technique was used to reconstruct the 3D coordinates of selected anatomical and racquet landmarks. The kinematic patterns were derived in terms of the linear velocities of the segmental endpoints, the 3D resultant joint angular velocities and the anatomical joint angles and angular velocities. The anatomical joint angles of the trunk segment and at the shoulder, elbow, radio-ulnar and wrist joints of the striking arm were calculated as Cardan angles. These angles were defined by the relative orientation of orthogonal reference frames embedded in adjacent

segments such that the joint angles corresponded to the clinical definitions of flexion/extension, abduction/adduction and internal/external rotation.

The PD sequencing was clearly demonstrated in the peak resultant linear endpoint velocities and the 3D resultant joint angular velocities. In addition, their peak velocities were successively higher proximally to distally.

The same sequential pattern was not apparent in the peak anatomical joint angular velocities, at least not in the anatomical sense. The movements primarily contributing to racquet motion at ball contact were trunk left rotation, shoulder internal rotation and adduction and wrist flexion of which shoulder internal rotation was most dominant. Even though shoulder internal rotation is anatomically proximal to wrist flexion, it had a functional significance on the distal endpoint speed via a wheel-and-axle arrangement at the time of impact. Therefore, the PD sequence may be inferred in the anatomical joint angular velocity profiles in a functional sense.

Contrary to previous observations, forearm rotation did not play a significant role in generating high racquet speeds at the instant of impact in the strokes analyzed. Another notable feature in the anatomical joint angular velocity profiles was an indication of counter-movement occurring across the joints as the angular velocity would proceed in one direction immediately followed with motion in the opposite direction. This pattern may be implicated in the beneficial use of the stretch-shortening cycle of muscle, but kinetic analysis is required to verify such use.

Of the three kinematic measures investigated two of them suggested similar temporal patterns. However, the resultant linear velocities of the endpoints and the 3D resultant joint angular velocities were limited in their completeness of the movement

description and potential for kinetic analyses. On the other hand, anatomical joint angles provided a more precise account of the segmental movements. Albeit complex and temporally ill-defined in terms of the peak values, the anatomical joint angular velocities were seen to be associated with a PD sequencing of the linear velocities of the segmental endpoints and 3D resultant joint angular velocities. A kinematic description using anatomical joint angular velocities may be conducive to the training and coaching of athletes and the clinical aspects of the sport due to the familiarity of anatomical definitions of joint movement.

# Dedication

I dedicate this thesis to my family:

my parents, Dick and Jean, and

Philip, Allen and Jennifer

whose unconditional love and support have

*brightened the dark times,*

*carried me through the rough times,*

*but most of all, laughed with me during the good times.*

# Acknowledgments

I would like to acknowledge the following people for their contributions to this thesis.

I wish to thank the members of my supervisory committee. Arthur, thank you for the opportunity to grow intellectually and as a scientist. Dave, thank you for your perseverance, patience and understanding. Igor, thank you for your uncanniness.

I would also like to thank Mary Ann for her abiding friendship and support. Your contributions to this thesis and my life have been invaluable and I can only hope to return the favour someday.

Thank you, Takeji, for your technical support and friendship.

Thanks to Karen and Joyce for their spirited support.

And thank you to all my friends who have shown me the meaning of friendship.

# Quotation

*"... The ultimate measure of a man*
*is not where he stands in moments*
*of comfort and conveniences,*
*but where he stands during*
*challenge and controversy. ..."*

Martin Luther King, Jr.

# Table of Contents

# List of Tables

# List of Figures

# Chapter 1
# PURPOSES

The overall purpose of this thesis was to perform a kinematic analysis of a complex, multisegmental, multiplanar activity. The squash forehand stroke of an elite player was analyzed with the following objectives.

1) Biomechanists and motor behaviourists are interested in the general movement patterns of skilled performance for the purposes of understanding human movement and achieving optimal performance. The segmental coordination during the squash forehand stroke had not been analyzed previously. One of the objectives of this thesis was to obtain kinematic profiles of the trunk, upper arm, forearm and hand/racquet segments during an elite squash forehand stroke. The kinematic profiles consisted of the linear velocities of the segmental endpoints, the 3D resultant joint angular velocities, and the anatomical joint angles and angular velocities.

2) Casual observation and conventional coaching wisdom suggest that optimal performance in multisegmental ballistic sporting skills such as in throwing, kicking, and striking skills is achieved by using a proximal to distal (PD) sequential order of segmental coordination. This movement pattern is generally apparent in ballistic skills when maximal endpoint velocity or maximal range is important. The movement patterns based on these various kinematic measures mentioned above were used to evaluate the temporal coordination of the segmental movements in the squash forehand stroke of an elite player. These parameters have been commonly used to describe the sequential nature of ballistic skills. However, the question has not been addressed previously concerning how these parameters may be similar or different in describing the same complex activity. Any

differences would have important implications on the interpretation of the temporal sequence in segmental coordination.

Several factors can vary the timing considerably resulting in departures from the PD sequence. These factors include differences in the physical attributes of the athlete and projectile, the speed and accuracy demands of the skill, and the joint configurations and ranges of motion which ultimately influence the segmental interactions and resulting motion of the segments. Another goal was to determine the extent to which the squash stroke follows or departs from the PD order of segmental motion.

3) A supplemental objective was to compare the anatomical joint angular velocity profiles between two elite squash players performing a forehand stroke. The similarities and differences of dominant features of the movement patterns were used to identify important characteristics of an elite stroke as opposed to those specific to an individual player.

# Chapter 2
# INTRODUCTION

The majority of analyses of sports biomechanics in the past have been in two dimensions (2D) due to its relatively simplicity. Such filming requires only one camera situated with its optical axis perpendicular to the plane of motion. The spatial representation of body landmarks or segments is straightforward and unambiguous in its interpretation. However, the applications of 2D techniques are limited because very few sporting skills confine their primary movements to a single plane. Even in 'planar' skills such as walking, running and cycling, there are movements outside the principle plane which are unaccounted for in 2D analyses. In describing multiplanar skills, it is not only inadequate, but also inappropriate to employ 2D techniques. In this case, a three dimensional (3D) analysis is necessary for a more accurate assessment of the movement.

The complexities in acquiring 3D coordinate data have deterred investigators in the past from performing multiplanar analyses. However, recent advances in mathematical techniques and computer technology have simplified the acquisition process considerably resulting in a rapid increase in 3D biomechanical studies.

## *A. THE DIRECT LINEAR TRANSFORMATION (DLT) TECHNIQUE*

There have been a number of photogrammetrical techniques developed to locate objects in 3D space. However, certain restrictions have made some of these methods cumbersome and unattractive for common use. Some requirements include knowing the exact locations of the cameras (Penrose et al., 1976) and having the optical axes intersect

(Cappozzo, 1983). Abdel-Aziz and Karara (1971) introduced the direct linear transformation (DLT) method which has since been commonly used in biomechanics to locate body landmarks in 3D space.

The DLT method is a relatively simple technique to implement and obviates the necessity for intersection of the optical axes of the cameras; the positions of the cameras are arbitrary and need not be measured; only a minimum of two camera images are necessary and additional cameras can be accommodated (Challis and Kerwin, 1992). Its major drawback is that the known control points used in calibrating the cameras must be well-distributed within the activity space, otherwise significant errors can occur in the data reconstruction (Wood and Marshall, 1986).

The 3D real space is represented by a Cartesian coordinate system comprising three perpendicular axes, X, Y and Z. A calibration frame consisting of several known control points establishes an arbitrary origin and the orientation of the axes. The frame is placed within the views of all cameras and approximates the volume where the motion occurs. The spatial location of a given point is represented by its 3D real or object coordinates (x, y, z) which are the projections of the point onto each of the three axes.

Challis and Kerwin (1992) provided an excellent description of the DLT technique. A minimum of two distinct camera views of each point is required to reconstruct its 3D coordinates. Each camera describes the point from a unique planar view in terms of 2D image coordinates $U_1,V_1$ and $U_2,V_2$, respectively. The process by which the DLT is used to reconstruct the 2D image coordinates (U,V) into 3D object coordinates (X, Y, Z) may be better understood if separated into two distinct steps. The initial step is referred to as the calibration of the associated image space when the object-to-image transformation is performed. It involves the estimation of eleven unknown DLT parameters or calibration

coefficients. Each set of coefficients is specific to a camera and defines the relationship of the 3D real space to the camera and the digitizer or motion analyzer. The accuracy of the estimation of this relationship determines the accuracy of the data recontruction.

The eleven calibration coefficients are estimated using at least six known, non-planar control points in object space. The object and image coordinates of each control point produce two DLT equations. The general form of these equations are:

$$U_d + \Delta U_d = \frac{A\mathbf{X} + B\mathbf{Y} + C\mathbf{Z} + D}{I\mathbf{X} + J\mathbf{Y} + K\mathbf{Z} + 1.0} \tag{2.1}$$

$$V_d + \Delta V_d = \frac{E\mathbf{X} + F\mathbf{Y} + G\mathbf{Z} + H}{I\mathbf{X} + J\mathbf{Y} + K\mathbf{Z} + 1.0} \tag{2.2}$$

where $U_d$, $V_d$ = the 2D (U,V) image coordinates
$\Delta U_d$, $\Delta V_d$ = the errors associated with the image coordinates
$\mathbf{X}$, $\mathbf{Y}$, $\mathbf{Z}$ = the 3D (X,Y,Z) object coordinates
$A$ - $K$ = the DLT calibration coefficients

With six control points, a system of twelve simultaneous equations results from a two camera setup. Therefore, an overdetermined system is available to estimate the eleven unknown variables. The solution of such a redundant system can be derived using linear least squares (LLS) approximations. Fewer than six control points yields an underdetermined system whereby a unique solution is impossible, therefore it is recommended that more than six well-distributed control points are used to improve the final estimate of these calibration coefficients.

The second step of the DLT method is the image-to-object transformation where the 3D space is reconstructed. From this step, the 3D (X,Y,Z) object coordinates of any selected point are estimated. By rearranging equations (2.1) and (2.2), the object coordinates may be estimated.

$$\begin{pmatrix} (A-EU) & (B-FU) & (C-CU) \\ (H-EV) & (J-FV) & (K-CV) \end{pmatrix} \begin{pmatrix} \mathbf{X} \\ \mathbf{Y} \\ \mathbf{Z} \end{pmatrix} = \begin{pmatrix} (U-D) \\ (V-L) \end{pmatrix} \tag{2.3}$$

The eleven calibration coefficients and the 2D image coordinates of the point produce only two equations from which to estimate the three unknown quantities corresponding to the point's 3D object coordinates (equation 2.3). If there is information from only one camera, an underdetermined system is generated, therefore it is impossible to determine its 3D object coordinates. However, if two distinct 2D images of the point are available, thus forming four equations, the resulting overdetermined system may be solved using LLS approximations. For each additional camera used, two more equations are added to the system, thus improving the redundancy of the system and the accuracy of the solution.

### *A.1 ACCURACY OF THE DLT RECONSTRUCTION*

There have been several ways to assess the accuracy of the DLT reconstruction of the 3D coordinates. Some researchers have compared estimated lengths with known lengths (eg. van Gheluwe, 1978) while others used known points (eg. Wood and Marshall, 1986). A comparision of the actual and reconstructed coordinates of known points is commonly used. The level of accuracy is indicated by calculating the Root Mean Square (RMS) of the differences in the coordinates. The set of known points has often been the

same as that used to determine the DLT calibration coefficients. Challis and Kerwin (1992) stated that such a procedure is inappropriate as it is not an independent measure of the DLT technique's ability to locate unknown points. Instead, it is testing the accuracy of the mathematical techniques utilized by the DLT technique and any unaccountable aspects of the photogrammetric model including noise. Much higher RMS errors were associated with estimating the locations of a set of unknown points than when estimating the same known points as were used for the calibration.

A number of factors influence the accuracy of the DLT reconstruction. These factors include the number, distribution and configuration of the known control points. The use of more control points consistently produced smaller RMS errors along the X, Y and Z directions (Wood and Marshall, 1986). More importantly, the same study emphasized the importance of ensuring that the control points are well distributed throughout the object space because significant errors of up to 100% were associated with reconstruction of unknown points outside the control point distribution space.

The configuration of the control points also plays an important role in improving the RMS error. In the past, the 'Christmas tree' configuration which had control points clustered about the central vertical axis was popular. However, it was the least accurate compared to more cuboid configurations (Challis and Kerwin, 1992). Among the cuboid structures investigated, superior results were obtained when the control points surrounded the activity space than when the points were located within it. The number of control points was found to be unimportant since the RMS errors were comparable with varying number of control points located on the perimeter of the calibrated space.

The configuration of the cameras with respect to the activity space is another factor which influences the accuracy of the data reconstruction (Wood and Marshall,

1986). If the cameras and the centre of the activity space were considered to be corners of a triangle, it was found that an arrangement resembling an equilateral triangle was superior to a right triangle configuration. In a equilateral triangle arrangement, the cameras were located to the right and left of the centre of the activity space, whereas in the right triangle arrangement, the cameras were located directly in front and to the right of the centre of the activity space. A distance:base ratio of approximately 1:2 corresponding to an equilateral triangle arrangement produced better results than in a right triangle configuration with a 1:1 ratio. The distance was defined as the perpendicular distance from the line connecting two cameras to the centre of the activity space.

## *B. ACQUISITION OF 3D COORDINATE DATA*

A motion analysis system must incorporate the four steps of a 3D analysis which are calibration, data collection, determination of the 2D image coordinates and the determination of the 3D object coordinates by the DLT technique. The three main types of 3D motion analysis systems are videography, optoelectric, and cinematography (or cine) systems. All systems are widely used in biomechanical analyses and one system is not necessarily better than another in terms of the accuracy of the data reconstruction. The decision as to which to use is based largely on the nature of the movement and the objective of the analysis. The latest systems have become increasingly automated. This may appear to be a convenient and attractive feature at first, but it severely reduces the flexibility and manual intervention required in some analyses. The following sections describe the main features of each system focussing on their advantages and disadvantages.

## *B.1 VIDEOGRAPHY*

With the recent increase in popularity of video equipment, the newest types of motion analysis systems (eg. Peak Performance, Kodak EktaPro 1000) have adopted video into their packages. Most of the packages include the video cameras, VCR and computer which are specifically designed for the purposes of motion analysis. The video based systems have incorporated several advantageous features of both the cine and optoelectric systems. They are designed to reduce the costs and time consuming tasks (eg. manual digitization) of film while maximizing the convenience featured by the automated optoelectric systems.

Video is similar to cine film in that a permanent image is captured. The only advantage film has over video is that film has higher resolution and clarity. However, by keeping the image size large on video, the resolution is adequate for most purposes.

The cameras are usually conventional video cameras with VHS format. The maximal frame rate is 60 Hz which limits their usage to qualitative assessments or the analysis of relatively slow and cyclical movements. Faster movements would appear blurry and indistinguishable on video due to the longer exposure time. However, high speed video cameras have been developed equipped with special shutters, but at considerably higher costs. These cameras can record up to speeds of 2000 frames per second by splitting a full frame or screen into multiple horizontal images. For example, a screen from a 60 Hz camera can be split into five images by separating each image by 1/300th of a second. The result is an effective film speed of 300 frames per second. Some disadvantages result from increasing the film speed in this fashion. The vertical resolution of the image is reduced since the screen is shared by several images. Higher film speeds

require specific lighting needs and/or a strobe due to the limited exposure time. In most cases, high speed video is associated with packaged systems requiring expert technical assistance at considerable costs.

The video system utilizes passive, hemi-spherical, reflective markers of various sizes which are firmly affixed on the skin surface above anatomical landmarks. The reflective nature of the markers and the relatively slow frame rate of conventional video cameras obviates the need for special lighting, thus allowing filming to occur under normal laboratory or field conditions.

The time consuming task of manual digitization has been replaced by a semi-automatic process whereby the illuminated markers are automatically located and tracked during the movement. The computer searches, detects and calculates the centroids of the markers providing a set of image (U,V) coordinates. This procedure is automatically repeated as long as the markers are visible and contrast with the background. When the computer encounters a situation where markers are crossing or hidden from camera view, the automatic digitizing process is interupted and the operator is asked to intervene by making the appropriate location decision. This bypasses the problem of having "missing data" introduced during the data collection.

## *B.2 OPTOELECTRIC SYSTEMS*

The optoelectric motion analysis systems are designed to take advantage of modern computer technology. They are completely automated and require minimal operator assistance in the acquisition of 3D coordinate data. These systems are usually marketed as integrated packages including specialized cameras, calibration frame, the central computer unit and the acquisition and analysis software and hardware (eg. WATSMART, OptoTrack, Selspot).

The WATSMART is a commonly used optoelectric motion analysis system in biomechanics. It comprises two cameras specifically designed to detect infrared pulses emitted by external markers called IREDs (InfraRed light Emitting Diodes). Each camera provides a unique set of image (U,V) coordinates of where the IREDs are located, thus enabling the system to reconstruct the 3D coordinates. The diodes are driven electronically via a cable connection to the computer and infrared pulses are strobed through the IREDs in sequence. The maximal sampling frequency or strobing is limited to approximately 400 Hz by the acquisition hardware. As more IREDs are employed, the maximal sampling frequency declines. This may present a problem in terms of sampling at the Nyquist frequency which states that data should be sampled at a rate at least twice the highest frequency of the movement in order to avoid aliasing or misinterpretation of the data.

Precautions must be taken to locate the IREDs accurately. Any possibility of infrared light being within or entering the data collection space must be removed. This includes natural light through windows and doors and any reflective material. The cameras may erroneously detect the point of reflection as a marker. Reflections present a

serious problem, therefore the use of these types of systems is limited to highly controlled laboratory environments.

The use of IREDs is convenient in the analysis of simple and confined movements (eg. pointing, reaching and grasping) where it is highly likely that the markers remain in camera view throughout the movement. However, this may not be the case with more complex sporting skills. In multisegmental skills, it is common to have body segments crossing in front of each other, thus obscuring markers from camera view. For example, the arm may swing across in front of the body blocking markers on the trunk, or longitudinal rotations may cause the markers to turn away from either or both cameras. When the IREDs cannot be detected, the system interprets the data as missing since a minimum of two cameras must view the marker simultaneously for its 3D coordinates to be determined. A possible solution is to use additional cameras, but the effectiveness of this solution is questionable since the obscured markers are usually well hidden between the body segments. Another possibility used by some systems is interpolation of the missing data. However the problem with this solution is that the missing data may occur over a prolonged period of the movement and interpolation may not correctly estimate the trajectory of the marker.

### *B.3 CINEMATOGRAPHY*

High speed cinematography or cine film has been the traditional method of data capture. Borrowed from 2D analyses, 3D techniques have been developed using cine film which makes it a viable option in multiplanar analyses. A cine system is manual and requires operator assistance. Custom-made software is needed for data analysis. The high speed cameras use 16 mm film and operate up to speeds of 500 frames per second. A

basic knowledge of photography is required because appropriate camera settings and lighting become increasingly important as frame rate rises. Although time consuming and cumbersome, cine systems have the flexibility and versatility to conduct a variety of analyses.

As cine film systems are not usually sold as complete packages, many piecemeal systems have been developed. It may be necessary to construct a calibration reference structure. Most reference structures included in packaged systems are relatively small and do not encompass the volume of most sporting activities unless multiple calibrations are performed. Multiple calibrations are tedious and vertical spacing of the frame is difficult. It is sometimes convenient to have the flexibility of constructing a reference structure to suit one's specifications in terms of size and control point distribution and configuration.

Synchronization of multiple high speed cameras is a problem. The most favourable technique is to have an electronic linkage between the cameras whereby the shutters are phase locked and driven simultaneously. This connection is usually permanent which may not be possible or preferred, therefore other means of synchronization are necessary. An alternative is to use an external timing signal or pulse of light within the views of both cameras identifying the 'starting' frame of film. However, the accuracy of this method depends on whether the film speeds are the same and whether a phase shift exists between films. The greatest possible error is half of the time interval between frames. If the error is considered too large, a possible solution is to interpolate information between frames from one of the films, so that a closer temporal match may be achieved with the other film.

Several factors need to be considered to improve the visibility of the anatomical landmarks so as to avoid confusion during the digitization process. Adequate lighting is required for sufficient exposure of the film, especially at higher frame rates. However, at

high speeds, the intense heat of the lights may limit the time of exposure of the subject. Additional precautions must be taken to enhance the contrast between both the markers and the subject, and the subject and the background. The subject should either wear minimal clothing or tight-fitting clothing of uniform colour to improve the contrast between the markers and the subject. Highly visible external markers or body paint are commonly used to locate the anatomical landmarks.

The 2D image (U,V) coordinates of the selected points are acquired by the manual digitization of the films. It is generally very time consuming and labourious. Random measurement error known as digitizer error is introduced during this stage because the locations of the points are subjectively determined by the operator. The accuracy and reliability of the digitization are often dependent upon the judgement and experience of the operator.

Manual digitization allows complete control over which points are digitized which is sometimes advantageous. External markers are usually not used as digitization points, but rather as aids in locating joint centres or segmental endpoints. This is unlike the automated systems where the joint centres and external markers are commonly assumed to be one and the same. There are several problems with this assumption. Unless the exact spatial relationship between the external marker and the joint centre is known, then it is inappropriate to use the external marker to represent the joint centre. Furthermore, the instantaneous location of the joint centre may change with joint angle which complicates the problem. There is also considerable relative movement between the external markers and the underlying bony structures due to movement of the skin and soft tissue particularly in high accelerative movements.

Another major drawback of a cine system is the need to develop custom-made software for data analysis. There may be computer programs available for specific functions such as smoothing and reconstruction of data, but there does not exist an integrated software package which analyzes data from cine techniques. Although, this requires a considerable amount of programming, custom-made software allows flexibility and convenience which is not available with more automated systems. This allows the operator to incorporate existing equipment and define appropriate measurement conventions suitable for the movement (eg. coordinate systems, joint angles). The operator has complete control over every aspect of the experiment at the expense of considerable time and work.

## *C. THREE DIMENSIONAL SPATIAL REPRESENTATION*

In addition to there being several ways to acquire 3D coordinate data, there are as many ways, if not more, to define the configuration of a joint in 3D space. There is no argument as to how joint motion may be described in 2D space as it exhibits only three degrees of freedom ($x,y,\theta$). However, there is considerable debate regarding the representation of 3D joint motion which has six degrees of freedom: 3 translational and 3 rotational components. Different coordinate systems, reference systems and analytical methods often make comparison of results difficult and ambiguous.

Possible coordinate systems include the spherical, cylindrical and orthogonal (Cartesian) systems in locating points in 3D space. Orthogonal systems with XYZ axes are the most commonly used, but even so, there are different ways of describing the location of a point. Conventionally, a right-handed orthogonal reference frame is used, but there is no concensus as to the orientation of the X, Y and Z axes. This has important

implications in not only the description of the coordinates of a point, but also in the resulting rotational transformations which describe the orientation of a body in 3D space. Therefore, the coordinate system must be clearly defined.

Another possible source of confusion is whether the points are described in terms of an inertial global reference system or a non-inertial body-fixed reference system in the calculation of segment or joint angles, respectively. The problem is further complicated by investigators choosing different anatomical landmarks or nomenclature in their definition of embedded reference systems.

The greatest source of confusion and debate concerns the choice of analytical method by which to describe 3D joint motion. Andrews (1984) stated three criteria which can be used to gauge the suitability of any analytical method used to describe the configuration of an anatomical joint. Firstly, the method should provide useable results which aid in the physical interpretation of the joint kinematics. From a clinical perspective, the objective is to determine three meaningful and interpretable independent parameters that represent flexion/extension, abduction/adduction and internal/external rotation, respectively. Secondly, singularities should not occur. Singularities or 'gimbal-lock' exists when the joint configuration does not produce unique joint coordinate values. In this case, the rotational angles are unidentifiable or indeterminant. Thirdly, the calculations should be computationally efficient and require minimal computer time.

There have been four primary analytical methods used to describe 3D joint motion in biomechanical studies. These methods are based on techniques borrowed from classical rigid body dynamics, or slight modifications thereof, to represent more accurately anatomical joint motion. The methods include the use of projected angles, Cardan or Euler angles, the floating axis system and the finite helical screw axis (FHA).

Projected angles have commonly been used in the past by clinicians and physicians who are interested in examining pure flexion/extension, abduction/adduction and internal/external rotation as required by functional tests. These angles are defined as the projections of the local segment coordinate axes which are embedded in the body segment onto the XY, YZ and ZX planes of the fixed global frame of reference or the sagittal, coronal and transverse planes of movement (Figure 2.1).

Although projected angles are simple to define and implement, they are unreliable for describing segment angles and are incorrect for joint angles. This approach is valid only when the movement is purely planar or if the segment angle is relatively small with respect to the reference attitudes. For example, if the knee joint remained motionless, but the global frame of reference changed, the joint angle will vary. The use of projected angles is justifiable in analyzing the kinematics of simple, planar movements, but not for complex sporting skills. This method should be avoided entirely, if possible, as other forms of attitude representation are considered more appropriate.

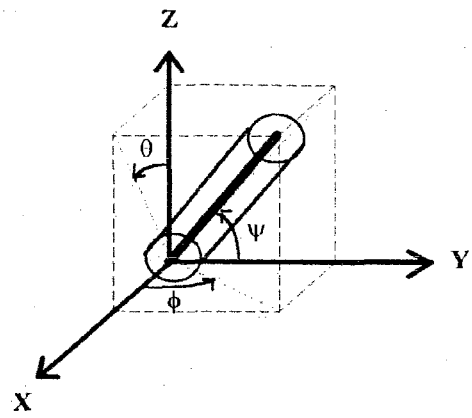


Figure 2.1 Projected angles ($\phi$, $\theta$, $\psi$) of the segment vector on the XY, XZ and YZ planes.

## *C.2 EULER OR CARDAN ANGLES*

Euler angles have traditionally been used in the study rigid body mechanics. The term Euler angles has been used rather loosely in biomechanics as have its applications. More appropriately, Cardan nct Euler angles have been used to describe joint motion, although the terms are used interchangeably. Euler angles refer to a specific rotational sequence occurring about the X, Y and X axes whereas Cardan or Bryant angles correspond to a rotational sequence about the X, Y and Z axes. The latter method is more appropriate for describing joint motion.

Joint movement may be defined as the movement of a distal segment with respect to its proximal neighbour. If an orthogonal coordinate system is embedded in the 'fixed' proximal segment and another orthogonal coordinate system is embedded in the 'moving' distal segment, the relative orientation of the two segments may be represented as a vector connecting the origins of the coordinate systems and a set of three ordered rotations ($\phi$,$\theta$, $\psi$). The three rotations correspond to the rotational sequence about the original and intermediate axes required to align the axes of both systems (Figure 2.2). It is these rotations which are known as the Cardan angles. The rotational sequence varies in the literature depending on the orientation of the axes. Each sequence uniquely defines a different body orientation. The transformation equations are derived from the multiplication of the three rotational matrices corresponding to each of the Cardan angles. Because of the non-commutative nature of matrix multiplication, the resulting transformation equations are sequence-dependent. The sequence dependency can be easily demonstrated by manipulating a book. The final orientation of the book will differ as a result of changing the order of the axes about which the book rotates. Therefore, the

coordinate systems and rotational sequence must be clearly defined, otherwise the interpretation and comparison of results may be confusing and difficult.

Another drawback of using Cardan angles is the possibility of singularities especially in describing shoulder and hip motion. A singularity occurs when the rotations become ill-determined. For example, in the description of shoulder rotation, if the three points (eg. shoulder, elbow and wrist joint centres) defining the joint configuration are colinear which occurs when the elbow joint is fully extended, then it is not possible to quantify the longitudinal rotation.

Despite the disadvantages, Cardan angles are commonly used because of their anatomical relevance. Each rotation about a given axis corresponds to an anatomical joint rotation which is appealing to clinicians, physicians and sports biomechanists. Most joint rotation conventions have flexion/extension ($\phi$), abduction/adduction ($\theta$), and internal/external rotation ($\psi$) angles corresponding to the first, second and third rotations required to align the axes. In the analysis of hand and finger motion, Small et al. (1992) related these joint angles to the rotational sequence about the Z, y' and x" axes. Conversely, Tupling and Pierrynowski (1987) used the same nomenclature of joint angles to correspond to a rotational sequence about the Z, X and Y axes. It appears that the sequence of the joint angles are similar, but are not about the same axes. The sequence of rotations will differ depending on the orientations of the axes and the sign conventions of the rotations.

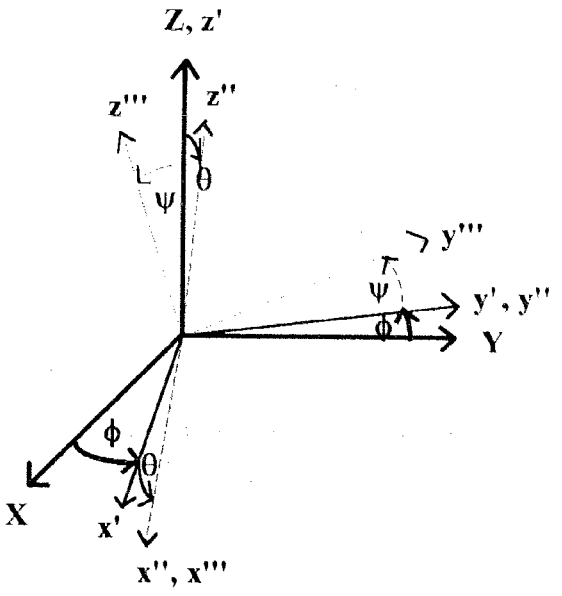


Figure 2.2 The Cardan angles ($\phi$, $\theta$, $\psi$) about the Z, y' and x'' axes representing abduction/adduction, flexion/extension and internal/external rotation angles at a joint.

### *C.3 FLOATING AXIS SYSTEM*

Grood and Suntay (1983) introduced a similar alignment-based system as Cardan angles, but without the sequence dependency. In analyzing the movement of the knee, they used two non-orthogonal anatomically based axes (**e**1 and **e**3) to represent the orientations of the two adjacent segments (Figure 2.3). The third axis, **e**2, referred to as the floating axis was normal to the plane of **e**1 and **e**3. The rotational angles $\alpha$, $\beta$, and $\gamma$ corresponded to flexion/extension, abduction/adduction and internal/external rotation, respectively. These angles were derived from the rotations about **e**1, **e**2 and **e**3. Small et al. (1992) compared the results obtained using Cardan angles versus floating angles and found identical results when taking into consideration the differences in axes definitions

and sign conventions. Given the specified coordinate systems, the rotational relationships between both systems may be as simple as $\alpha = -\phi$ (flexion angle), $\beta = \pi/2-\theta$ (adduction angle), and $\gamma = -\psi$ (external rotation).

Although the floating axis system is not sequence dependent, singularities may still occur. Because the locations of the axes are known in space, the order of rotations is unimportant. This is unlike Cardan systems where the orientations of the intermediate axes are unknown. As in the example cited above where the embedded axes are parallel, the direction of the floating axis is ill-defined, therefore no unique solution is possible.

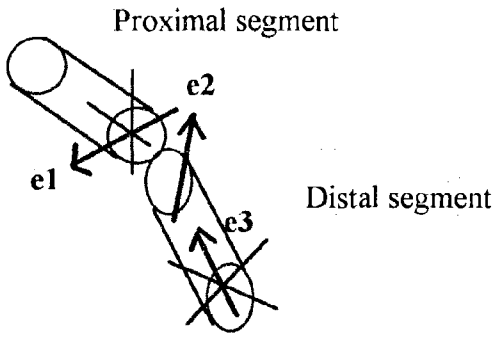


Figure 2.3. The Floating Axis System where the first axis (**e1**) is in the fixed body, the second axis (**e3**) is in the moving body and the third axis (**e2**) is normal to **e1** and **e3**. Rotations about these axes correspond to flexion/extension, internal/external rotation and abduction/adduction, respectively.

### *C.4 FINITE HELICAL AXIS*

Another method by which a finite movement from a reference orientation to a current position can be described is using the finite helical axis (FHA) technique. It is

advantageous in describing joint motion because it is not sequence dependent nor is it susceptible to singularities. The movement is defined as undergoing a finite rotation ($\theta > 0$) about an axis with unit vector **n** (Figure 2.4). Woltring (1991) stated that the helical angles may be identical to those under any Cardan convention, but did not explicitly describe how. However, Small, et al. (1992) stated that a simple correlation between the helical angles and Cardan angles is non-existent unless the helical or functional axis of motion is aligned with a coordinate axis. Although the FHA technique conveniently avoids the mathematical pitfalls inherent in the other representations, it is a rather cumbersome and mathematically-laden method for clinical and common use.

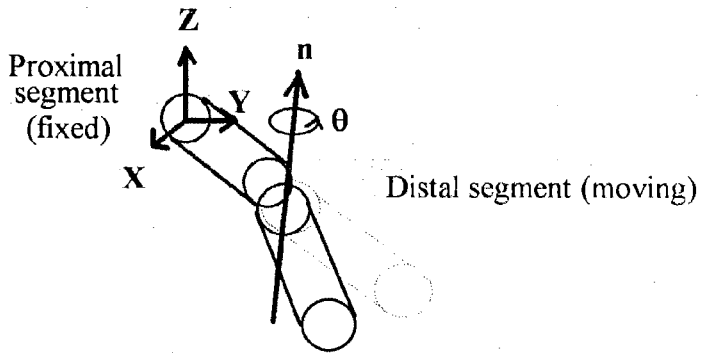


Figure 2.4 The rotational angle θ about the Finite helical Axis.

## *D. TECHNIQUE*

In most sporting activities, coaches emphasize the use of proper technique in achieving optimal performance. Technique is usually concerned with the mechanics of the movement whereby the athlete must properly coordinate the movements of the body

segments spatially and temporally to be successful. The proper technique for a given athlete executing a skill is dependent on a number of factors such as the athlete's physical and muscle attributes, the environmental conditions and the objective of the skill. There appears to be a general movement pattern common to the elite performance of a group of multisegmental, ballistic-type skills which include throwing, kicking and striking. The objective of these skills is either to maximize endpoint speed or projectile range. Most of these skills are characterized by the segments moving progressively in a proximal to distal (PD) sequence with each more distal segment becoming successively faster. The similarity in the segmental movement pattern suggests that there may be some underlying, fundamental mechanism which governs the strategy by which the segments move (Chapman and Sanderson, 1990).

The PD sequence has been observed in a variety of ballistic-type sporting skills. A PD order of peak segmental endpoint velocities occurred in striking a field hockey ball (Elliot and Chivas, 1988), tennis serve (van Gheluwe and Hebbelinck, 1985) and a tennis topspin forehand drive (Elliot et al., 1989). Throwing skills also demonstrated a similar PD sequence of resultant linear endpoint velocities such as in javelin throwing (Whiting et al., 1991; Luo et al., 1993), overarm throwing in female handball players (Joris, et al., 1985) and cricket bowling (Stockill and Bartlett, 1993). The PD sequential pattern has also been described in terms of peak resultant joint angular velocities in the serving arm of experienced volleyball players (Luhtanen, 1988), successful badminton smashing technique (Hong, 1993) and the windmill pitch (Alexander and Haddow, 1982). Putnam (1983) indicated that this same PD sequence of peak joint angular velocities also occurred in the lower leg during punt kicking.

Although most ballistic-type sporting skills are multiplanar, many of the analyses have been in 2D. It is questionable whether it is appropriate to assume that movements

outside the principle plane are insignificant or negligible. Throwing skills have been analyzed both in 2D and 3D. Similar PD patterns of linear velocities were found in a planar analysis of javelin throwing (Whiting et al., 1991) and in a multiplanar analysis of cricket bowling (Stockill and Bartlett, 1993). However, a PD sequence was not apparent in a 3D analysis of fastball baseball pitching in terms of resultant joint angular velocities (Elliot et al., 1985) nor anatomical joint angular velocities (Feltner and Dapena, 1986). The latter analyses found that the elbow motion peaked prior to shoulder motion. Therefore, the segmental movement pattern is dependent on the kinematic parameter implemented.

A variety of measures have been used to describe kinematically the sequential pattern of segmental movement during ballistic-type skills. The use of resultant linear velocities of segmental endpoints has clearly demonstrated the PD sequence. The maximal speeds of the endpoints not only occur sequentially, but also become faster in a PD fashion. Such an analysis reveals the instantaneous, kinematic contributions of individual segments to the distal endpoint speed. Resultant joint angular velocities also provide a clear description of the PD sequencing of motion. Because human movement is typically thought of as a series of joint rotations, the information obtained from these analyses is straightforward and easy to visualize. This type of analysis can also indicate the individual segmental contributions to the distal endpoint speed. Anatomical joint angular velocities have not been used as frequently as the other criteria in the description of sporting skills because of the complexities and difficulties in defining the joint angles. However, they provide a more detailed description of joint motion because three degrees of freedom may be defined at a given joint. The PD sequence was not illustrated when using anatomical joint angular velocities to describe the motion of the arm during throwing (Feltner, 1986). Whether these various kinematic measures equally describe the temporal coordination of body segments in the same complex skill is unknown.

There are two conflicting mechanical principles which explain how the body segments shall move to achieve high distal endpoint speeds. It has already been recognized that most ballistic-type skills are characterized by a PD progression of segmental motion. However, it is inituitively more appropriate from a kinematic perspective alone that the segmental movement pattern follow the principle of optimal coordination of partial momenta (van Gheluwe and Hebbelinck, 1985). It states that maximal speed at the distal endpoint of an open-linked system is achieved when the angular speeds of all segments peak simultaneously. Given that the speed of the distal end of a segment is proportional to the segment's length and angular speed, it would seem logical that all joints be fully extended and all segments rotate with the same angular speed at the instant maximal endpoint speed occurs. This pattern has been observed in the volley and in the forehand ground stroke in tennis (Deporte et al., 1990), but it is not typical.

Most ballistic skills seem to follow the principle of summation of speed which states that maximal endpoint speed is attained when the movement begins with the more proximal segment and progresses to the more distal segments such that each segment starts its motion at the instant of greatest speed of the preceding segment and reaches a maximum speed greater than its predecessor (Bunn, 1972). Although not stated in the principle, this movement pattern implies that the speeds of the proximal segments have diminished considerably by the time the most distal segment has reached maximal speed. This transition is known as the deceleration-acceleration (DA) pattern and had been associated with enhanced performance (Alexander, 1983; Herring and Chapman, 1988). In fact, the timing of the deceleration may be considered to be a more critical factor than maximal limb velocity in the successful execution of ballistic movements (Alexander, 1983). Many investigators have referred the DA transition to a whip-like action whereby the deceleration of the proximal segments precedes or even causes the

acceleration of the distal segments to higher speeds via transfer of segmental momenta (eg. Joris et al., 1985; Edmondstone and Chapman, 1991). The mechanism by which the deceleration of the proximal segment takes place remains inconclusive. It has been suggested that it is due to muscle activity or a consequence of segmental interaction (Putnam, 1993).

Several factors may account for slight deviations in the PD sequential pattern among ballistic skills. The timing can vary considerably depending on differences in the speed and accuracy demands of the task (Putnam and Dunn, 1987), the ranges of motion of the participating joints, the properties of the musculature involved (Chapman and Sanderson, 1990) and the segmental interaction resulting from such differences as in the physical characteristics of the athlete. However the relative effects of these factors on the overall movement are unknown because of the complex interactions of all the contributing factors.

It is apparent that the PD pattern is not shown as clearly in some skills as in others. This is particularly evident in analyses which quantify the longitudinal rotation about body segments. For example, in the tennis serve, peak forearm pronation motion precedes that of shoulder internal rotation in generating high racquet velocities. Similarly, peak elbow angular velocity occurs prior to peak upper arm internal rotation velocity in baseball pitching (Feltner and Dapena, 1986).

### *E. THE SQUASH STROKE*

Even though the game of squash racquets or squash has gained widespread popularity, there have been very few studies analyzing the movements involved. The

forehand stroke is one of its fundamental movements. It is necessary that a player develop an accurate and powerful forehand stroke to achieve any degree of success in playing the game. Behm (1987) recognized that such strokes result from biomechanically correct technique, but he did not quantify the stroke.

Coaches of the game advocate that the general movement pattern starts with rotation of the trunk, then the arm swings forward leading with the elbow until the forearm pronates rapidly while the wrist is radially deviated at impact. In a 2D frontal view of the striking arm and racquet during a forehand stroke, the linear velocities of the segmental endpoints in the direction of the stroke peaked in the order of the shoulder, elbow, wrist and finally, the racquet (Chapman, 1985a). This implied that the segmental movements occurred in a proximal to distal (PD) sequence. However, this observation did not accurately represent the multiplanar nature of the squash stroke.

Extensive forearm rotation is advocated as a primary movement in generating high racquet head speeds at ball contact in a squash forehand stroke (Chapman, 1985a). This is a significant feature of the squash stroke, particularly among elite players, and also of other racquet sports. Sprigings, et al. (1992) found the greatest contributions to the racquet motion at impact to be internal rotation of the upper arm and forearm pronation in a squash forehand stroke. Similar segmental movements were observed at impact in a tennis serve (van Gheluwe and Hebbelinck, 1985).

# Chapter 3
# METHODS

## *A. SUBJECT*

A male elite squash player was used as the subject in the present experiment. While performing the squash stroke, the subject wore only white tennis shorts. The visibility of the joint centres was enhanced by painting two centimetre wide black bands about the subject's waist at the level of the suprailiac crests and neck region at the level of the suprasternal notch. Similar black bands were placed about the shoulder, elbow and wrist joints of the striking arm. To indicate forearm rotation, an external marker was firmly attached about the subject's forearm proximal to the wrist joint on the anterior lateral surface with a velcro strap. This location was considered optimal as the marker remained in camera view for a relatively long period throughout the stroke. The marker was a flourescent red hemisphere with a diameter of 2 cm and a height of 1 cm.

Four highly visible fluorescent red stickers were placed on the squash racquet. One of these markers was located on the shaft just above the grip and another marker on the shaft identified the racquet's centre of mass. The final two markers were on the head of the racquet, one on the side of the head of the frame and the other at the racquet tip.

### *B. TASK*

The subject was required to perform the stroke referred to as the forehand stroke or drive. Under game conditions during a forehand drive, the ball is hit with a relatively high velocity towards the front wall at a height just above the tin. He was required to produce as 'hard' a stroke as possible while maintaining consistency of motion. Therefore, these were not maximal effort strokes. The experimental task required the subject to replicate this stroke by hitting a squash ball towards a 8"x11" cardboard target placed 3 m to his left with the centre of the target at a height of 50 cm. The subject was given a warm-up period to familiarize himself with the task and testing environment. He repeatedly performed the task until he felt he was ready to perform the stroke consistently. During the filming process, the consistency in the stroke could only be assessed on the basis of the subject's judgement and those of the observers' and whether the subject successively hit the target.

The subject was filmed performing five consecutive trials. Each trial consisted of the following protocol. The subject initiated the trial by yelling, "Go!", at which time the camera operators started the two high speed cameras, thus allowing sufficient time for the cameras to accelerate to the appropriate film speed. After a brief pause, the subject dropped the squash ball in front of his feet from head height. Just as the ball dropped out of the subject's hands, an experimenter initiated a photographic flash within both camera views. This flash served as a visual signal for the temporal synchronization of both films. The ball was then struck after the first bounce towards the target. To ensure that the height of the bounce was adequate and reasonably consistent, a yellow dot squash ball was kept at approximately game temperatures (42 degrees Celcius) by having it sit in warmed water. The cameras were stopped once ball contact was heard.

## *C. DATA ACQUISITION*

### *C.1 EXPERIMENTAL SETUP*

A pilot study indicated that the best method to acquire coordinate data in the squash forehand stroke was high-speed cinematography. An optoelectric motion analysis system, the WATSMART, was not viable because the complexity of the segmental movements obscurred several of the IREDs resulting in missing data for lengthy periods during the stroke. This was particularly a problem with the markers on the trunk and forearm. In addition, the use of external markers did not provide the 3D location of the joint centres without knowing their spatial relationships between them. Videography was also considered to be impractical because of the high expense of high-speed video systems and the same problems encountered when using external markers as in optoelectric systems.

The experimental setup included two LOCAM high speed cameras arranged in a quasi-equilateral triangle with the centre of the activity space where the subject was located as illustrated in Figure 3.1. The distances between the cameras and the subject were restricted to the dimensions of the laboratory, but effort was made in locating the cameras as far away from the central testing space as possible to maximize the cameras' fields of view. Cameras A and B were situated 8.5 m and 7.6 m from the centre of the activity space and 8.8 m apart. Both cameras were secured atop tripods which in turn were sitting on table tops. The vertical heights of the cameras were about 2.5 metres above the floor which improved the visibility of the markers as the optical axes of the cameras were directed slightly downwards toward the subject.

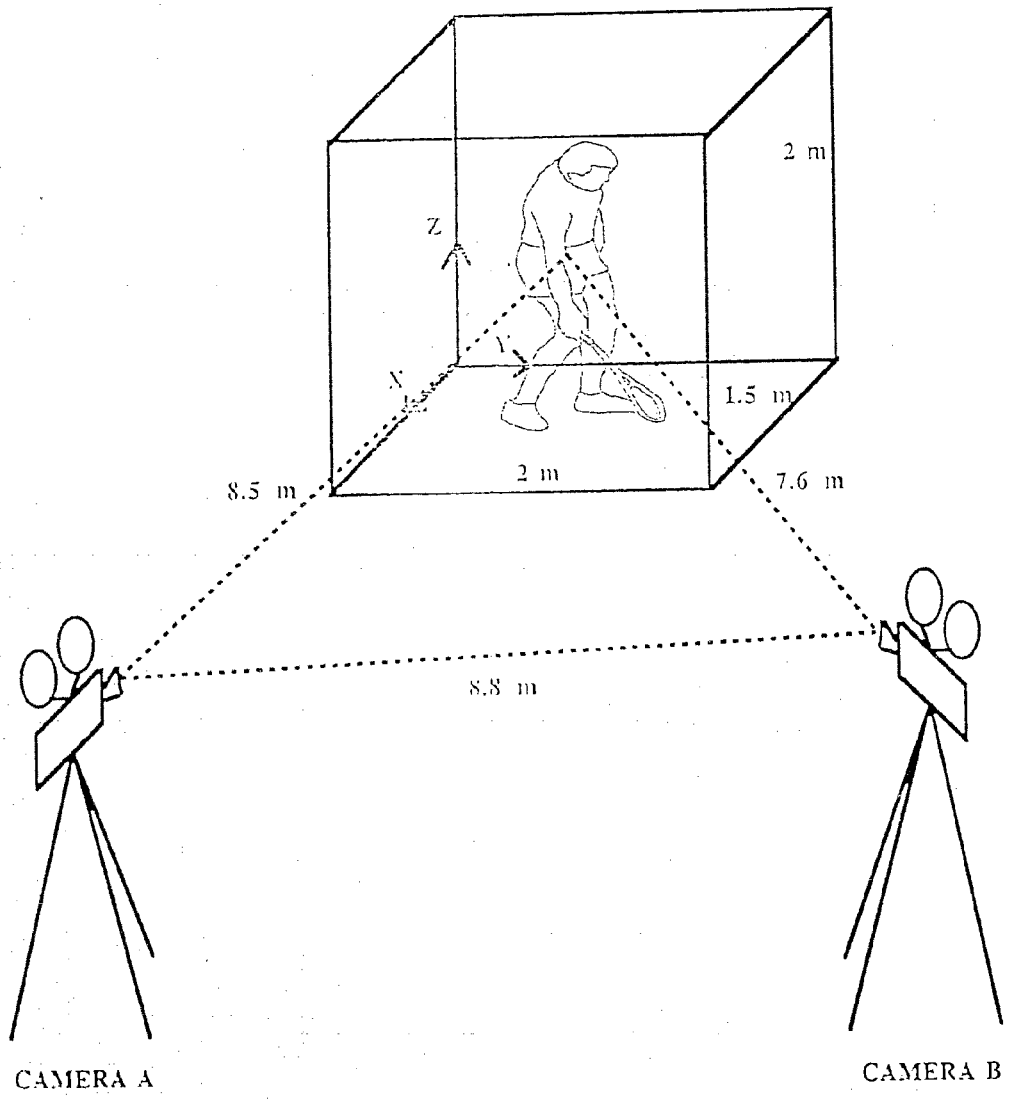


Figure 3.1 A schematic diagram of the experimental setup. The origin of the fixed global frame of reference ($R_1$) was located at the bottom, left, back corner of the activity space.

Both cameras used 400 ASA 16 mm Kodak colour film. The camera settings included a film speed at 400 frames per second with a shutter speed of 1/2000 second and a shutter angle of 1/6. A fast film rate was chosen in order to capture ball contact and the rapid movements of the racquet near the time of ball contact. Because the ball stays in contact with the racquet for about 2.5 ms, any slower frame rate might not have captured contact.

To ensure adequate film exposure for such high film speeds, nearly 600 foot candles of illumination was necessary. The background was covered with plain white cloth to improve the contrast between subject and background. A counter was also placed in the background to indicate the trial number.

### *C.2 THE FILMING AND DIGITIZING PROCESSES*

The filming and digitizing processes used to obtain the 2D (U,V) image coordinates consisted of three stages. Firstly, the calibration structure containing the known control points was filmed. It was then removed prior to filming the subject in the reference position. Lastly, the subject was filmed performing repeated trials of the squash forehand stroke. The specifications of the filming process are described in the following sections.

The 2D (U,V) image coordinate data were acquired from manual digitization of selected points on both films. The image size was increased by projecting the films onto a mirror which reflected onto the digitizing tablet. Films A and B were digitized on a Numonics Model 2200 digitizing tablet which had an error of ±0.25 mm. One film was completely digitized before proceeding onto the second film. The 3D coordinate data

reconstruction was performed by using the DLT technique incorporating these sets of 2D (U,V) image coordinates.

### *C.2.1 CALIBRATION PROCEDURE*

A semi-rigid, cubic reference structure was constructed encasing the known control points for calibration purposes (Figure 3.2). The rigid outer frame which consisted of steel side supports and stabilizing steel struts had dimensions of 2 metres x 1.5 metres x 1.5 metres. The size of the calibration frame was sufficiently large to encompass the subject and the racquet during the entire squash stroke.

The top surface was made of lightweight aluminum supports from which nine translucent strings hung. These strings were arranged in a 3 x 3 hexagonal formation as viewed from the top. Each string acted as plumb line with a small weight attached at the bottom end keeping the line vertical. The string was damped by having the weight sit in a small container of water. For easier identification of the strings on film, the strings were coded with different coloured stickers labelling the front, middle and back rows. From left to right, the back row contained strings #1 to #3. The middle row had strings #4 to #6 and strings #7 to #9 were located in the front row.

Six control points were suspended on each string resulting in a total of 54 control points available for calibration. The control points were red and white plastic spheres with 2 centimetre diameters. They were well distributed within the calibration frame with the points spaced 20 to 40 centimetres apart vertically along each string.

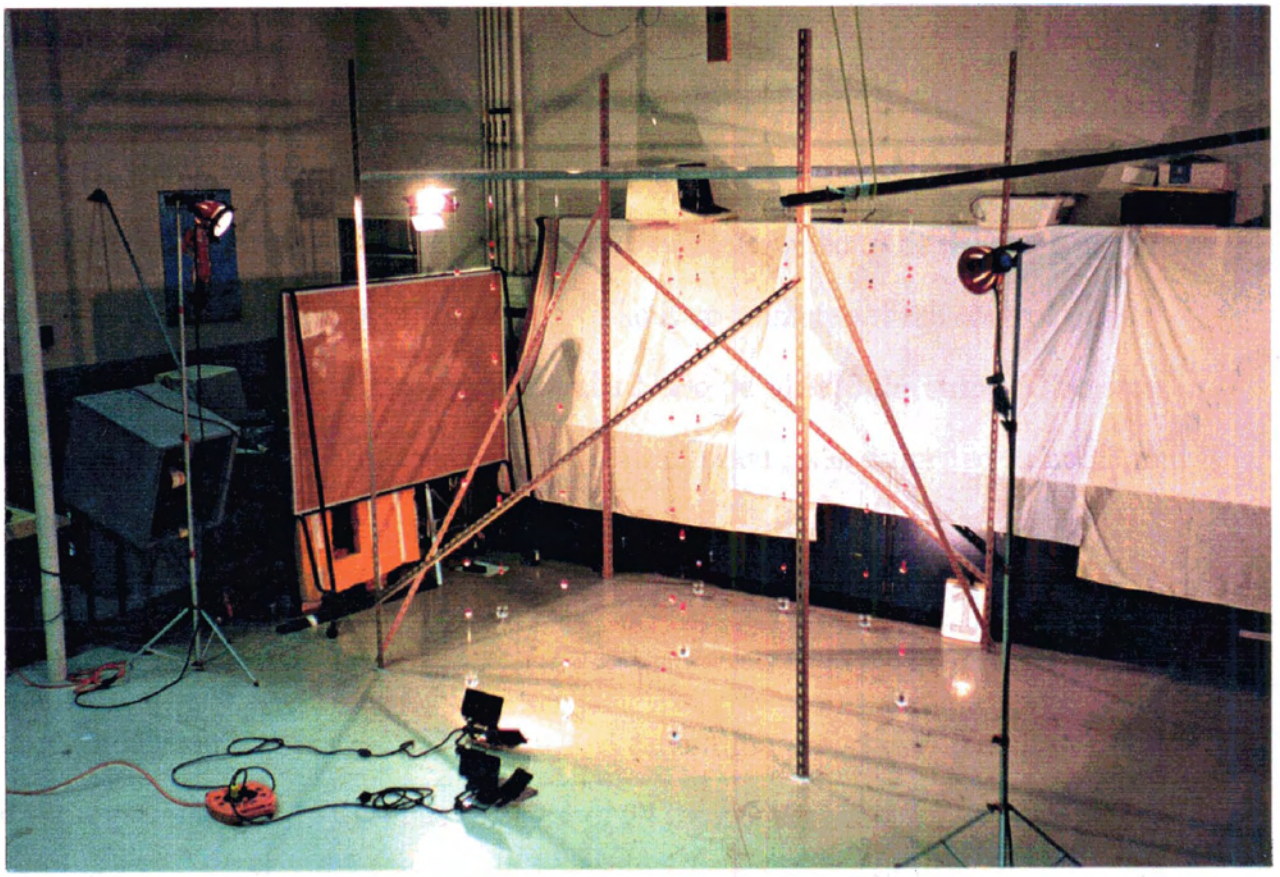

Figure 3.2 A photograph of the calibration frame containing the known control points.

The object (X,Y,Z) coordinates of the control points corresponded to the centroid of the sphere. They were measured with respect to a right-handed orthogonal reference frame referred to as the inertial global reference frame ($R_I$). Its origin was located at the back, left, bottom corner of the calibration frame from camera view (Figure 3.1). The Z axis was directed vertically, the Y axis pointed laterally to the right, and the X axis was oriented in the anterior direction towards the cameras. The X and Y coordinates of each string were measured by projecting the strings towards the floor. Because the strings hung vertically and passed through the centres of the control points, the X and Y coordinates of all control points on any one string were assumed to be the same as the measured X and Y coordinates of that string. The Z coordinates of the control points were measured with a vertical measuring standard held parallel to the string. The error in measurement of the X,Y,Z coordinates of the control points was estimated to be $\pm 3$ mm along each of the axes. A single measurement of these coordinates was made.

Once the 3D object coordinates of the control points within the frame were measured, the frame was not moved prior to the calibration procedure. The frame was filmed for approximately 15 seconds at a rate of 24 frames per second. After the calibration frame was filmed, it was removed from camera view and the subject was filmed in the same object space. The cameras were not moved hereafter to ensure a valid calibration throughout the whole experiment.

Not all of the control points of the calibration frame were digitized. Although all 54 control points were visible on both films, the image of the calibration frame extended beyond the active borders of the digitizing tablet leaving only 40 usable points. The missing points were located on the top row and string #7 (front left). The remaining points were well distributed within the calibration frame. The usable control points were

digitized from ten consecutive frames of film. These frames of film were chosen during an interval after the cameras had reached the appropriate film speed.

### *C.2.2 THE REFERENCE POSITION*

Once the calibration procedure was completed, the subject was filmed in the reference position (RP) for approximately 15 seconds at a frame rate of 24 frames per second. In this position, the subject stood stationary facing directly between the cameras with his shoulder, elbow and wrist joints of the striking arm aligned in a vertical plane. In addition, his forearm and wrist were in anatomically neutral positions while holding onto the racquet with a standard handgrip.

The rationale for using the reference position was to establish reference angles of the forearm and wrist. As the most distal segment comprised the hand and racquet, the extension of the racquet coming out of the hand when using the standard handgrip indicated some wrist extension and abduction even though the wrist was in an anatomically neutral position. The angles between the hand/racquet segment and the longitudinal axis of the forearm were referred to as the reference angles of the wrist. These angles were subtracted from subsequently calculated wrist angles to obtain true wrist joint angles.

A similar procedure was required to establish a reference angle for the external marker on the forearm with respect to the neutral plane defined by the shoulder, elbow and wrist joint centres. Since the optimal location of this external marker in terms of visibility by the cameras was not in this neutral plane, the reference angle of the forearm marker was subtracted from subsequent calculations of forearm rotation.

A total of thirteen points were digitized with the subject in the reference position. These points were the same as those digitized during the stroke (see below). Ten consecutive frames of the subject in the reference position were digitized. Again, it was unecessary to synchronize the films at this point for same reasons as stated above in the digitization of the calibration frame. From these 10 sets of data, a set of averaged UV coordinates was calculated.

### *C.2.3 THE SQUASH FOREHAND STROKE*

The subject was filmed while performing five strokes labelled Strokes #1 to #5. In every trial, he successfully hit the target. These trials were performed successively such that the ball only needed re-warming after the second trial.

Thirteen points were digitized in each frame for all five trials. Although the body was marked, the markings surrounding the joint centres of the striking arm were not used as points of digitization, but rather as an aid in locating the joint centres on film. The following points were digitized:

1) a fixed reference point,
2) the right hip point located on the right suprailiac crest (RHIP),
3) the midhip point at the level of the suprailiac crests representing the inferior end of the longitudinal axis of the trunk segment (MHIP),
4) the left hip point located on the left suprailiac crest (LHIP),
5) the sternal point representing the superior end of the longitudinal axis of the trunk segment (STRN),

6) the shoulder joint centre (SHLD),

7) the elbow joint centre (ELB),

8) the wrist joint centre (WRST),

9) the external marker on the forearm (FORE),

10) the marker on the shaft of the squash racquet (SHFT),

11) the marker representing the centre of mass of the racquet (CM),

12) the marker on the head of the racquet (HEAD), and

13) the marker on the tip of the racquet (RTIP).

There were no markings on the body representing the side hip points (RHIP and LHIP). These points were later considered to be necessary to calculate the trunk rotation angle as being relative to the position of the pelvis rather than an absolute angle.

In the synchronization of both films, the number of frames of film were counted from the instant the photographic flash was seen to the instant of ball contact in both films. Ball contact was captured in a single frame of film. There was a small difference in film speeds (Film A = 397 frames/s; Film B = 398 frames/s) as verified by the internal timing marks on the films. This difference was also seen as a slight difference in the deformation of the ball while in contact with the racquet head. This accounted for a temporal error of less than a frame or 0.0025 s.

The number of frames in which to digitize per stroke was established in Stroke #1. Each frame was digitized from the initial frame when the photograhic flash was seen until 140 frames of film which provided at least 20 frames of film after ball contact. This number was considered to be sufficient for providing enough data prior to the initiation of movement and after ball contact so as to capture the entire stroke and to avoid distortion due to the filtering process. In the other trials, 140 frames of film were also digitized, but

there were not an additional twenty frames after ball contact. Ball contact varied between frames #114 - 127 in all trials.

For the purpose of examining the accuracy and reliability of the results, the intra and inter-digitizer variabilities were analyzed in terms of the anatomical joint angular velocity profiles of Stroke #2. The intra-digitizer reliability was determined by the same individual digitizing Stroke #2 three times repeatedly (Digitizer A). Digitizer A was the same individual who digitized all trials. It was considered to be superfluous to digitize 140 frames since the peak velocities occurred within approximately 40 frames prior to ball contact. Therefore only 60 frames were digitized of which Frame #50 was ball contact.

A new DLT calibration was required to reconstruct the 3D (X,Y,Z) object coordinates for the intra-digitizer investigation yielding an RMS error of 3.67 cm.. Although the reconstruction error was relatively high in this case, further reduction of the RMS error would not have altered the general shape of the anatomical joint angular velocity profiles (Appendix A). Therefore, no attempt was made to reduce the RMS error. Details of the how the accuracy of the reconstruction was assessed are described later.

Inter-digitizer variablity was investigated similarly by having a second person (Digitizer B) digitize Stroke #2 once. This was performed to illustrate the validity of the digitization process. Again, the anatomical joint angular velocity profiles from this trial were compared to those obtained by Digitizer A. Digitizer B digitized a total of 140 frames.

## *C.3 DATA ANALYSIS*

The data analysis followed the scheme shown in Figure 3.3. The following sections discusses each stage after acquiring the image coordinate data. There was no concensus in the literature regarding a systematic approach in analyzing 3D data. Through a series of investigations comparing various data analysis strategies, the scheme shown below was found to be the most appropriate for this study.

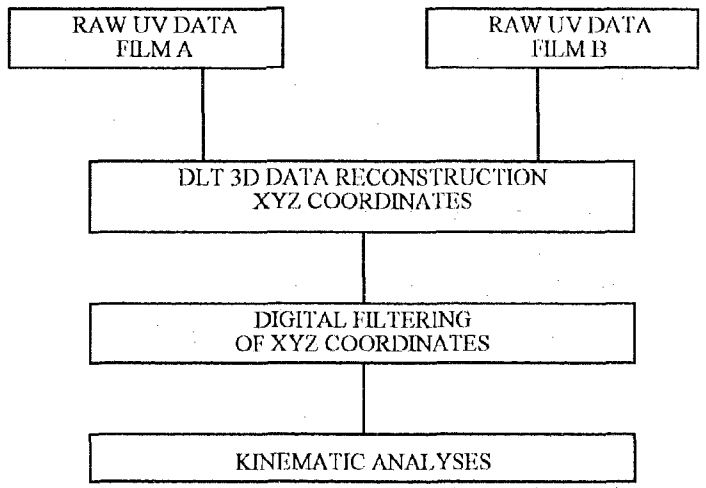


Figure 3.3 A flow diagram of the data analysis.

### *C.3.1 3D COORDINATE DATA RECONSTRUCTION*

The 3D (X,Y,Z) coordinates of the selected points in the reference position and during the strokes were reconstructed by the DLT technique. The following sections describe the steps implemented in the determination of the appropriate calibration

coefficients and the removal of discontinuities in the 2D (U,V) image coordinate data prior to reconstruction.

### *C.3.1.1 CALIBRATION*

The initial step of the data reconstruction process was the calibration of the cameras with the activity space. The ten sets of digitized (U,V) image coordinates of the known control points produced ten corresponding sets of estimated calibration coefficients for each camera. These sets were averaged producing a single set of averaged calibration coefficients for each camera.

The accuracy of the 3D data reconstruction was assessed by calculating the overall root mean square (RMS) error of the differences in the actual and estimated XYZ coordinates of the control points used in the calibration. This was not in accordance with Challis and Kerwin (1992) who recommended that the same points used in the calibration should not be used to evaluate the accuracy of the reconstruction. The use of the same points significantly underestimated the accuracy. The RMS error was calculated using equation 3.1 (Nike Sport Research Review, 1991):

$$RMS = \frac{\sum_{i=1}^{N} \sqrt{(Rx - Cx)^2 + (Ry - Cy)^2 + (Rz - Cz)^2}}{N} \qquad (3.1)$$

where $Rx, Ry, Rz$ = reconstructed XYZ coordinates
$Cx, Cy, Cz$ = known control point XYZ coordinates
$N$ = the number of control points

The overall RMS error using all 40 control points was 3.81 cm. A stepwise approach to reduce this error was taken by successively removing control points which yielded relatively high residuals (Appendix A). Calibrations were performed using 40, 29, 21 and 9 control points. The RMS error declined as more control points were removed. The lowest error was 1.09 cm when 9 control points were used. However, these control points were not well distributed within the activity space which was one of the criteria of the DLT technique. It was necessary to compromise between a higher RMS error and an even distribution of the control points, so CALIB21 was the calibration used with 21 control points and an RMS error of 1.67 cm. RMS errors were also calculated for the individual axes in each case and the accuracy was consistently the poorest in the X direction representing the depth on the sagittal axis.

Futhermore, the effect of the various calibrations on the joint angular velocity profiles of Stroke #2 was investigated to ensure that an appropriate calibration was chosen before the remaining trials were analyzed. Similar velocity profiles were obtained regardless of the number of control points used (Appendix A).

### *C.3.1.2 SOURCES OF ERROR IN THE RAW UV COORDINATES*

Random and non-random errors were introduced to the data during the digitizing process. The sources of random error include those by the digitizer and the misalignment of the frame of film within the gate of the projector.

The purpose of digitizing a reference point was to avoid errors due to misalignment of the film in the projector. This may be accomplished by defining all 2D (U,V) image coordinates with respect to a fixed reference point in each frame of film. However, an analysis investigating the accuracy of the reconstructed 3D (X,Y,Z) object coordinates of the squash ball during free fall as it fell from the subject's hand to the floor indicated that using a reference point was inappropriate. Unreasonable results were obtained as the raw reconstructed 3D (X,Y, Z) object coordinates suggested the ball was outside the activity space (Appendix B). The coordinates of the reference point were not subtracted from the coordinates of the remaining points in each frame of film. Any potential errors ocurring from the misalignment of the film were assumed to be removed by the filtering process.

Some discontinuities were also introduced during the digitization of the strokes. In one of the films, Film A, the image size was sometimes too large to stay within the frame of film, thus affecting the vertical (V) image coordinates. In particular, the markers on the side (RHEAD) and tip (RTIP) of the racquet head went out of view when the racquet was held above the subject's head at the beginning of the stroke and during the racquet's lowest trajectory around the time of ball contact. The acquisition of program required a certain number of data entries. Therefore, these missing points were temporally replaced by 'dummy' coordinates representing points just within the digitizing tablet boundaries, but with the correct horizontal (U) coordinates.

The 'dummy' coordinates at the beginning of the stroke did not present a problem because the data analysis did not include this period of the stroke. However, this was not so during the critical frames around ball contact. The vertical (V) image coordinates of the RTIP marker bottomed out as it went below the lower limits of the digitizing tablet. To estimate its trajectory, a cubic spline was used to interpolate its coordinates in the

frames that the marker was out of view. Only the data within these critical frames were modified. In the kinematic analysis, the RTIP marker was only used in the calculations of linear velocities not joint angles.

### *C.3.2 DIGITAL FILTERING OF THE XYZ COORDINATES*

The literature provided no rationale as to the stage at which data should be filtered. The possibilities include the 2D (U,V) image coordinates prior to 3D data reconstruction, the 3D (X,Y,Z) object coordinates, or the kinematic data. Primarily, investigators have smoothed the 3D (X,Y,Z) object coordinates or the displacment data, but it is uncertain as to whether filtering data at different stages may result in different velocity profiles. The effect of filtering the data at each possible stage was investigated by comparing the anatomical joint angular velocity profiles from filtered UV coordinate data, filtered 3D (X,Y,Z) OBJECT coordinate data and filtered joint angles of Stroke #2 using cutoff frequencies of 12 Hz and 20 Hz. The results of this investigation are presented in Appendix C. There was little difference between the various filter sequences at 12 Hz which was closer to the cutoff frequency later found to be suitable for this study. Some of the angular velocities profiles from filtering the UV coordinates at a higher cutoff frequency were dramatically different from the other filter sequences at the same cutoff frequency suggesting an adverse effect in filtering coordinate data prior to data reconstruction. Therefore, filtering either the 3D (X,Y,Z) OBJECT coordinates or joint angles appear to be preferable since their profiles were not substantially different. In this study, the 3D (X,Y,Z) OBJECT coordinates were filtered because certain distal anatomical joint angle calculations were based on the angles calculated at more proximal joints. Filtering the 3D (X,Y,Z) OBJECT coordinates also ensured that the data would only be filtered once and at the same time.

The removal of random noise from the 3D (X,Y,Z) OBJECT coordinate data was accomplished using a zero-lag, fourth order Butterworth digital filter (Winter, 1990). This passes the low frequency signal while attenuating the high frequency noise. A fourth order filter is achieved by a double pass of a second order filter, once in the forward direction and then in the reverse direction. The second pass is necessary to remove the phase lag created by the first pass. The higher order filter had a sharper cutoff response causing less distortion of data at frequencies close to the cutoff frequency.

A residual analysis described by Winter (1990) was conducted to decide the optimal cutoff frequency in filtering the 3D (X,Y,Z) OBJECT coordinate data (Appendix D). It indicated that 8 Hz was the most appropriate cutoff frequency based on the criterion that an equal amount of signal and noise was passed through the filter at the cutoff frequency.

#### *C.3.2.1 EXTRAPOLATION OF THE XYZ COORDINATE DATA*

The Butterworth digital filter is recursive in nature so that the value of each data point is predicted from its previous two data points. This inevitably results in some distortion of the data at the beginning and end of the data set. Extra data points are required as a padded region at either end allowing the data to settle so as not to affect the true region of interest.

A range of thirteen to twenty six frames were digitized after ball contact in the five trials. This number of frames was considered to be sufficient to avoid distortion of data within the critical time around and at impact. However, when analyzing the intra-digitizer

variability data, the padded region was found to be as many as twenty frames. Therefore, an additional twenty points were extrapolated onto both ends of the unfiltered 3D (X,Y,Z) object coordinate data sets to endure no distortion would occur during filtering. The extra points were extrapolated by a reflection method about the boundary points. This method was easily implementable and most effective (Smith, 1989). If $P_n$ was the boundary point where P was the coordinate value and n was the number of the boundary point, then $P_{n+i}$ would equal $P_{n-i}$ where $i$ is the number of extra points. The extrapolated sets of unfiltered 3D (X,Y,Z) OBJECT data were then filtered and analyzed.

### *C.4 3D KINEMATICS*

A open-linked model consisting of five rigid-body segments of fixed lengths joined together by ideal joints was used to investigate the movements of the trunk and upper extremity during a squash forehand stroke. The joints consisted of the hip, sternoclavicular, shoulder, elbow and wrist of the striking arm and the five rigid segments were referred to as the trunk, clavicular, upper arm, forearm and hand/racquet segments. Table 3.1 summarizes the anatomical landmarks defining the segments.

Table 3.1 The anatomical landmarks representing the endpoints of the body segments.

| SEGMENT | PROXIMAL POINT | DISTAL POINT |
|---|---|---|
| Trunk | MHIP | STRN |
| Clavicular | STRN | SHLD |
| Upper Arm | SHLD | ELB |
| Forearm | ELB | WRST |
| Hand/Racquet | WRST | CM |

The filtered 3D (X,Y,Z) object coordinate data were used in the calculation of the following kinematic parameters:

i) linear velocities of the segmental endpoints,
    a) resultant linear velocities
    b) linear velocities in the X, Y and Z directions

ii) 3D resultant joint angular velocities, and

iii) the anatomical joint angular velocities.

### *C.4.1 LINEAR VELOCITIES OF THE SEGMENTAL ENDPOINTS*

The segmental endpoints were the MHIP, STRN, SHLD, ELB, WRST, and CM points corresponding to the hip, sternal, shoulder, elbow, wrist and distal endpoint of the hand/racquet segment. The RTIP marker located at the distal end of the racquet was only used in the calculations of the linear velocities because of the uncertainty associated with the accuracy of the cubic spline in estimating the trajectory of the RTIP coordinates. Because the CM marker was visible throughout the stroke, it was used to represent the distal endpoint in the calculations of the 3D resultant joint angles and anatomical joint angles.

The linear velocities were calculated using finite differentiation in their respective directions with respect to the inertial global frame of reference ($R_1$). The resultant velocities were determined subsequently indicating the speed at which the endpoints were travelling.

The 3D resultant joint angles were calculated as the angle between the longitudinal axes of adjacent segments as shown in Figure 3.4. If a proximal segment (segment #1) is defined by as vector $\mathbf{V}_1$ and segment #2 was the adjacent distal segment defined by vector $\mathbf{V}_2$, the resultant 3D joint angle ($\theta$) would be the angle between the two vectors.

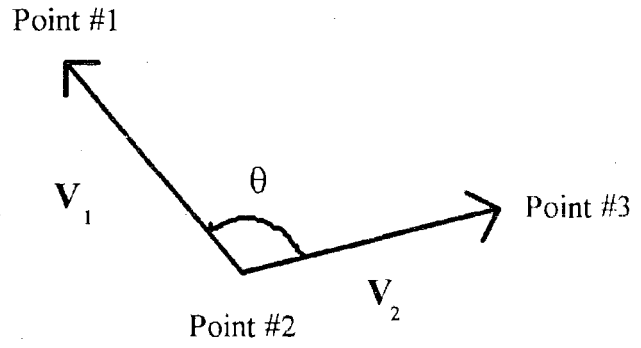


Figure 3.4 The 3D resultant joint angle ($\theta$) is the angle between vectors $\mathbf{V}_1$ and $\mathbf{V}_2$. (Point #1 is $(X_1, Y_1, Z_1)$; Point #2 is $(X_2, Y_2, Z_2)$; Point #3 is $(X_3, Y_3, Z_3)$).

where $$\mathbf{V}_1 = (X_1 - X_2)\mathbf{i} + (Y_1 - Y_2)\mathbf{j} + (Z_1 - Z_2)\mathbf{k} \quad (3.2a)$$

$$\mathbf{V}_2 = (X_3 - X_2)\mathbf{i} + (Y_3 - Y_2)\mathbf{j} + (Z_3 - Z_2)\mathbf{k} \quad (3.2b)$$

The resultant joint angle was calculated using the following general equation for determining the angle between two vectors.

$$\cos\theta = \frac{\mathbf{V}_1 \bullet \mathbf{V}_2}{\|\mathbf{V}_1\|\|\mathbf{V}_2\|} \qquad \text{where} \quad -\frac{\pi}{2} \le \theta \le \frac{\pi}{2} \qquad (3.3)$$

where $\theta$ = the angle between the vectors $\mathbf{V}_1$ and $\mathbf{V}_2$

$\|\mathbf{V}_n\|$ = the modulus of the vectors $\mathbf{V}_1$ and $\mathbf{V}_2$

The angular velocities were determined by finite differentiation. A positive angular velocity indicated that the resultant 3D joint angle was increasing whereas a negative angular velocity referred to a decreasing angle.

### *C.4.3 ANATOMICAL JOINT ANGULAR VELOCITIES*

The equations used to calculate the anatomical joint angles were derived from an analytical method similar to that presented by Small et al. (1992) in evaluating hand and finger motion. Cardan angles were used to assess the anatomical relationship of the distal segment relative to its proximal neighbour. The trunk was defined with respect to the orientation of the pelvis. The choice of Cardan angles over other analytical methods in the spatial representation of the body segments was based on its direct anatomical relevance of the angles and its widespread use. Its sequence-dependency is not a problem as long as the orientations of the axes and sign conventions are clearly stated. The motion of the shoulder joint may be susceptible to singularities, but the configuration of the arm during the majority of the stroke avoided this problem.

In the determination of the Cardan angles, local, right-handed orthogonal coordinate systems or reference frames were embedded in each of the segments to describe their respective orientations. A series of translations and rotations were required to align the axes of the coordinate systems. The relative orientations of the coordinate systems were defined in terms of a vector connecting the origins and a set of three ordered

rotations. It is these rotations known as the Cardan angles which describe anatomical joint motion.

The general concept behind this alignment-based system is that the fixed frame of reference (FFR) has axes X, Y and Z with unit vectors **I**, **J** and **K** embedded in the proximal segment (Segment A) with the unit vector **I** aligned along its longitudinal axis. The moving frame of reference (MFR) is embedded in the neighbouring distal segment (Segment B) and has axes x, y, and z with unit vectors **i**, **j** and **k**. The unit vector **i** of the MFR is directed along the longitudinal axis of the segment. Both reference frames originate at the proximal endpoint of each segment and are defined with respect to the inertial global reference frame ($R_I$). Figure 3.5 illustrates the relationship between the local coordinate systems embedded in adjacent segments.

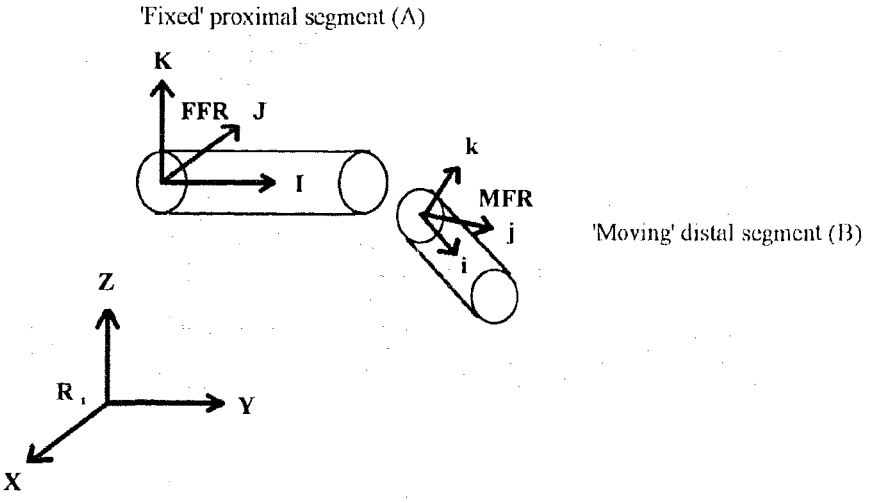


Figure 3.5 Illustration of the relative orientation of the FFR and MFR in the proximal (A) and distal (B) segments.

Equation 3.4 was the general mathematical relationship between the unit vectors of the FFR (**I**, **J**, **K**) and the MFR (**i**, **j**, **k**) where $S_f$ was the vector connecting the origins of both reference frames.

$$\begin{pmatrix} \mathbf{i} \\ \mathbf{j} \\ \mathbf{k} \end{pmatrix} = (B) \begin{pmatrix} \mathbf{I} \\ \mathbf{J} \\ \mathbf{K} \end{pmatrix} + \mathbf{S}_f \qquad (3.4)$$

The transformation matrix [B] was derived from the multiplication of three rotational matrices (equations 3.5a-c) corresponding to the three sequential rotations or Cardan angles, $\phi$, $\theta$, and $\psi$, which were required to align the axes of the two reference frames. The appropriate order of rotations in this analysis was about the Z, y' and x" axes.

Rotation matrix about the Z axis (first rotation):
$$\begin{pmatrix} \cos\phi & \sin\phi & 0 \\ -\sin\phi & \cos\phi & 0 \\ 0 & 0 & 1 \end{pmatrix} \qquad (3.5a)$$

Rotation about the y' axis (second rotation):
$$\begin{pmatrix} \cos\theta & 0 & -\sin\theta \\ 0 & 1 & 0 \\ \sin\theta & 0 & \cos\theta \end{pmatrix} \qquad (3.5b)$$

Rotation about the x" axis (third rotation):
$$\begin{pmatrix} 1 & 0 & 0 \\ 0 & \cos\psi & \sin\psi \\ 0 & -\sin\psi & \cos\psi \end{pmatrix} \qquad (3.5c)$$

The multiplication of the three matrices in the rotational order about the Z, y' and x" axes produced the transformation matrix $[B]$, (equation 3.6).

$$[B] = \begin{pmatrix} \cos\phi\cos\theta & \sin\phi\cos\theta & -\sin\theta \\ -\sin\phi\cos\psi + \cos\phi\sin\theta\sin\psi & \cos\phi\cos\psi + \sin\phi\sin\theta\sin\psi & \cos\theta\sin\psi \\ \sin\phi\sin\psi + \cos\phi\sin\theta\sin\psi & -\cos\phi\sin\psi + \sin\phi\sin\theta\cos\psi & \cos\theta\cos\psi \end{pmatrix} \qquad (3.6)$$

The matrix $[B]$ may also be expressed in terms of direction cosines from porjecting the unit vectors **i**, **j**, and **k** onto **I**, **J** and **K** (equation 3.7).

$$[B] = \begin{pmatrix} \mathbf{i} \bullet \mathbf{I} & \mathbf{i} \bullet \mathbf{J} & \mathbf{i} \bullet \mathbf{K} \\ \mathbf{j} \bullet \mathbf{I} & \mathbf{j} \bullet \mathbf{J} & \mathbf{j} \bullet \mathbf{K} \\ \mathbf{k} \bullet \mathbf{I} & \mathbf{k} \bullet \mathbf{J} & \mathbf{k} \bullet \mathbf{K} \end{pmatrix} \tag{3.7}$$

By equating equations 3.6 and 3.7, the Cardan angles may be determined by the following equations:

$$b_{13} = \mathbf{i} \bullet \mathbf{K} = -\sin\theta \qquad \text{therefore, } \theta = \sin^{-1}(-\mathbf{i} \bullet \mathbf{K}) \qquad \text{where } -\frac{\pi}{2} \le \theta \le \frac{\pi}{2} \tag{3.8}$$

$$b_{12} = \mathbf{i} \bullet \mathbf{J} = \sin\phi\cos\theta \qquad \text{therefore, } \phi = \sin^{-1}(\mathbf{i} \bullet \mathbf{J} / \cos\theta) \qquad \text{where } -\frac{\pi}{2} \le \phi \le \frac{\pi}{2} \tag{3.9}$$

$$b_{23} = \mathbf{j} \bullet \mathbf{K} = \cos\theta\sin\psi \qquad \text{therefore, } \psi = \sin^{-1}(\mathbf{j} \bullet \mathbf{K} / \cos\theta) \qquad \text{where } -\frac{\pi}{2} \le \psi \le \frac{\pi}{2} \tag{3.10}$$

Anatomically, the Cardan angles corresponded to the following joint angles as proposed by Small, et al. (1992):

i) $\phi$ = abduction/adduction

ii) $\theta$ = flexion/extension

iii) $\psi$ = internal/external rotation

Details of the calculation of individual anatomical joint angles appear in Appendix E.

### *D. INTER-SUBJECT VARIABILITY*

The temporal coordination of a forehand stroke of another elite male squash player (Subject B) was analyzed in a similar manner as previously described. He was filmed performing several trials of the same experimental task. A single trial was selected for analysis based on the best visibility of the markers. The purpose of this investigation was to distinguish commonalities and differences between the players' strokes possibly providing some insight as to the dominant features of an elite squash forehand stroke. The comparison was between the anatomical joint angle and angular velocity profiles obtained in Stroke #2 of Subject A and that of Subject B.

# Chapter 4
# RESULTS

It was not possible to normalize the period over which each of the strokes were performed because there was no distinct starting event initiating the movement. Therefore, the kinematic profiles obtained for each the trial were aligned with respect to the absolute time of ball contact (t = 0.3175 s).

The subject's stroke was highly consistent as indicated by the similarity of the kinematic profiles. Although the absolute magnitudes and timings of the peak velocities may differ slightly between trials, the general trends of the profiles were quite similar. Appendix F presents the anatomical joint angle and anatomical joint angular velocity profiles from all trials. Included in Appendix F are the mean profiles with plus and minus one standard deviation indicating the variability throughout the stroke for each parameter.

Further support of the consistency in the task and subject was indicated by the motion of the squash ball. Its kinematics were derived from the raw XYZ coordinate data because filtering would have resulted in data distortion due to the limited number of frames which were recorded between the time of ball contact and when the ball had gone out of camera view. The ball was struck low at heights of 39.0, 38.5, 45.9, 38.2 and 34.4 cm in Strokes #1 to #5, respectively. The speed at which the ball travelled after impact was defined as the average speed in the frames when the ball had reached terminal velocity. The ball speeds were 47.8, 47.4, 48.0, 44.4 and 47.7 m/s, in Strokes #1 to #5, respectively. In addition, the subject hit the target successively in all trials. These measures establish the high consistency of the subject's stroke and the conditions under which the experimental task was performed.

The variability in the data was further analyzed in terms of the intra-digitizer and inter-digitizer variability. The anatomical joint angular velocity profiles obtained from these digitizations are presented in Appendix G. Good reliability by Digitizer A was indicated by the similarity of the profiles particularly during the period around impact. The greatest variation occurred at the beginning and end sections of these profiles even with additional points extrapolated to the limited original data set. In terms of the inter-digitizer variability, the general shapes of the anatomical joint angular velocities were similar between the two Digitizers, but the absolute temporal pattern were not the same. This was most likely due to slight differences in the interpretations of the joint centre locations. Greater judgemental errors was inherently associated with larger proximal segments. Due to the nature of the calculations, this error may be propagated to the distal joints as shown by a large variability in the wrist angular velocities.

To simplify this description, only the results from a single trial will be presented in detail with reference to the other trials. This is justifiable in light of the subject's high reliability. Stroke #2 was considered representative of the subject's stroke.

To aid in the visualization of the squash stroke, the following two figures are the 3D (X,Y,Z) object coordinates plotted terms of the global frame of reference ($R_1$) of the digitized landmarks and markers of Stroke #2. Figure 4.1 is the projection of the points on the YZ plane as if viewing the stroke from the front down along the X axis. The sweeping motion of the racquet is clearly visible. Figure 4.2 is a side view of the stroke along the Y axis opposite the direction of ball travel with the points projected on the XZ plane. This figure indicates that motion in the X direction was much less than in the Y and Z directions.

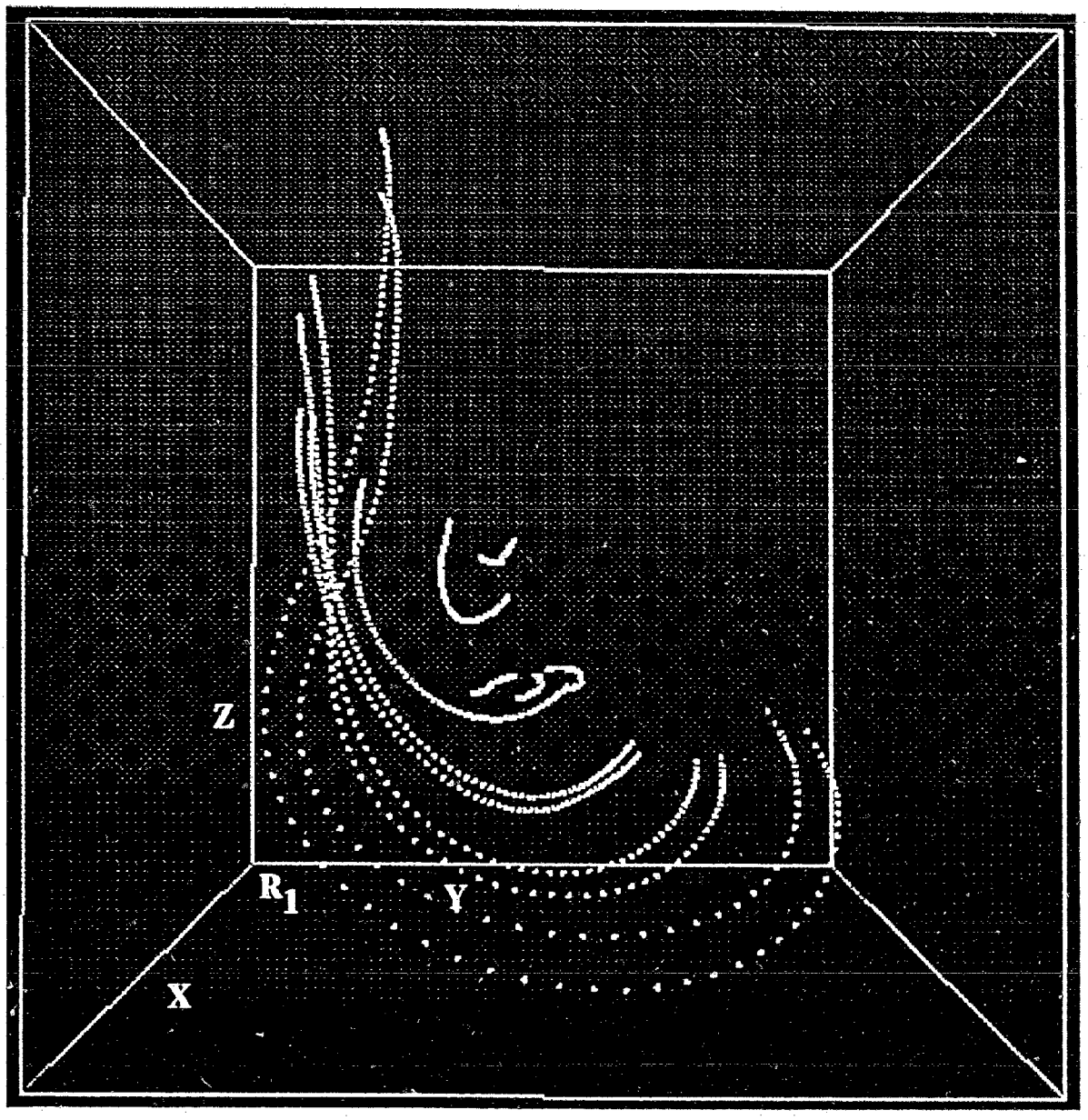


Figure 4.1 The projections of the digitized points on the YZ plane providing a frontal view of Stroke #2 (down the X axis).

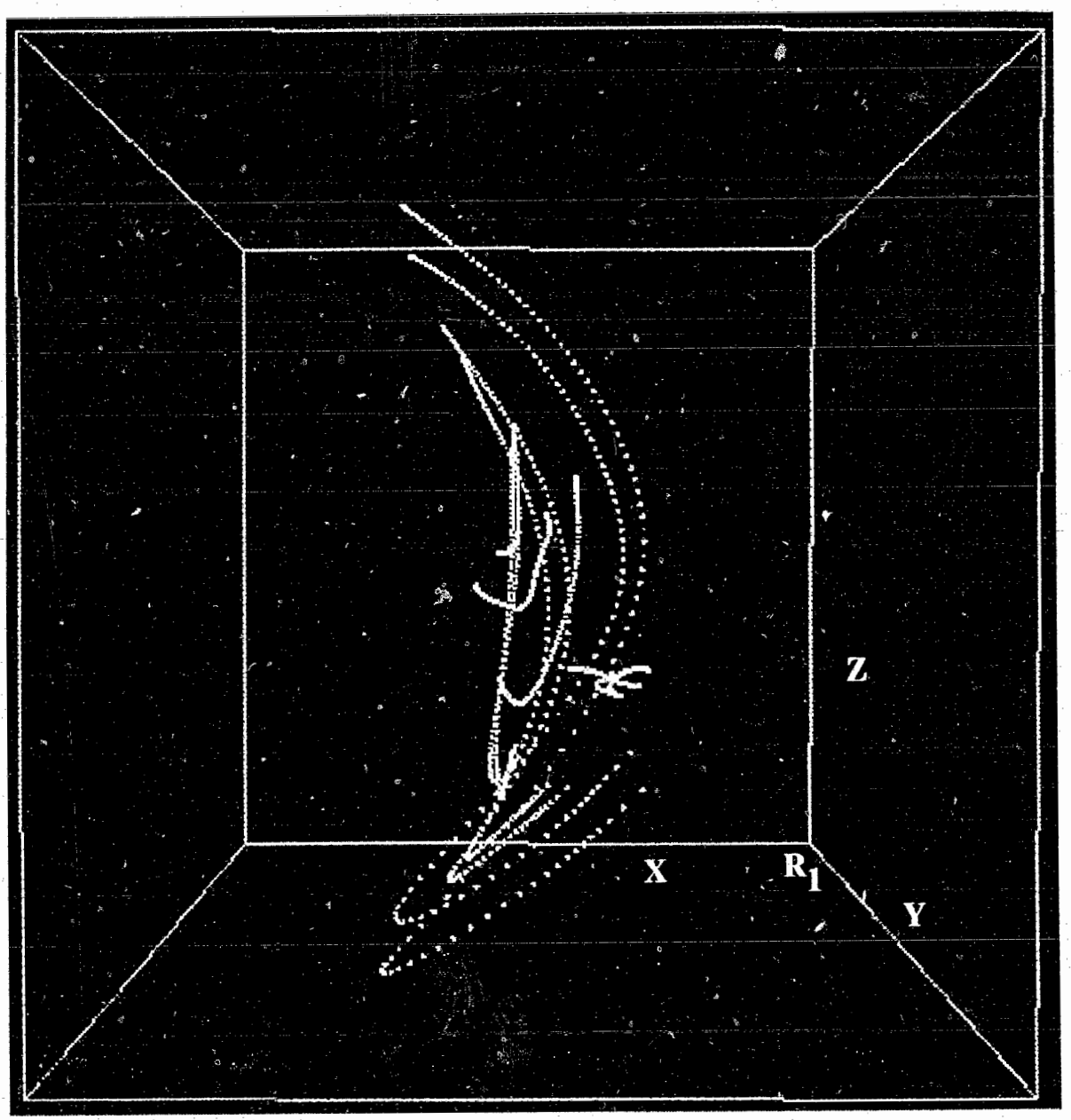


Figure 4.2 The projections of the digitized points on the XZ plane providing a side view of Stroke #2 (opposite the direction of ball travel).

## *A. RESULTANT LINEAR VELOCITIES OF THE SEGMENTAL ENDPOINTS*

The profiles of the segmental endpoint resultant linear velocities of Stroke #2 are shown in Figure 4.3 and the peak values and their times of occurrence are tabulated in Table 4.1. The magnitudes of the peak resultant linear velocities of the segmental endpoints increased progressively from proximal to distal. The lowest peak velocity was 0.86 m/s by the STRN point whereas the greatest velocity, achieved by the most distal point, RTIP, was 30.5 m/s. Maximal RTIP velocity did not occur at ball contact rather it peaked 0.0125 seconds prior to impact. This progressivly increasing pattern in the magnitudes of the peak velocities was seen in all five trials.

The temporal sequence of the peak resultant linear velocities occurred in an approximate proximal to distal fashion. The endpoint linear velocities peaked in the order of the STRN, MHIP, SHLD, ELB, WRST and RTIP points. The STRN reached its greatest velocity 0.0150 s prior to that of the MHIP point. This temporal pattern was observed in four out of the five trials. However, in these trials, the time intervals separating the STRN and MHIP peak velocities were less than 0.0075 s. The only trial that demonstrated true PD sequencing of peak endpoint velocities was Stroke #3.

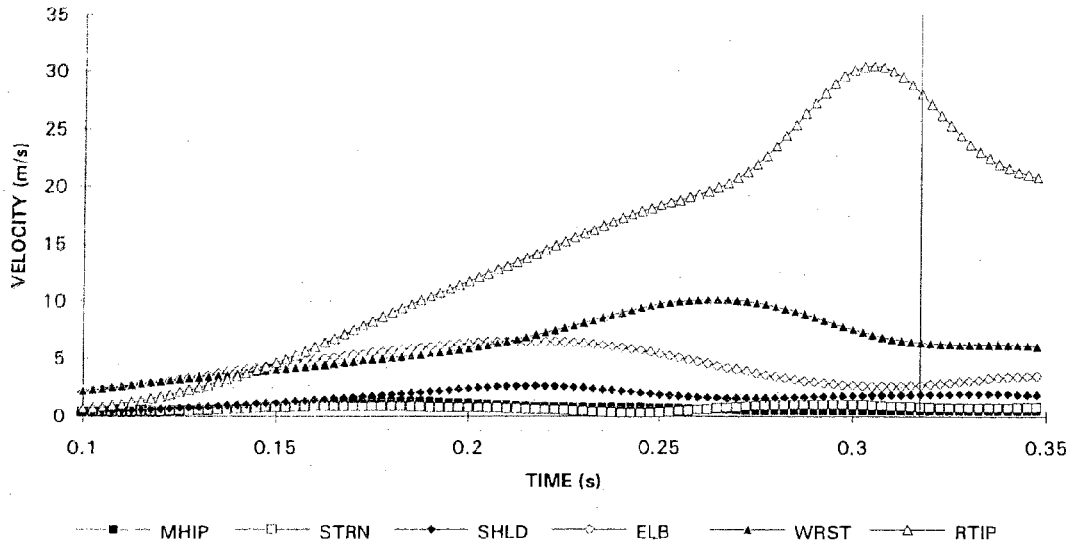


Figure 4.3 The segmental endpoint resultant linear velocity profiles of Stroke #2 (ball contact was at t = 0.3175 s as indicated by the vertical line).

Table 4.1 The peak resultant linear endpoint velocities, times of occurrence and the resultant linear velocities at the time of impact (t = 0.3175 s) of Stroke #2.

| ENDPOINT | PEAK VELOCITY (m/s) | TIME (s) | $V_{impact}$ (m/s) |
|---|---|---|---|
| MHIP | 1.3 | 0.1875 | 0.4 |
| STRN | 0.9 | 0.1725 | 0.8 |
| SHLD | 2.6 | 0.2175 | 1.9 |
| ELB | 6.5 | 0.2175 | 2.7 |
| WRST | 10.1 | 0.2625 | 6.4 |
| RTIP | 30.5 | 0.3050 | 28.0 |

## *A.1 COMPONENTS OF THE RESULTANT LINEAR VELOCITY*

Resultant linear velocities do not indicate direction rather just the speed of the movement. Directional information may be obtained from analyzing the component velocities or the velocities in the X, Y and Z directions. Relative to the subject, a positive X velocity referred to movement anteriorly, a positive Y velocity was motion towards the left primarily in the direction of ball travel, and a positive Z velocity was a movement upwards.

### *A.1.2 LINEAR VELOCITIES IN THE X DIRECTION (sagittal)*

In Figure 4.4, the X velocity profile indicated minimal movement in the sagittal plane until just prior to ball contact. The majority of the movement was by the racquet tip as it was brought forward during the foreswing. The peak positive X velocities of the endpoints were less than 1.2 m/s with the exception of the RTIP which had a peak velocity of 16.7 m/s (Table 4.2). The sequence of the peak X velocities was the STRN, MHIP, ELB, WRST, RTIP, and SHLD. All other trials showed the same temporal pattern of the peak X velocities in the striking arm.

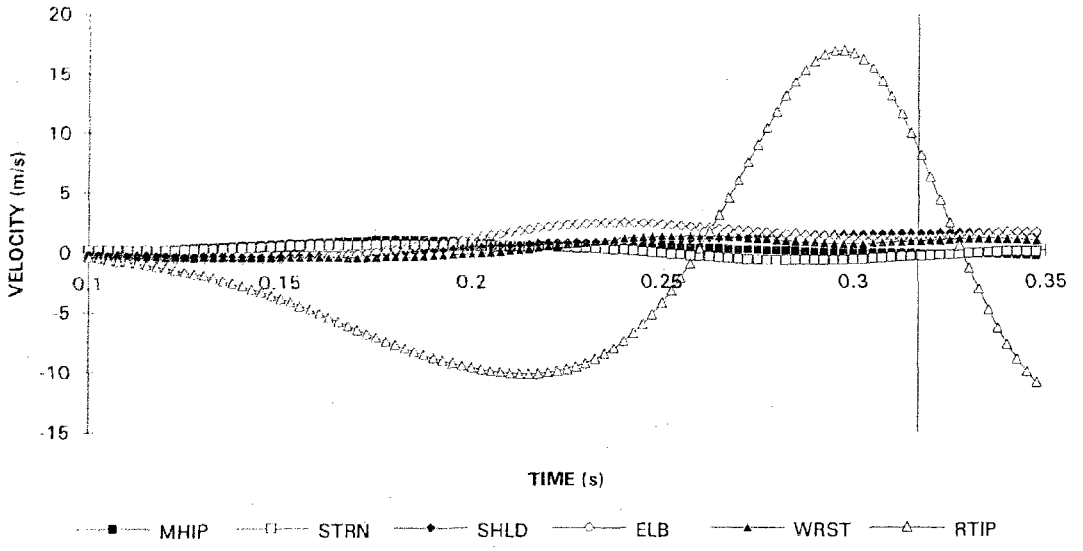


Figure 4.4 The segmental endpoint X linear velocity profiles of Stroke #2 (ball contact was at t = 0.3175 s as indicated by the vertical line).

Table 4.2 The peak linear endpoint velocities in the X direction of Stroke #2.

| ENDPOINT | PEAK VELOCITY (m/s) | TIME (s) | $V_{impact}$ (m/s) |
|---|---|---|---|
| MHIP | 0.9 | 0.1825 | -0.3 |
| STRN | 0.5 | 0.1800 | -0.4 |
| SHLD | 1.5 | 0.3325 | 1.4 |
| ELB | 2.3 | 0.2375 | 1.0 |
| WRST | 1.2 | 0.2575 | 0.8 |
| RTIP | 16.7 | 0.2975 | 8.0 |

### *A.1.3 LINEAR VELOCITIES IN THE Y DIRECTION (lateral)*

Figure 4.5 illustrates the Y velocity profiles (i.e. in the direction of ball travel) of the segmental endpoints for Stroke #2 and Table 4.3 summarizes the peak velocities and their times of occurrence. The magnitudes of the peak positive Y velocities of the endpoints were progressively greater in the distal segments compared to the more proximal segments, but the same PD pattern was not observed in the temporal sequence. The peak velocities ranged from 0.7 m/s, at the STRN, to 26.6 m/s at the distal endpoint, RTIP. The Y velocities peaked in the order of the STRN, MHIP, ELB, WRST, SHLD, and finally, RTIP. Maximum velocity of RTIP occurred at the instant of ball contact.

The temporal sequence in the peak Y velocities of the striking arm was similar in four out of the five trials. In two of the five trials, the peak velocity in the Y direction of the distal endpoint, RTIP, occurred simultaneously with ball contact and within 0.005 s of ball contact in the other trials. This was expected as the ball was projected primarily in the Y direction.

Characteristic of the Y velocity profiles of the endpoints in the striking arm was a deceleration-acceleration pattern. The Y velocity of the wrist did not begin to increase appreciably until the velocity of the ELB reached its peak. As the WRST velocity continued to increase surpassing the maximal velocity of the elbow, the ELB velocity decreased substantially. The WRST velocity peaked later than that of the ELB. The same pattern was also seen between the WRST and RTIP with the distal point developing maximal velocity which peaked higher and later than the proximal endpoints.

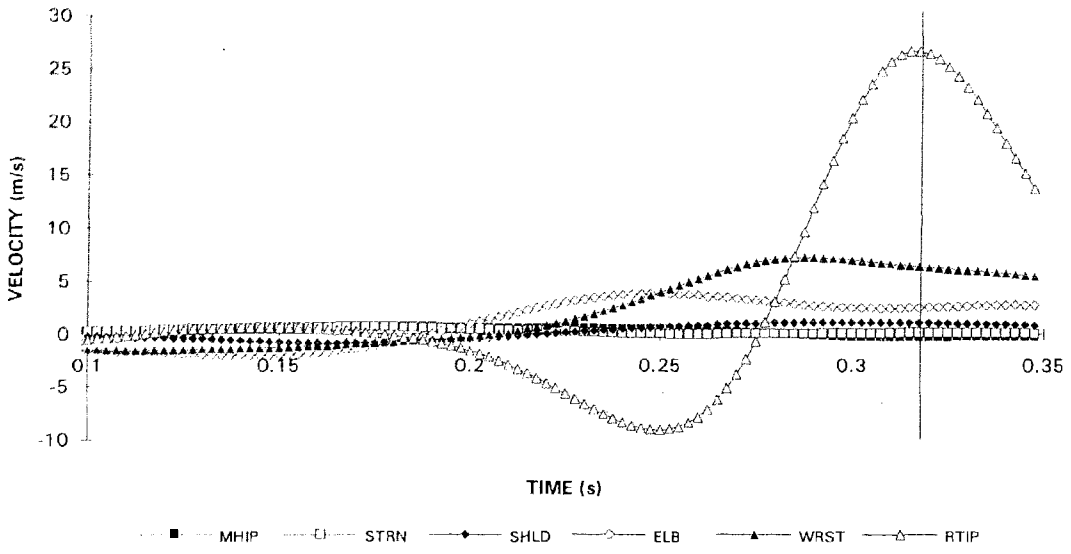


Figure 4.5 The segmental endpoint Y linear velocity profiles of Stroke #2 (ball contact was at t = 0.3175 s as indicated by the vertical line).

Table 4.3 The peak linear endpoint velocities in the Y direction of Stroke #2.

| ENDPOINT | PEAK VELOCITY (m/s) | TIME (s) | $V_{impact}$ (m/s) |
|---|---|---|---|
| MHIP | 0.7 | 0.1875 | -0.3 |
| STRN | 0.7 | 0.1725 | -0.1 |
| SHLD | 1.1 | 0.3025 | 1.1 |
| ELB | 3.8 | 0.2475 | 2.5 |
| WRST | 7.2 | 0.2900 | 6.3 |
| RTIP | 26.6 | 0.3175 | 26.6 |

### *A.1.3 LINEAR VELOCITIES IN THE Z DIRECTION (longitudinal)*

The Z velocity profiles of the segmental endpoints are shown in Figure 4.6. Table 4.4 lists the peak velocities and times of occurrence. The magnitudes of the peak Z velocities increased progressively from proximal to distal ranging from -0.3 m/s for MHIP to -20.2 m/s for RTIP. The downward swing of the racquet produced a sequential pattern of the peak Z negative velocities in the order of the MHIP, STRN, ELB, SHLD, WRST and RTIP. This temporal sequence was apparent in all trials. The maximal Z velocities of RTIP were reached well before ball contact. As expected, all endpoint velocities were approximately zero at ball contact.

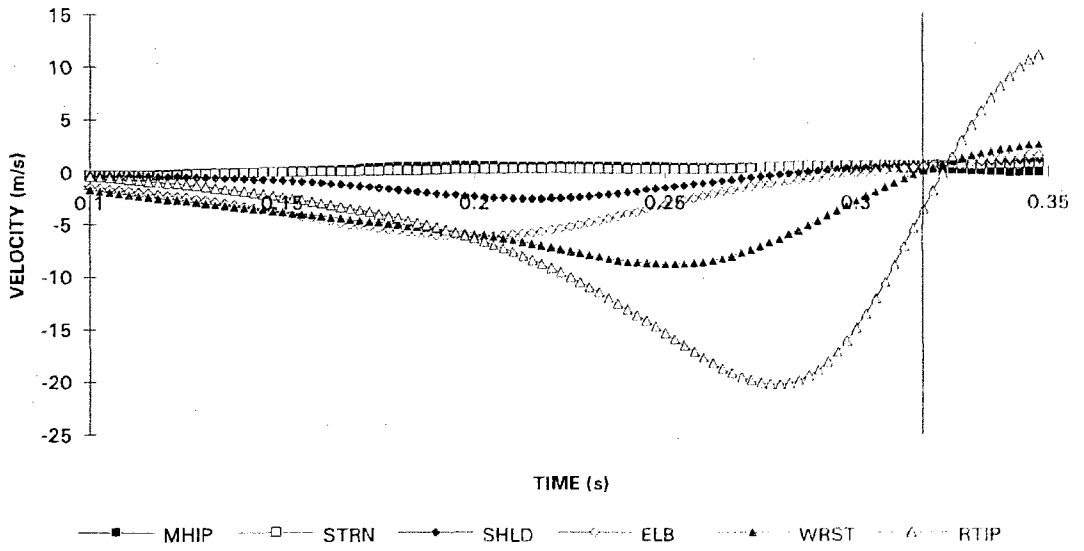


Figure 4.6 The segmental endpoint Z linear velocity profiles of Stroke #2 (ball contact was at t = 0.3175 s as indicated by the vertical line).

Table 4.4 The peak linear endpoint velocities in the Z direction of Stroke #2.

| ENDPOINT | PEAK VELOCITY (m/s) | TIME (s) | $V_{impact}$ (m/s) |
|---|---|---|---|
| MHIP | -0.3 | 0.1075 | 0.1 |
| STRN | -0.3 | 0.1125 | 0.6 |
| SHLD | -2.6 | 0.2175 | 0.7 |
| ELB | -6.1 | 0.2000 | 0.5 |
| WRST | -8.8 | 0.2500 | 0.6 |
| RTIP | -20.2 | 0.2800 | -3.6 |

## *B. 3D RESULTANT JOINT ANGULAR VELOCITIES*

An increasing 3D resultant joint angle was indicated by a positive 3D resultant joint angular velocity. Conversely, a negative joint angular velocity was defined by a decreasing joint angle. The temporal pattern of the peak joint angular velocities contributing to racquet motion in the direction of ball travel was determined. Therefore, the relevant velocities of the trunk and at the shoulder were negative and velocities at the elbow and wrist were positive.

According to the above criterion, the 3D resultant joint angular velocities peaked in a proximal to distal order from the trunk, shoulder, elbow, and finally, the wrist. In addition, the magnitudes of the peak velocities were successively higher from proximal to distal (Figure 4.7 and Table 4.5). Similar patterns were observed in four out of the five trials with the exception of Stroke #1 where the velocity at the shoulder reached maximal prior to that of the trunk. At ball contact, the 3D resultant angular velocities of the elbow and wrist joints have diminished considerably so as to be considered non-contributors to racquet motion at this time.

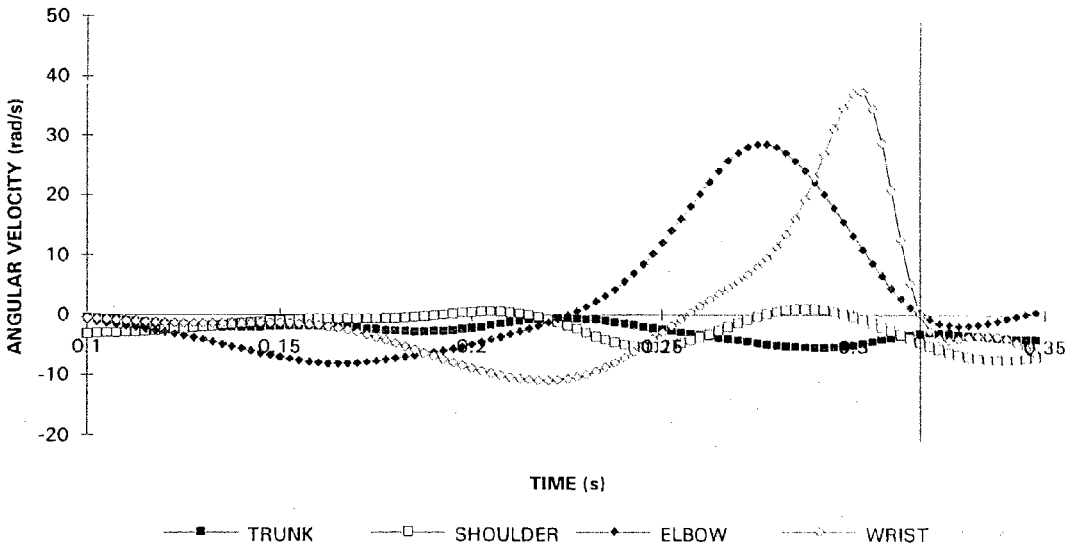


Figure 4.7 The profiles of the 3D resultant joint angular velocities of Stroke #2 (ball contact was at t = 0.3175 s as indicated by the vertical line)

Table 4.5 The peak 3D resultant angular velocities, times of occurrence and the 3D resultant angular velocity at impact of Stroke #2

| JOINT | $\dot{\theta}_{peak}$ (rad/s) | $t_{peak}$ (s) | $\dot{\theta}_{impact}$ (rad/s) |
|---|---|---|---|
| TRUNK | -0.6 | 0.2225 | -3.1 |
| SHOULDER | -5.4 | 0.2450 | -4.6 |
| ELBOW | 28.7 | 0.2775 | 0.1 |
| WRIST | 37.4 | 0.3025 | 0.2 |

## *C. ANATOMICAL JOINT ANGLES AND ANGULAR VELOCITIES*

### *C.1 JOINT ANGLES*

The anatomical joint angle profiles of Stroke #2 are illustrated in Figures 4.8-11. In the following sections, the joint angles are described for each joint during the interval between the initial position, where the racquet was held above the head, until ball contact at 0.3175 s. Across all trials, the same general trends were observed in the angular profiles although the magnitudes and temporal patterns often differed slightly. Appendix F presents the anatomical joint angle profiles of all trials.

#### *C.1.1 HIP JOINT*

The profiles of the anatomical angles of the trunk segment of Stroke #2 are illustrated in Figure 4.8. The changes in trunk flexion and lateral flexion angles were relatively small. The trunk segment remained in the flexed position throughout the stroke reaching a maximal flexion angle of 0.7 rad at 0.2475 s. The positive lateral flexion angle indicated that the subject was always leaning slightly to the right reaching a maximal angle of 0.5 rad at 0.2975 s. After peaking, the trunk segment straightened and approached initial angles as the trunk flexion and lateral flexion angles decreased to 0.6 rad and 0.5 rad, respectively, by the time of ball contact. The majority of the trunk movement was in the longitudinal rotation. The trunk segment rotated continually towards the left from -1.2 rad to 1.1 rad at impact, covering a range of 2.3 rad.

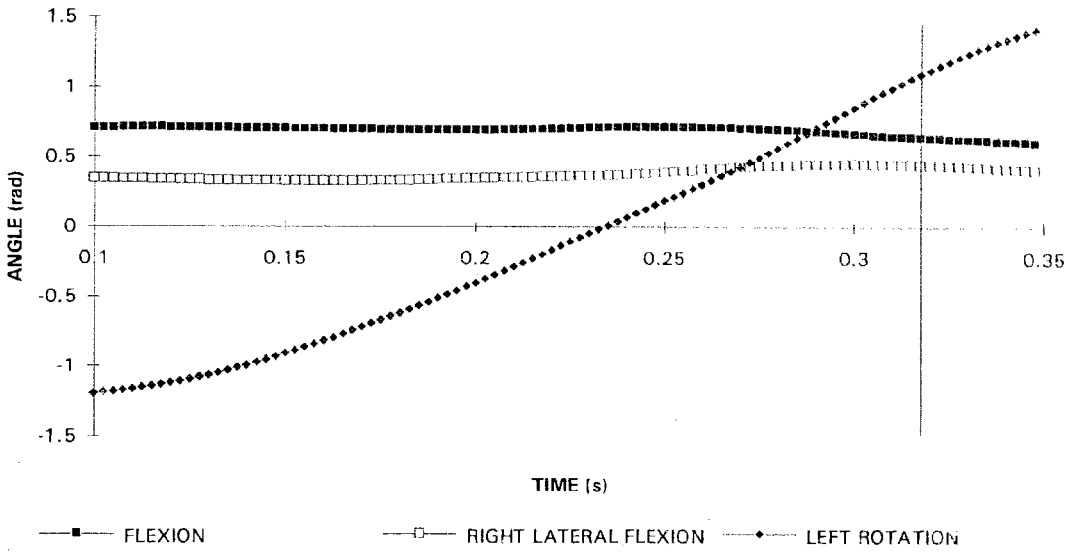


Figure 4.8 The profiles of the anatomical angles of the trunk segment of Stroke #2.

### *C.1.2 SHOULDER JOINT*

In Figure 4.9 the profiles of the anatomical angles at the shoulder joint of Stroke #2 are shown. At the beginning of the downswing from the initial position, the upper arm was in an abducted position (0.1 rad). The upper arm was adducted continuously until ball contact when it reached an angle of 0.6 rad. This movement contributed to bringing the upper arm down and in front of the body. During the period between 0.15 s to 0.23 s, the upper arm was held in a position of horizontal adduction and slight internal rotation. This small change in the horizontal adduction angle indicated that there was no movement of the elbow in a horizontal plane in the direction of the stroke. After 0.23 s, the upper arm was horizontally adducted to a maximal angle of 0.5 rad at 0.2650 s, resulting in the elbow being brought in towards the body. This movement was accompanied by considerable external rotation of the upper arm which peaked at a angle of 0.6 rad at

0.2950 s. However, it quickly dropped to 0.3 rad at ball contact which was only 0.0225 s later.

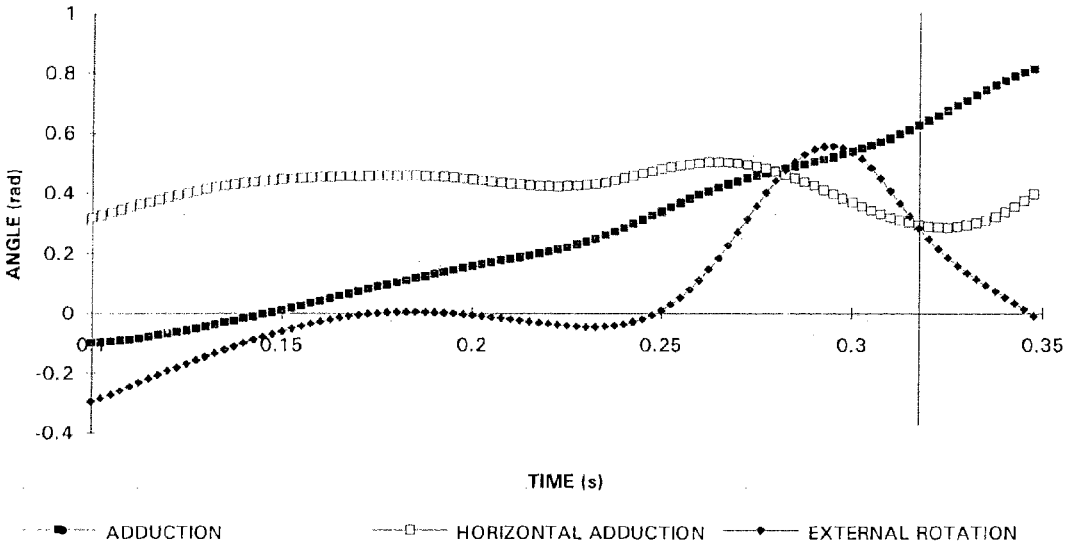


Figure 4.9 The profiles of the anatomical shoulder joint angles of Stroke #2.

### *C.1.3 ELBOW JOINT*

As indicated in Figure 4.10, the elbow joint began in an extended position of approximately -2 rad. From this initial position, the elbow began to flex as the arm was dropped. A minimum angle of -1.5 rad was reached at 0.225 s. As the upper arm was in extreme external rotation, the elbow joint extended rapidly to an angle of -2.8 rad at impact, thus partly establishing the vertical height of the racquet head for ball contact. The elbow angle extended to -2.8 rad at about 0.3050 s and remained at that angle until well after ball contact.

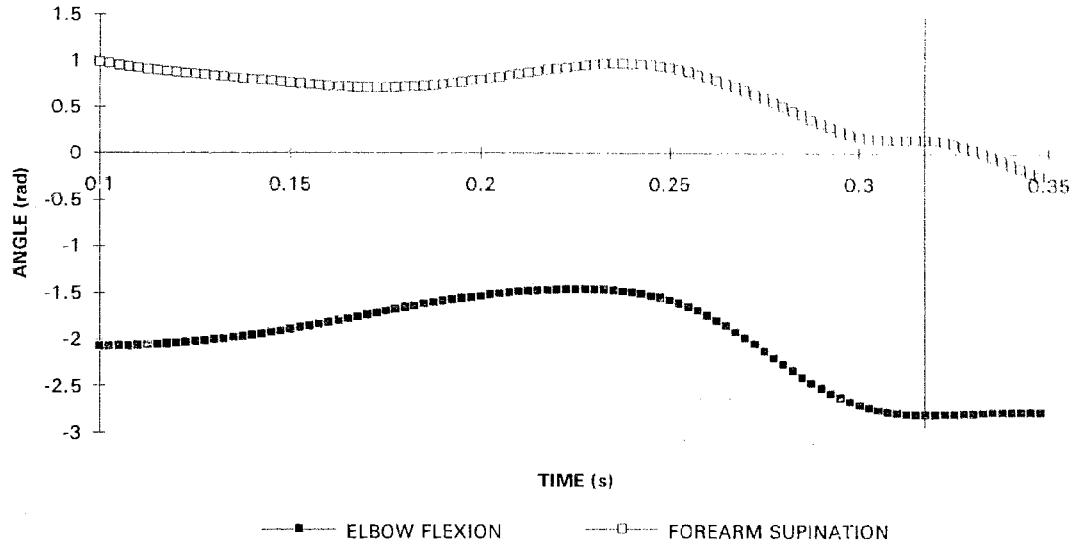


Figure 4.10 The profiles of the anatomical elbow and forearm angles of Stroke #2.

### *C.1.4 FOREARM ROTATION*

The forearm began in a supinated position and was maintained at approximately 0.8 rad of supination for the first portion of the stroke. At 0.2375 s, the forearm supinated further to an angle of 1.0 rad. From this instant until 0.3050 s, the forearm quickly pronated, approaching the neutral position. At ball contact, the forearm was slightly supinated at 0.2 rad. Similarly to the elbow joint angle, the forearm angle experienced relatively little change in the 0.0175 s prior to ball contact. The profile of the forearm rotation angle of Stroke #2 is shown in Figure 4.10.

### *C.1.5 WRIST JOINT*

At the wrist joint, the hand/racquet segment was initially in a slightly extended and abducted position having approximate angles of 0.3 rad and 0.2 rad, respectively (Figure 4.11). From this position, the wrist began to flex. The wrist was maximally flexed at an angle of 0.1 rad. In this particular trial, the maximal wrist flexion angle indicated slight extension, but in three out of five trials the wrist was actually flexed. Greatest wrist flexion was concurrent with the period (0.1 to 0.22 s) when the upper arm was moving from internal rotation to zero angle and the elbow was flexing from an extended position. At the beginning of the forewing, the wrist extended rapidly to 1.5 rad at 0.27 s. Thereafter, the wrist began to flex approaching the neutral position. However, it was slightly extended (0.3 rad) at the time of ball contact.

From the initial abducted position, the wrist was further abducted to a maximal angle of 0.8 rad at 0.2425 s. This was the same time as when the wrist was rapidly extending. After reaching maximal abduction, the wrist adducted towards the neutral position in preparation for ball contact. As was seen in the elbow and forearm angles, the wrist adduction angle was maintained for approximately 0.01 s prior to ball contact, thus establishing the vertical height of the racquet head in concert with the elbow angle. At ball contact, the wrist was slightly adducted at 0.1 rad.

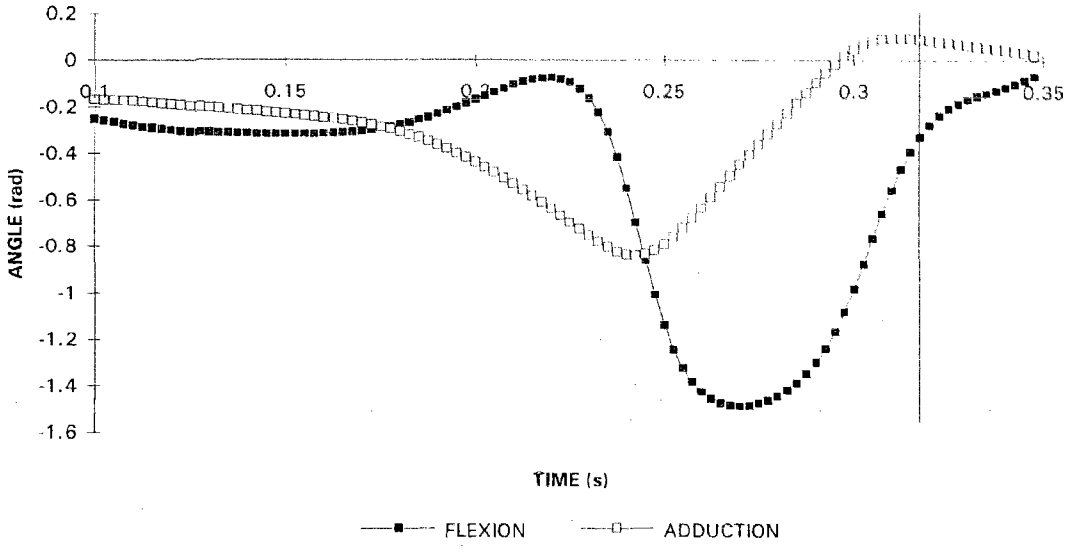


Figure 4.11 The profiles of the anatomical wrist joint angles of Stroke #2.

### *C.1.6 SUMMARY OF ANATOMICAL JOINT ANGLES*

In the initial position, the subject began the stroke with the racquet held above his head. The subject's trunk segment was flexed, laterally flexed to the right, and rotated to the right. The upper arm was abducted, horizontally adducted and internally rotated. The elbow was relatively extended, the forearm supinated, and the wrist slightly extended and abducted.

During the downswing, the racquet was brought down to the front of the body. This phase was characterized by segmental movements in the opposite directions as those during the foreswing. The trunk segment was in maximal flexion and rotated beyond its neutral position towards the left. The elbow was relatively flexed, the forearm was in extreme supination, and the wrist was in its most flexed and abducted positions. From this position, the elbow and wrist joints began to extend rapidly. Additionally, there was

considerable shoulder external rotation and forearm pronation ending with the upper arm reaching maximal external rotation (0.0225 s prior to impact).

During the foreswing, the racquet was accelerated by rapid forearm pronation and partly by shoulder internal rotation. The segmental movements which primarily contributed to racquet motion at the time of impact were the longitudinal rotations about the trunk and upper arm segments, shoulder adduction and wrist flexion. The elbow and wrist adduction angles played important roles in maintaining the vertical position of the racquet head whereas the forearm rotation was responsible for maintaining proper orientation of the racquet head for ball contact.

Table 4.6 summarizes the anatomical joint angles at ball contact. Figure 4.12 is a drawing of the subject at the time of ball contact from the perspective of Camera A.

Table 4.6 The anatomical joint angles at ball contact of Stroke #2.

| JOINT ANGLE | ANGLE (rad) |
|---|---|
| Trunk Flexion | 0.7 |
| Trunk Right Lateral Flexion | 0.5 |
| Trunk Left Rotation | 1.1 |
| Shoulder Adduction | 0.6 |
| Shoulder Horizontal Adduction | 0.3 |
| Shoulder Outward Rotation | 0.3 |
| Elbow Flexion | -2.8 |
| Forearm Supination | 0.2 |
| Wrist Flexion | -0.3 |
| Wrist Adduction | 0.1 |

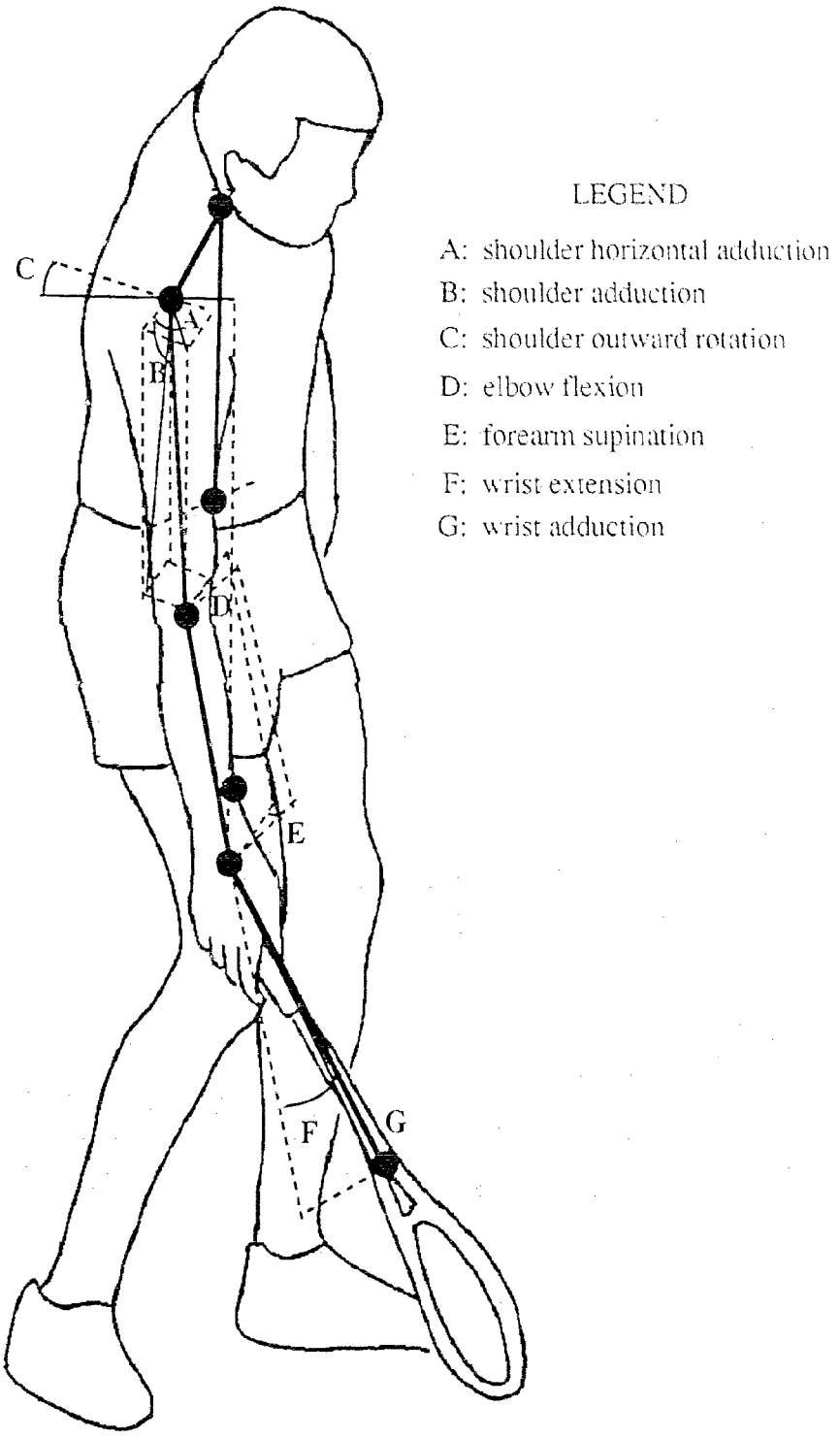


Figure 4.12 A drawing of the subject at the time of ball contact from the perspective of Camera A.

*C.2 JOINT ANGULAR VELOCITIES*

As was the case with the anatomical joint angles, there were differences between the trials in terms of the absolute magnitudes and temporal patterns of the anatomical joint angular velocity profiles. In fact, the temporal pattern could not be generalized for all trials because the sequence of peak velocities was specific to each trial. However, the general shapes of the profiles were similar. The following description presents the results obtained from Stroke #2. Rather than describing the angular velocities results in terms of each specific joint, a chronological description may better demonstrate the sequence of movements. The anatomical joint angular velocity profiles are depicted in Figures 4.13-16 and the peak velocities and their times of occurrence of Stroke #2 are summarized in Table 4.7. Appendix F presents the anatomical joint angular velocity profiles of all trials and Table F.1 summarizes the peak anatomical joint angular velocities, times of occurrence and the angular velocities at ball contact.

From the initial position, the trunk segment flexed continuously until it reached a maximal velocity of 0.8 rad/s at 0.2275 s (Figure 4.13). The elbow flexion velocity was zero at this time as it began to extend from its most flexed position as depicted in Figures 4.13 and 4.8, respectively. The elbow was then brought towards the midline of the body as the shoulder horizontal adduction velocity peaked (3.1 rad/s) at 0.2450 s (Figure 4.15). Subsequently, the striking arm straightened as the wrist adducted and the elbow extended achieving maximal velocities of 18.6 rad/s at 0.2650 s (Figure 4.16) and 28.7 rad/s at 0.2775 s (Figure 4.15), respectively. However, the racquet was lagging considerably as the wrist was in extreme extension at this time. Much of the effort required to bring the racquet around was accomplished by pronation of the forearm. The maximal forearm pronation velocity was 18.9 rad/s at 0.2850 s which slightly preceded maximal elbow

extension velocity (Figure 4.15). By this time, the elbow was relatively extended and the wrist slightly adducted. Just prior to ball contact, the maximal values for trunk rotation velocity was 14.6 rad/s at 0.2925 s (Figure 4.13), wrist flexion velocity was 43.8 rad/s at 0.3050 s (Figure 4.16) and shoulder internal rotation velocity was 16.8 rad/s at 0.3125 s (Figure 4.14).

The movements primarily contributing to the racquet motion at ball contact were trunk left rotation (12.8 rad/s), shoulder adduction (6.2 rad/s) and internal rotation (15.3 rad/s), and wrist flexion (22.7 rad/s). Even though the upper arm was adducting constantly throughout the stroke, the maximal shoulder adduction velocity did not occur until well after ball contact (6.9 rad/s at 0.33 s) indicating its role in the follow-through.

No angular velocities peaked at the same time as ball contact. This was apparent in the other trials as well. With the exception of trunk rotation, shoulder adduction and rotation, and wrist flexion, all other angular velocities approached zero velocity at ball contact. In particular, forearm pronation did not contribute substantially to the racquet speed at this time. Most angular velocity profiles, except trunk rotation and shoulder adduction, demonstrated some counter-movement across the joints as the joint motion was initiated in one direction and immediately followed by motion in the opposite direction.

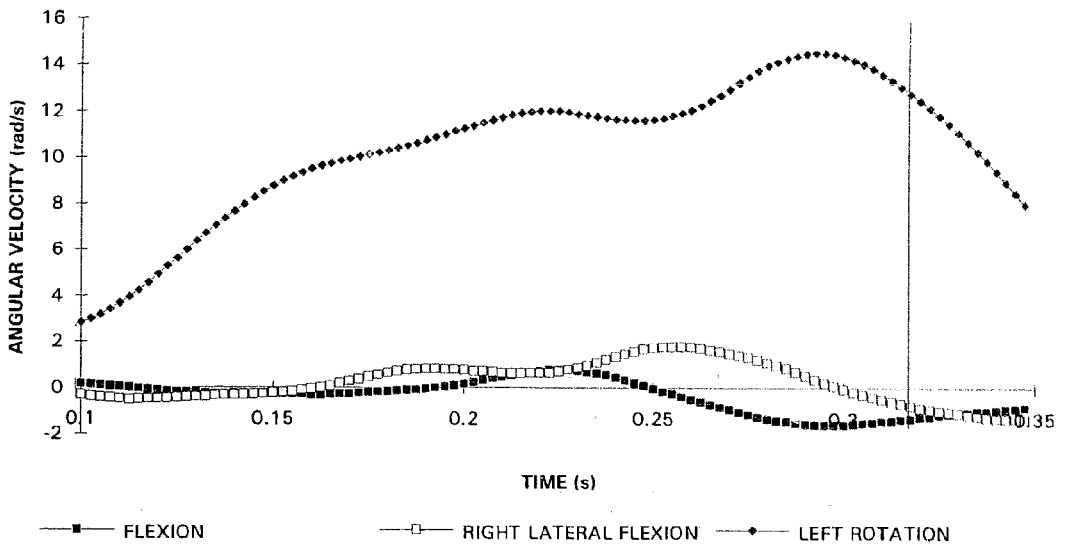


Figure 4.13 The anatomical trunk angular velocity profiles of Stroke #2.

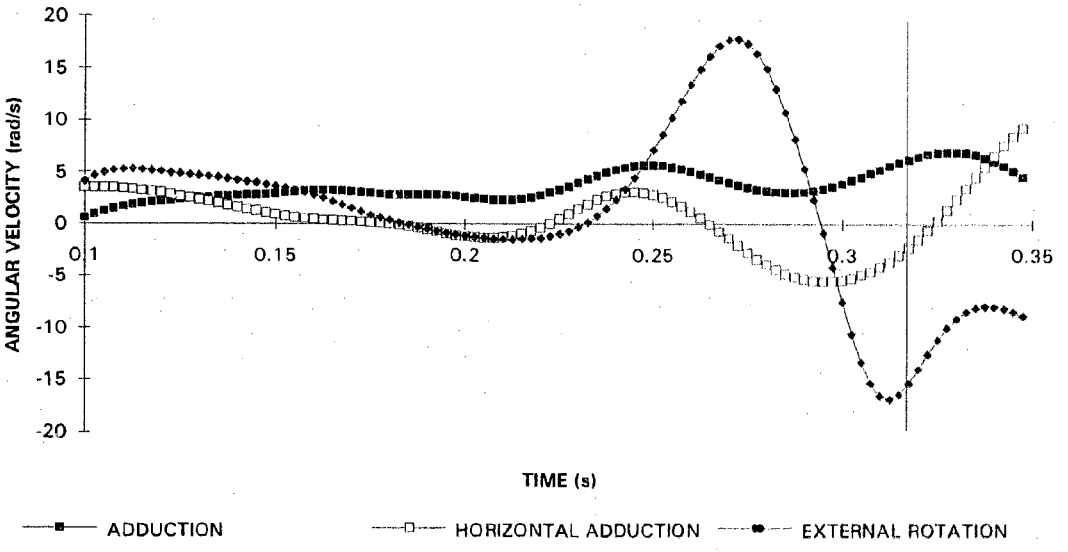


Figure 4.14 The anatomical shoulder angular velocity profiles of Stroke #2.

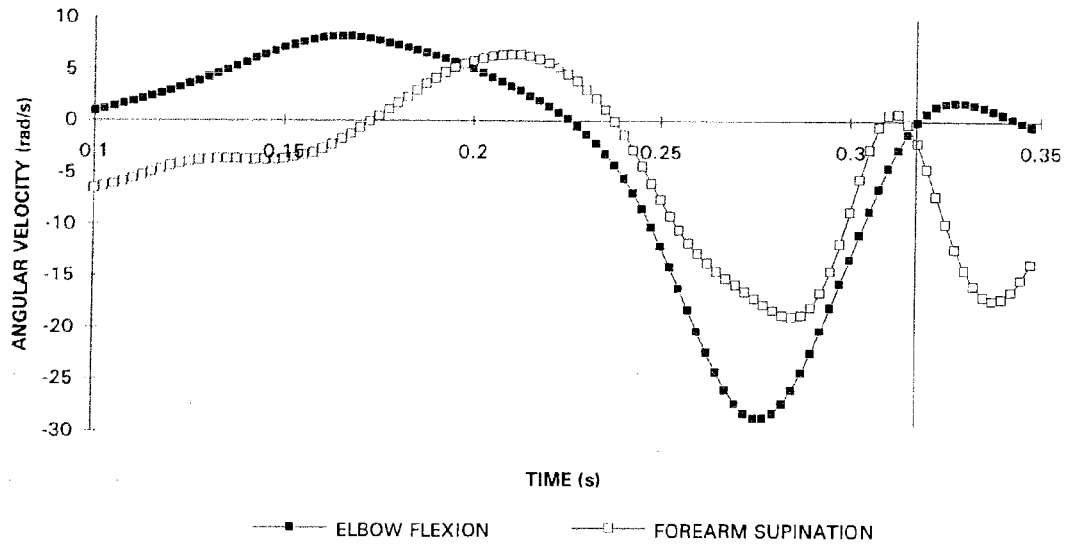


Figure 4.15 The anatomical elbow and forearm angular velocity profiles of Stroke #2.

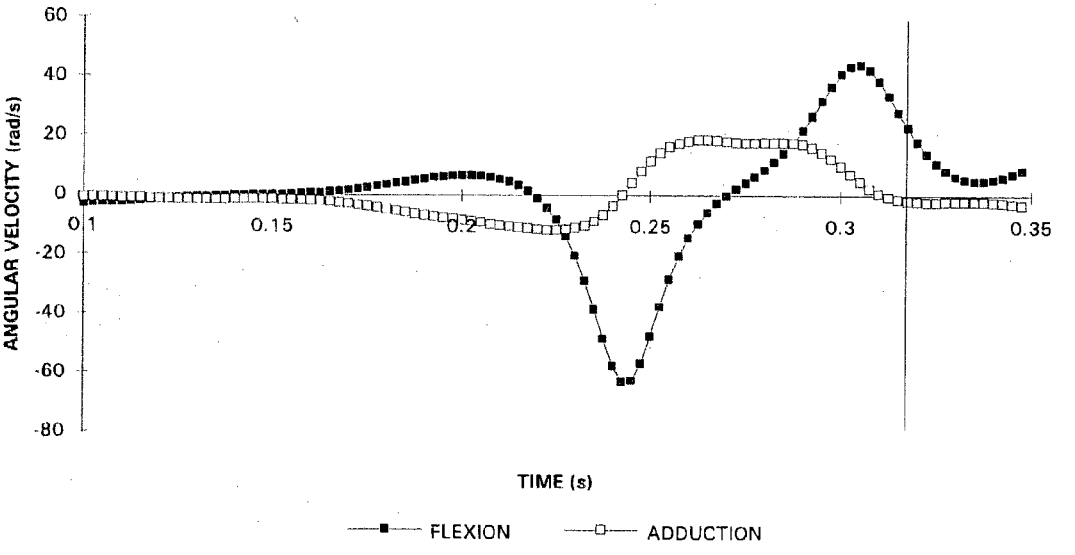


Figure 4.16 The anatomical wrist angular velocity profiles of Stroke #2.

Table 4.7 The peak joint anatomical angular velocities, times of occurrence, and the angular velocities at the time of impact ($\dot{\theta}_{impact}$) for Stroke #2. Negative values indicate movement in the opposite direction.

| | $\dot{\theta}_{peak}$ (rad/s) | $t_{peak}$ (s) | $\dot{\theta}_{impact}$ (rad/s) |
|---|---|---|---|
| Trunk Flexion | 0.8 | 0.2275 | -1.3 |
| Trunk Right Lateral Flexion | -1.4 | 0.3500 | -0.8 |
| Trunk Left Rotation | 14.6 | 0.2925 | 12.8 |
| Shoulder Adduction | 6.9 | 0.3300 | 6.2 |
| Shoulder Horizontal Adduction | 3.1 | 0.2450 | -2.3 |
| Shoulder Outward Rotation | -16.8 | 0.3125 | -15.3 |
| Elbow Flexion | -28.7 | 0.2775 | -0.1 |
| Forearm Supination | -18.9 | 0.2850 | -2.1 |
| Wrist Flexion | 43.8 | 0.3050 | 22.7 |
| Wrist Adduction | 18.6 | 0.2650 | -1.7 |

## *D. INTER-SUBJECT VARIABILITY*

Although the experimental task was the same for both subjects, it was unknown whether the subjects performed under similar conditions making direct comparison of technique difficult. The ball kinematics were not determined for Subject B, therefore the vertical height of the ball at impact and its velocity after impact were not available. Based on the subject's judgement, the stroke was performed with consistency as the primary concern. Therefore, it was not a maximal effort stroke. Nonetheless, some important similarities and differences were found between the strokes.

The anatomical kinematic profiles were aligned with respect to the time of ball contact (t = 0.3175 s). Figures 4.17-20 illustrate the anatomical joint angle profiles of

Subjects A and B and the anatomical joint angular velocity profiles are shown in Figures 4.21-24. The peak anatomical joint angular velocities, times of occurrence, anatomical joint angular velocities at impact and anatomical joint angles at impact are tabulated in Table 4.8.

The general trends of the anatomical joint angles were similar. In particular, the joint angles were similar in both subjects at the time of ball contact. However, the exact temporal coordination differed even though both subjects did not show PD sequencing in their anatomical angular velocity profiles. The shoulder adduction and trunk left rotation velocities peaked relatively early (0.18 s and 0.2525 s, respectively) in the stroke of Subject B. The simultaneous peaking of the angular velocities of wrist adduction (14.9 rad/s at 0.2825 s), forearm pronation (21.2 rad/s at 0.2850 s), and wrist flexion (49.4 rad/s at 0.2825 s) in Subject B differed from the sequential pattern of the same angular velocities in Subject A. These movements were primarily responsible for accelerating the racquet forward at the beginning of the foreswing.

The movements contributing most to the racquet speed at impact in Subject B was shoulder internal rotation as its velocity peaked (12.3 rad/s) at the time of impact. All other angular velocities were virtually non-contributors. This was unlike Subject A who had trunk rotation, shoulder adduction and rotation and wrist flexion contributing to the instantaneous racquet speed at impact.

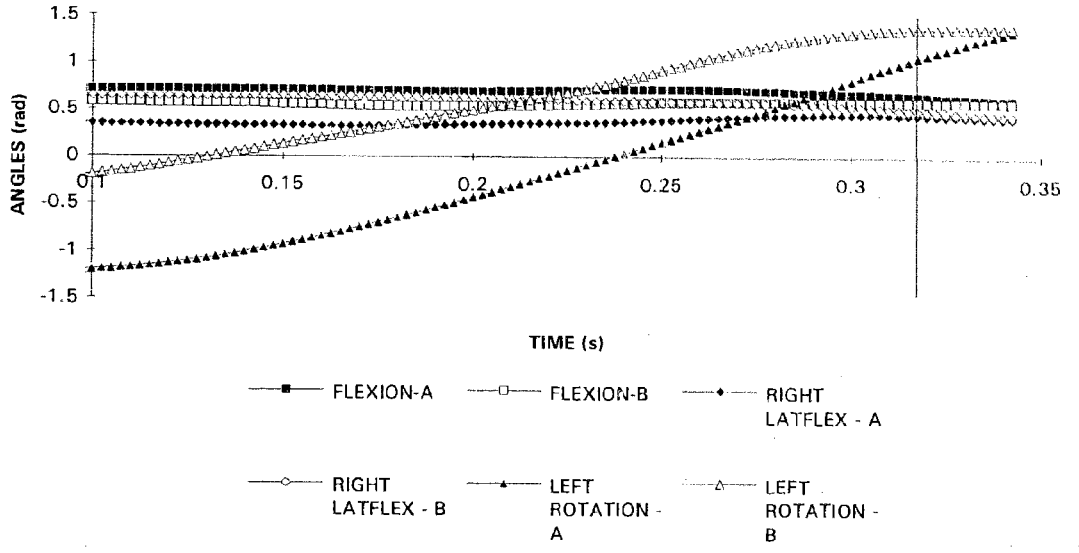


Figure 4.17 Inter-subject variability: anatomical joint angle profiles of the trunk.

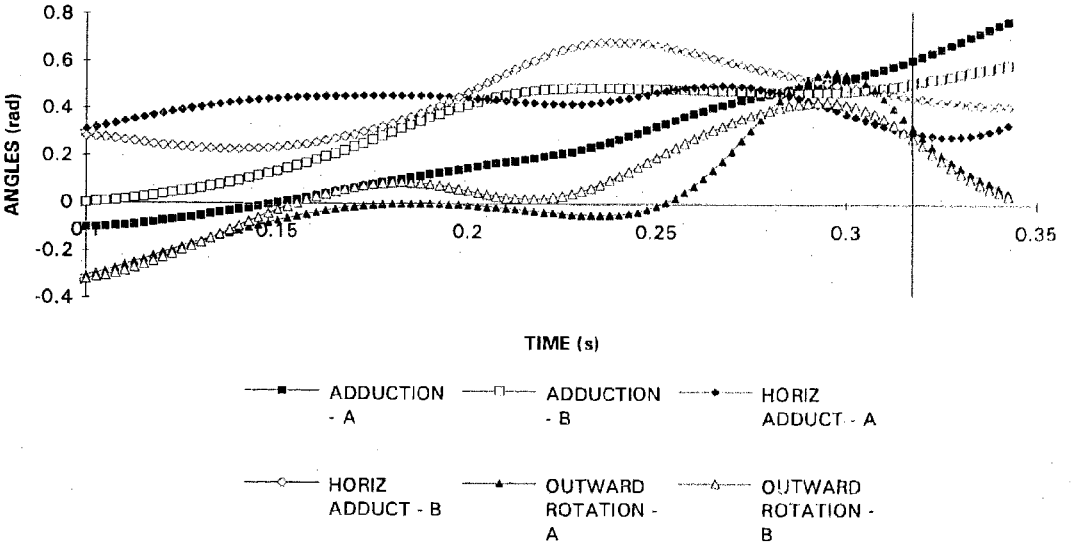


Figure 4.18 Inter-subject variability: anatomical joint angle profiles of the shoulder.

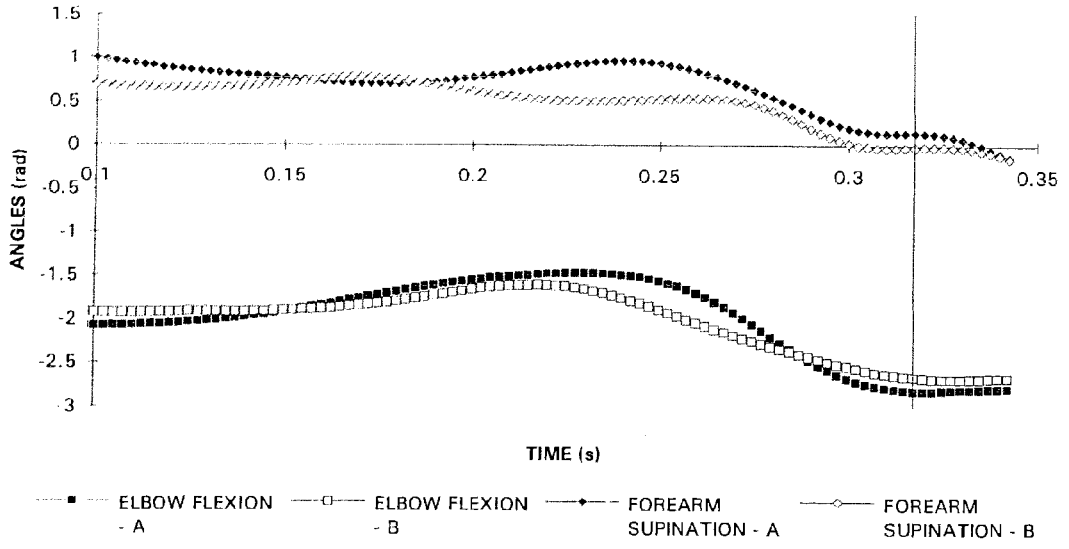


Figure 4.19 Inter-subject variability: anatomical joint angle profiles of the elbow and forearm.

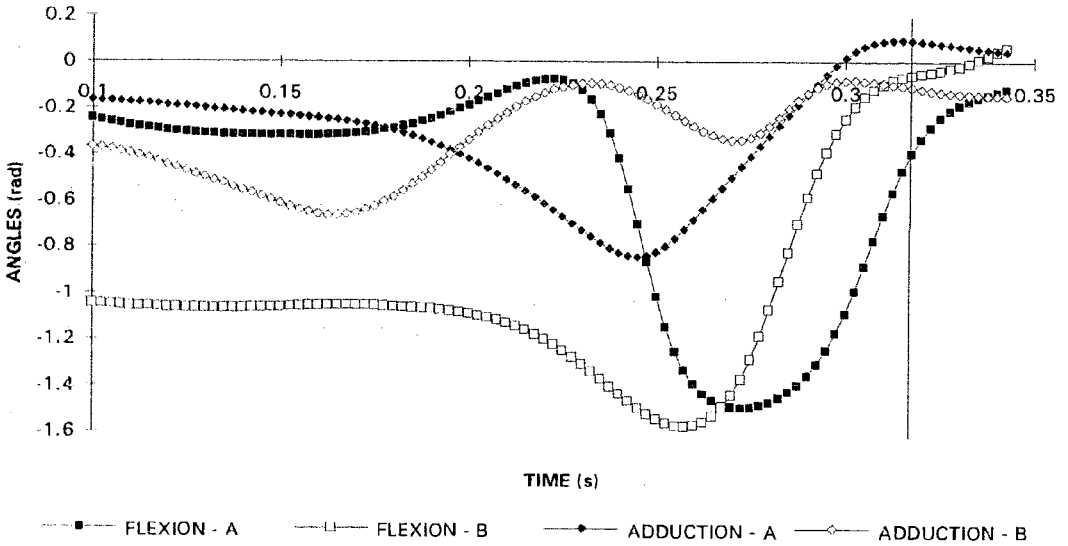


Figure 4.20 Inter-subject variability: anatomical joint angle profiles of the wrist.

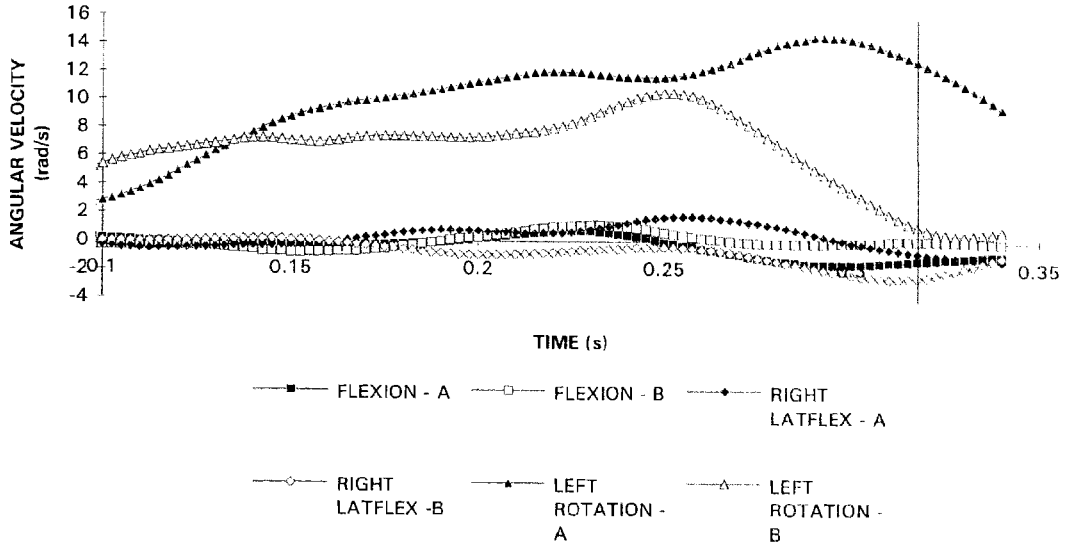


Figure 4.21 Inter-subject variability: anatomical joint angular velocity profiles of the trunk.

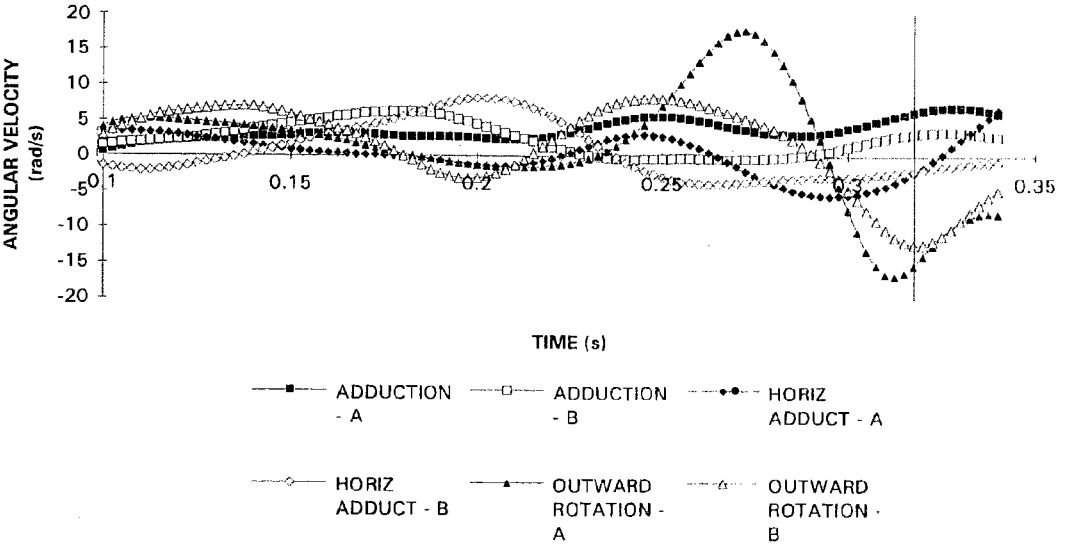


Figure 4.22 Inter-subject variability: anatomical joint angular velocity profiles of the shoulder.

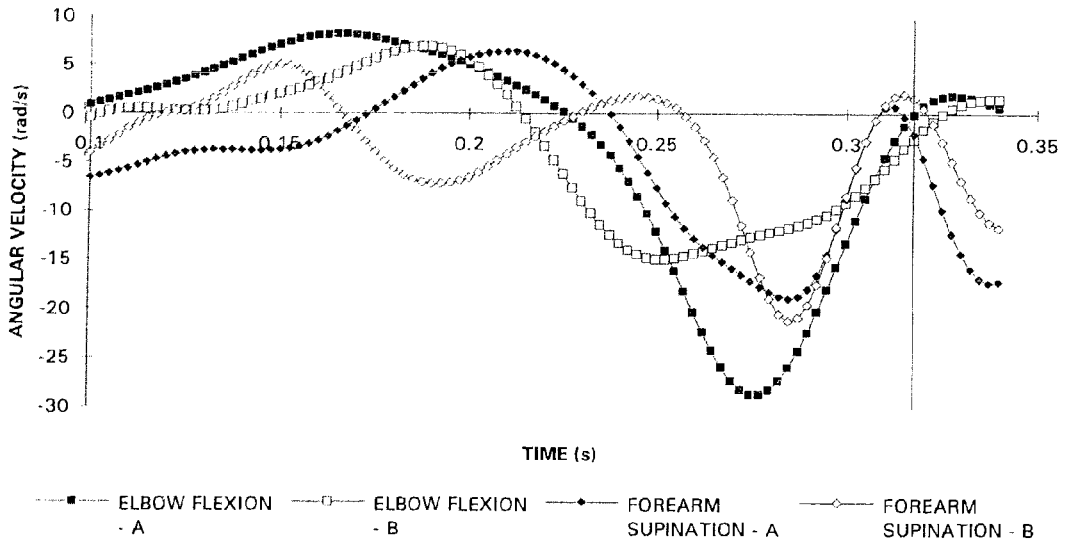


Figure 4.23 Inter-subject variability: anatomical joint angular velocity profiles of the elbow and forearm.

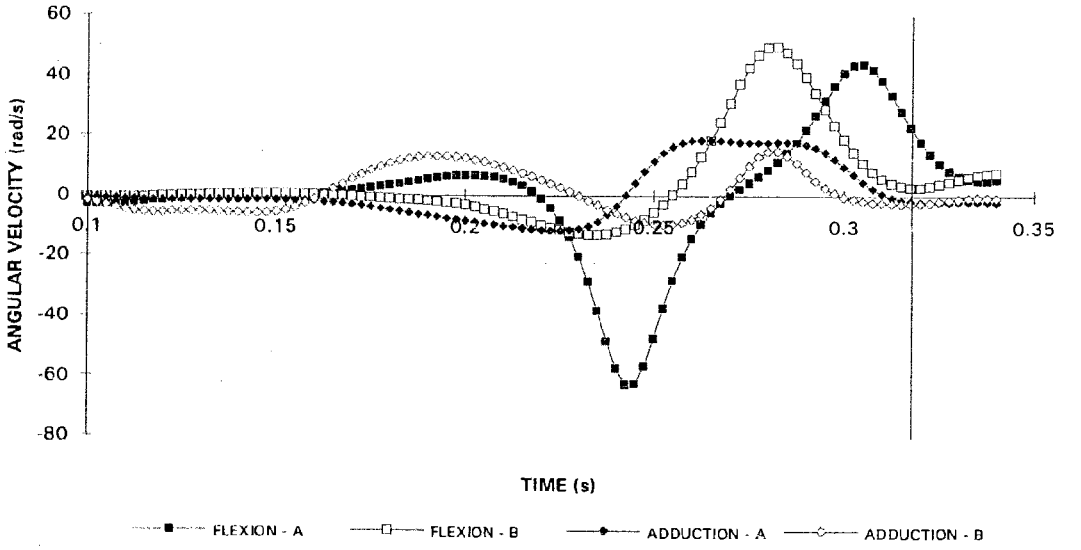


Figure 4.24 Inter-subject variability: anatomical joint angular velocity profiles of the wrist.

Table 4.8 Comparison of anatomical kinematic results between two separate squash players. (Subject A and Subject B).

| | SUBJECT A | | | | SUBJECT B | | | |
|---|---|---|---|---|---|---|---|---|
| | $\dot{\theta}_{peak}$ (rad/s) | $t_{peak}$ (s) | $\dot{\theta}_{impact}$ (rad/s) | $\theta_{impact}$ (rad) | $\dot{\theta}_{peak}$ (rad/s) | $t_{peak}$ (s) | $\dot{\theta}_{impact}$ (rad/s) | $\theta_{impact}$ (rad) |
| TRUNK FLEXION | 0.8 | 0.2275 | -1.3 | 0.7 | 1.2 | 0.2325 | 0.1 | 0.6 |
| TRUNK RIGHT LATFLEX | -1.4 | 0.3500 | -0.8 | 0.5 | -2.6 | 0.3125 | -2.5 | 0.5 |
| TRUNK LEFT ROTATION | 14.6 | 0.2925 | 12.8 | 1.1 | 10.6 | 0.2525 | 1.1 | 1.4 |
| SHOULDER ADDUCTION | 6.9 | 0.3300 | 6.2 | 0.6 | 6.3 | 0.1800 | 3.1 | 0.5 |
| SHOULDER HORIZ ADDUCT | 3.1 | 0.2450 | -2.3 | 0.3 | 8.1 | 0.2025 | -2.1 | 0.5 |
| SH OUTWARD ROTATION | -16.8 | 0.3125 | -15.3 | 0.3 | -12.3 | 0.3175 | -12.3 | 0.3 |
| ELBOW FLEXION | -28.7 | 0.2775 | -0.1 | -2.8 | -15.0 | 0.2525 | -2.6 | -2.7 |
| FOREARM SUPINATION | -18.9 | 0.2850 | -2.1 | 0.2 | -21.2 | 0.2850 | 1.5 | 0.0 |
| WRIST FLEXION | 43.8 | 0.3050 | 22.7 | -0.3 | 49.4 | 0.2825 | 2.7 | -0.1 |
| WRIST ADDUCTION | 18.6 | 0.2650 | -1.7 | 0.1 | 14.9 | 0.2825 | -2.6 | -0.1 |

# Chapter 5
# DISCUSSION

## *A. THE SQUASH STROKE*

The 3D kinematics of the trunk and upper extremity during the squash forehand stroke have neither been produced nor analyzed previously. The present study investigated the 3D kinematics of an elite squash player using various kinematic measures which are commonly found in descriptions of segmental coordination. The player's technique was evaluated in terms of the linear velocities of the segmental endpoints, 3D resultant joint angular velocities and anatomical joint angles and angular velocities.

The objective of a squash stroke is to generate substantial racquet speeds in a particular direction, so as to impart a high velocity to the ball. The summation of speeds principle stipulates that to maximize the speed of the most distal endpoint of a linked system, segmental movements occur in a PD sequence such that once a segment reaches its greatest speed, the neighbouring distal segment initiates its movement and reaches an even a higher speed. In accordance to this principle, the PD sequencing of segmental movements was clearly demonstrated in the peak resultant linear velocities of the segmental endpoints and the 3D resultant joint angular velocities. Furthermore, their magnitudes were successively higher proximally to distally.

The individual segmental contributions to the distal endpoint speed at ball contact may be obtained from analyzing instantaneous velocities. The resultant linear velocity of the most distal endpoint peaked 0.0125s prior to ball contact. Therefore, the racquet was

not travelling at maximal speed at the time of impact which may suggest poor timing in the player's technique. However, upon analysis of the directional components of the resultant velocities, it was revealed that the effective velocity was appropriately maximal at ball contact. Because the ball's trajectory from a forehand drive was virtually horizontal along the Y axis, it was not surprising that the peak speed in the Y direction coincided with ball contact. The Y velocity of the racquet tip was greatest (26.6 m/s) at the time of impact whereas the Z velocities of all endpoints were virtually zero indicating little vertical motion.

The Y velocity profiles of the endpoints were characterized by deceleration-acceleration (DA) patterns which are commonly associated with enhanced performance (Alexander, 1983). This movement pattern states that the speed of an endpoint increases rapidly once its proximal neighbour begins to slow down such that the speed of the proximal segments had decreased considerably by the time the most distal segment had reached maximal speed. The DA transition may be attributed to transfer of segmental momenta whereby the deceleration of the proximal segments precedes or even causes the acceleration of the distal segments similar to a whip-like action (eg. Joris et al., 1985; Edmondstone and Chapman, 1991). The cause of the deceleration of the proximal segment is inconclusive. It may be an active mechanism via muscle activity or a consequence of segmental interaction.

The drawback of using linear velocities of segmental endpoints to describe segmental coordination is its limited application towards the understanding of why segments are coordinated sequentially in a variety of multisegmental skills. A complete kinematic and kinetic description is required to understand the causal factors responsible for the resulting movement patterns. Kinetic information at the joints cannot be derived from resultant endpoint velocities of segmental endpoints alone. Instantaneous resultant

linear velocities and their respective components are beneficial in providing the segmental contributions to the distal endpoint speed at any one instant in time. One cannot appreciate the contributions of the proximal segments in sequential movements using instantaneous measures since it is their movement histories which ultimately contributes to the achievement of higher speed as the DA transition suggests.

Three dimensional resultant joint angular velocities provide a more complete description of joint motion since both angular and linear information may be determined. Human movement is a combination of linear and angular movements, therefore using 3D resultant joint angular velocities as a kinematic measure is also visually advantageous. In this study, the instantaneous 3D resultant joint angular velocities indicated that there was little angular joint motion at ball contact. The angular velocities at the elbow and the wrist joints rapidly approached zero velocity from their maxima by the time of impact. Quantifying joint motion in terms of 3D joint angular velocities was inadequate in providing a complete kinematic description since the instantaneous angular speeds did not totally account for the distal endpoint speed at impact.

The use of 3D resultant joint angular velocities is common and straightforward in evaluating the relative movement between segments. However, it fails to include contributions by longitudinal rotations about the segments. Even though the joint angle between two segments may not be changing, indicating zero joint angular velocity, any rotation about a longitudinal axis of a segment will affect the speed of the distal endpoint as long as the endpoint is not colinear with the axis of rotation. This is analogous to a wheel-and-axle arrangement where the advantage is in increasing the speed of the movement or the range of motion of the endpoint (Kreighbaum and Barthels, 1981). The axle is coincident with the longitudinal axis of the first segment. A second segment which articulates with the first segment at some angle comprises the wheel. For a given

longitudinal rotation about the first segment, the distal endpoint speed of the second segment is dependent on the perpendicular distance of the endpoint from the longitudinal axis of the first segment. For example, the speed of the hand is maximized if the elbow is flexed to 90° as the upper arm internally rotates.

The PD sequencing of segmental movements was not clear in the anatomical joint angular velocity profiles compared to those of the other measures. In fact, the temporal sequence of the peak anatomical joint angular velocities was not consistent between trials. The timing of the peak angular velocities was close such that a slight variation in the timing resulted in a different temporal pattern. Due to the complexity of the anatomical joint angular information, the temporal sequence was obscured. Nonetheless, an anatomical kinematic description provides a complete account of the segmental movements involved, possibly leading to a better understanding of the movement.

The necessity of the squash stroke to be compact due to the limited space available precludes a player from using a large windup to generate high racquet speeds such as the case of a groundstroke in tennis. In this particular subject, certain segmental movement strategies were apparent by which his stroke was confined to a relatively small space. However, a powerful and accurate stroke was still achieved. The majority of the motion was confined to a vertical frontal plane. During the downswing, the racquet was kept to the side of the body close to the shoulder as elbow flexion and wrist abduction were maximal. From this position, the upper limb began to straighten by extending the elbow and adducting the wrist while the upper arm was externally rotated. The racquet was accelerated in the direction of ball travel by rapidly pronating the forearm and internally rotating the upper arm. By the time of ball contact, elbow extension and wrist adduction had virtually stopped. Since the ball height was relatively low at impact, the extended

upper limb was in a vertical position so that the racquet head would be sufficiently low for a successful hit.

The distal endpoint speed depends on both the angular velocity and instantaneous position of the endpoint with respect to the segment's axis of rotation. In turn, the angular velocity is inversely related to the inertial characteristics of the system. Therefore, by keeping the segments close to the body initially during the downswing, the rotational inertia was minimized. If the rotational inertia of the system was low, a high angular velocity can then be achieved, thus a high distal endpoint speed was attained. The endpoint gained speed initially by reducing the system's inertia, then the endpoint speed was increased by extending the upper limb such that the distance between the distal endpoint and the rotational axes was increased.

The segmental movements contributing most to the racquet speed at ball contact were trunk left rotation, shoulder internal rotation and adduction and wrist flexion. The velocities peaked in the order of trunk left rotation (0.2925 s), wrist flexion (0.3050 s) and shoulder internal rotation (0.3125 s). Shoulder adduction velocity was greatest after impact suggesting a possible role in the follow through. These movements served to increase the speed of the racquet as each had a component of projection perpendicular to a virtually straight upper limb at impact.

The dominance of shoulder internal rotation at impact has been observed in squash (Sprigings, et al., 1992) and other movements such as a tennis serve (van Gheluwe and Hebbelinck, 1985) and baseball pitching (Feltner and Dapena, 1986). This movement contributes to the distal endpoint speed by taking advantage of the wheel-and-axle arrangement as previously described. In the squash stroke, the elbow was not entirely

extended at ball contact such that the internal rotation of the upper arm contributed appreciably to the racquet speed.

Forearm pronation did not contribute to the racquet speed at ball contact as previously reported (Sprigings, 1992). The pronation velocity at impact was 2.1 rad/s which was relatively low compared to its maximal value of 18.9 rad/s at 0.2850 s. With this movement peaking so early, it contributed more to the acceleration of the racquet during the initial stages of the foreswing than to generating high racquet speeds at impact. The forearm pronation velocity was diminished by the time of ball contact. This served to orient the face of the racquet properly for impact and prevent overpronation of the racquet face as was seen in the tennis serve (van Gheluwe, et al., 1987). As the longitudinal axes of upper arm and forearm were almost aligned by the time of impact, wrist flexion played a more important role in producing high racquet speeds than forearm pronation.

Elbow flexion and wrist adduction velocities were essentially zero at ball contact. These movements would not have contributed greatly to racquet speed at this time due to the vertical arm configuration, but they played an important role in the proper height of the racquet head for impact. The greater variability in the instantaneous wrist adduction angular velocities at impact suggested that fine tuned adjustments were made distally.

Although the main subject (Subject A) demonstrated high consistency in his stroke, the forehand stroke of another elite squash player was analyzed in terms of the anatomical joint angular kinematics to investigate the commonalities of elite stroking and idiosyncratic differences between strokes. It was assumed that the stroke of the second player, Subject B, was consistent, thus typical of his stroke. This assumption could not be validated since only one trial of Subject B was analyzed. Therefore the following discussion must be interpreted with caution. The general trends of the anatomical joint

angle profiles between Subjects A and B were similar except at the wrist. The differences at the wrist could either be due to differences in the stroke technique or ball position at impact. As observed in Subject A, vertical adjustments of the racquet head for proper impact were made distally at the wrist which could have accounted for the variation in the wrist adduction angle profile particularly between subjects. Since the ball kinematics were unknown for Subject B, this explanation could not be verified. By the time of ball contact, the joint angles were quite similar indicating the same positions of the trunk and striking arm.

The PD sequencing was also not apparent in the anatomical joint angular velocity profiles of Subject B as was observed in Subject A. However, the exact temporal patterns were not the same. The differences could be due to several factors such as differences in the experimental conditions (eg. ball height at impact) and effort put forth by each subject to satisfy the requirement that the stroke be consistent. Other factors may have included differences in the players' physical and muscular attributes (Chapman and Sanderson, 1990).

The downward acceleration of the racquet was mainly provided by shoulder adduction in the stroke of Subject B as opposed to its apparent role in the follow through in Subject A. In Subject B, wrist adduction, forearm pronation and wrist flexion velocities peaked simultaneously and were responsible for the forward acceleration of the racquet during the foreswing. This differed from the sequential pattern of these angular velocities in Subject A.

The movement primarily contributing to the racquet speed at impact in Subject B was shoulder inward rotation. Its velocity peaked (12.3 rad/s) at the time of impact. All other angular velocities were virtually non-contributors. This was unlike Subject A where

various segmental movements, including trunk rotation, shoulder adduction and rotation and wrist flexion, contributed to the instantaneous racquet speed at impact.

It was apparent in this study that the PD sequence was not a characteristic of segmental movements in terms of anatomical joint angular velocities. For example, the shoulder internal rotation velocity peaked after maximal wrist flexion velocity. The implications of the sequence of the peak velocities should not be considered in terms of their anatomical significance, but rather in light of their effect on the ball velocity at impact. Even though shoulder internal rotation is anatomically proximal to wrist flexion, it has a functional significance on the distal endpoint velocity at the time of impact. A similar argument was used by Alexander (1991) who simulated overarm throwing employing a simple, two-segment model. The best simulated throw was produced by horizontal flexion followed by internal rotation while the elbow remained flexed at 90°. Although both rotations occurred about the shoulder joint, internal rotation was considered to have a more distal influence because it accelerated only the distal forearm and hand segment while horizontal adduction accelerated both proximal and distal segments. Even though a consistent temporal pattern was not apparent in the peak anatomical joint angular velocities in the squash strokes analyzed, the complexity of the segmental movements manifested itself as a PD progression of peak linear velocities of the segmental endpoints. Therefore, it may be said that the PD sequence was not apparent in the joint angular velocity profiles in an anatomical sense, but rather in a functional sense.

Another notable feature in the anatomical joint angular velocity profiles was counter-movements occurring across the joints. The joint motion began in one direction and was immediately followed by movement in the opposite direction. For example, left rotation of the trunk, shoulder adduction and horizontal adduction resulted in the lagging of the distal forearm and hand/racquet segments as the upper arm was taken to extreme

external rotation. This was followed immediately by rapid internal rotation of the upper arm. Similar counter-movements were observed at the elbow and wrist joints which increased their ranges of motion resulting in greater distal endpoint speeds. In addition, such movements have been associated with enhanced performance due to intrinsic muscle properties whereby stretching an active muscle immediately prior to its shortening phase increased the work output of the muscle (Chapman, 1985b). However, the contribution of this phenomenon to the squash stroke would require kinetic and electromyographical verification.

Three analytical techniques were used to describe the temporal coordination of the upper body segments in an elite squash stroke. Different conclusions may be drawn from analyzing the same movement using either the method employing anatomical joint angles versus the simpler methods. Both the resultant linear endpoint velocity and the 3D resultant joint angular velocity methods provided a clear description of the PD sequencing seen in previous analyses of ballistic skills (Putnam, 1993). However, these techniques, by themselves, were found to be limited in terms of their completeness in describing the segmental motion and potential for future analysis. On the other hand, the sequential coordination was not as clear in the anatomical joint angular kinematics. Instead, a more precise account of the segmental movements was obtained, therefore the segmental contributions to distal endpoint speed may be identified. Albeit complex and temporally ill-defined in terms of the peak values, the anatomical joint angular velocities were seen to be associated with a PD sequencing of the linear velocities of the segmental endpoints and 3D resultant joint angular velocities. A kinematic description using anatomical joint angular velocities may also lead to a kinetic analysis of the segmental movement. With a complete kinematic and kinetic analysis of the skill, it is then possible to determine the causal relationships of segmental movement patterns observed. In addition, anatomical descriptions of joint motion are familiar to a wide range of people including athletes,

coaches, and clinicians making it easier to convey precisely, both descriptively and visually, what segmental movements are involved. This not only furthers the understanding of human movement, but also facilitates the development of training and teaching programs, and injury related concerns. However, such descriptions fall victim to differences in the analytical methods, definitions of joint angles, reference frames and sign conventions between investigators. This poses a serious problem when comparing results from different studies and warrants standardization of such sporting skill analyses in order for the findings to have general application.

## *B. DATA ANALYSIS*

Supplementary to the kinematic analysis of a squash forehand stroke were a series of investigations by which the data were analyzed. There does not exist a strict recipe stipulating how 3D biomechanical data are to be analyzed. The major stages of a 3D kinematic study are the 2D image coordinate acquisition, 3D object coordinate reconstruction, smoothing of the data and the kinematic calculations. At these various stages, questions arose as to the most appropriate strategy by which to analyze the data. Many of these concerns have not been directly addressed previously. This prompted a series of investigations which compared the effect of various methods at different stages of the data analysis on the anatomical joint angular velocity data.

## *B.1 CALIBRATION COMPARISON*

The accuracy of the DLT reconstruction was assessed by determining the RMS error between the actual and calculated coordinates of the control points used in the calibration. To reduce the RMS error, the control points with high residuals were arbitrarily removed without regard to the configuration of the remaining control points. Contrary to findings by Wood and Marshall (1986), the RMS error decreased substantially as the number of control points reduced. The most accurate calibration consisted of only nine control points which did not represent the activity space well. An appropriate calibration should not only have a low RMS error, but it should also have an even distribution of the control points within the activity space. A comparison was made between the anatomical joint angular velocity profiles of Stroke #2 using various calibrations to determine the appropriate compromise (Appendix A). Of the four calibrations investigated, there were no differences in the temporal pattern except for the slight delay in the peak wrist velocities using the calibration consisting of only nine points. The magnitudes of the peak velocities were slightly different between the calibrations. Therefore, care must be taken in choosing the appropriate calibration when magnitudes of the velocities are of major concern.

## *B.2 FILTER SEQUENCE*

Even though smoothing of raw data is considered necessary to remove noise, it is not often agreed upon as to which data to smooth; whether it be the 2D (U,V) image coordinates, 3D (X,Y,Z) object coordinates, or the displacement data. It was found that filtering either the 3D coordinates or the displacement data was appropriate as shown by

the no differences in the anatomical joint angular velocity profiles between these filter sequences (Appendix C). Filtering the coordinate data prior to data reconstruction was inappropriates since filtering the 2D (U,V) image coordinate data at the higher cutoff frequency produced angular velocity profiles which were vastly different from the other conditions.

## C. *FUTURE RESEARCH*

Possible future research based on the work presented in this thesis includes:

- *a 3D kinetic analysis of the segmental movements involved*

In conjunction with the kinematic results, it would be possible to determine what causes the motion of each segment in a linked system in terms of the complex segmental interactions.

- *timing in the squash stroke*

1) This was an analysis of a well practiced and highly consistent stroke of one individual while a second individual's stroke showed significant similarities. Generalizations about the sequential coordination during the execution of a squash forehand stroke cannot be made. Such statements require many more subjects and trials.

2) The timing may also be compared between elite players and novice players. Identifying the commonalities and differences between these strokes would identify features characteristic of the elite stroke.

# REFERENCES


Abdel-Aziz, Y.I. and Karara, H.M. (1971) Direct linear transformation from comparator coordinates into object space coordinates in close range photogrammetry. In *ASP Symposium on Close Range Photogrammetry*, pp. 1-18, American Society of Photogrammetry, Church Falls.

Alexander, M.J. (1983) The pattern of body segment movement in high speed sport skills. *Coaching Science Update*, Coaching Association of Canada, pp. 15-19.

Alexander, M.J. and Haddow, J.B. (1982) The kinematic analysis of an upper extremity ballistic skill: the windmill pitch. *Can. J. Appl. Spt. Sci.* 7(3), 209-217.

Alexander, R. McN. (1991) Optimum timing of muscle activation for simple models of throwing. *J. theor. Biol.* 150, 349-372.

Andrews, J. (1984) On the specification of joint configurations and motions. *J. Biomechanics*, 17(2), 155-158.

Behm, D.G. (1987) A kinesiological analysis of the squash stroke. *NSCA Journal*, 9(5), 4-14.

Bunn, J.W. (1972) *Scientific Principles of Coaching*, Prentice-Hall, Inc., Inglewood Cliffs, NJ.

Cappozzo, A. (1983) Stereophotgrammetric system for kinesiological studies. *Med. Biol. Engng Computing* 21, 217-223.

Challis, J.H. and Kerwin, D.G. (1992) Accuracy assessment and control point configuration when using the DLT for photogrammetry. *J. Biomechanics* 25(9), 1053-1058.

Chapman, A.E. (1985a) Biomechanics of squash technique. Biomechanics module of Level IV coaching certification, Canadian Squash Racquets Association, unpublished.

Chapman, A.E. (1985b) The mechanical properties of human muscle. *Exercise and Sports Sciences Reviews* 13, pp. 443-501.

Chapman, A.E. and Sanderson, D.J. (1990) Muscular coordination in sporting skills. In *Multiple Muscle Systems: Biomechanics and Movement Organization* (edited by Winters, J.M. and Woo, S. L-Y), pp. 608-620. Springer-Verlag, New York.

Deporte, E., van Gheluwe, B. and Hebbelinck, M. (1990) A three-dimensional cinematographic analysis of arm and racket at impact in tennis. *Biomechanics of Human Movement*, (edited by Berme, N. and Cappozzo, A.), pp. 460-467. Bertic Corp, Worthington, OH.

Edmondstone, M.A. and Chapman, A.E. (1991) An investigation of the mechanisms contributing to optimal performance in throwing. *Proceedings of the XIIIth International Congress on Biomechanics*, 415-416.

Elliot, B.C. and Chivas, L. (1988) A three dimensional cinematographical analysis of the penalty corner hit in field hockey. In *Biomechanics XI-B* (edited by de Groot, G., Hollander, A.P. Huijing, P.A. and van Ingen Schenau, G.J.), pp. 791-797. Free University Press, Amsterdam.

Elliot, B.C., Grove, J.R, Gibson, B.J. and Thurston, W. (1985) A three-dimensional cinematographic analysis of baseball pitching technique. *Aust. J. Sci. Med. in Sport* 4, 8-13.

Elliot, B.C., Marsh, T. and Overheu, P., (1989) A biomechanical comparison of the multisegmental and single unit topspin forehand drives in tennis. *Int. J. Sport Biomechanics* 5, 350-364.

Feltner, M.E. and Dapena, J. (1986) Dynamics of the shoulder and elbow joints of the throwing arm during a baseball pitch. *Int. J. Sport Biomechanics* 2, 235-259.

van Gheluwe, B. (1978) Computerised three dimensional cinematography for any arbitrary camera set-up. In *Biomechanics VI-A* (edited by Asmussen, E. and Jorgenson, K.), pp. 343-348. University Park Press, Baltimore.

van Gheluwe, B. and Hebbelinck, M. (1985) The kinematics of the service movement in tennis: a three-dimensional cinematographical approach. In *Biomechanics IX-B* (edited by Winter, D.A., Norman, R.W., Wells, R.P., Hayes, K.C. and Patla, A.E.), pp. 521-526. Human Kinetic Publishers, Inc., Champaign, Ill.

Grood, E.S. and Suntay, W.J. (1983) A joint coordinate system for the clinical description of three-dimensional motions: applications to the knee. *J. Biomed. Eng.* 105, 135-144.

Herring, R.M. and Chapman, A.E. (1988) Computer simulation of throwing: optimization of endpoint velocity and projectile displacment. *Proceedings of the 5th Biennial Conference of the Canadian Society of Biomechanics* (edited by Cotton, C.E., Lamontagne, M., Robertson, D.G.E. and Stothart, J.P.), pp. 76-77. Spodym Publishers, London, Ontario.

Hong, Y. (1993) The biomechanics of badminton smash technique. *Proceedings of the XIVth International Congress on Biomechanics*, 588-589.

Joris, H.J.J., Edwards van Muyen, A.J., van Ingen Schenau, G.J., Kemper, H.C.G. (1985) Force, velocity and energy flow during the overarm throw in female handball players. *J Biomechanics* 18(6), 409-414.

Kreighbaum, E. and Barthels, K.M. (1981) Biomechanics. A Qualitative approach for Studying Human Movement. Burgess Publishing Company, Minneapolis, Minnesota.

Luhtanen, P. (1988) Kinematics and kinetics of serve in volleyball at different age levels. In *Biomechanics XI-B* (edited by de Groot, G., Hollander, A.P. Huijing, P.A. and van Ingen Schenau, G.J.), pp. 815-819. Free University Press, Amsterdam.

Luo, S., Liao, T. and Ning, Z. (1993) Kinematic analysis of whip action in javelin throwing. *Proceedings of the XIVth International Congress on Biomechanics*, 814-815.

NIKE Sport Reseach Laboratory. (1991) Sport Research Review - Three Dimensional Kinematics. April/July. NIKE, Inc. Beaverton, Oregon.

Penrose, T., Wood, G. and Blanksby, B. (1976) The accuracy of positional data in tri-axial cinematography. *Aust. J. Health, Physical Education, Recreation* 71, 7-12.

Putnam, C.A. (1983) Interaction between segments during a kicking motion. In *Biomechanics VIII-B* (edited by Matsui, H. and Kobayashi, K.), pp. 688-694. Human Kinetic Publishers, Inc., Champaign, Ill.

Putnam, C.A. (1993) Sequential motions of body segments in striking and throwing skills: descriptions and explanations. *J. Biomechanics* 26(Suppl.), 125-135.

Putnam, C.A. and Dunn, E.G. (1987) Performance variations in rapid swinging motions: Effects on segment interaction and resultant joint moments. In *Biomechanics X-B* (edited by Jonsson, B.), pp. 661-665. Human Kinetics Publishers, Inc., Champaign, Ill.

Small, C.F., Bryant, J.T. and Pichora, D.R. (1992) Rationalization of kinematic descriptors for three-dimensional hand and finger motion. *J. Biomed. Eng.* 14, 133-141.

Sprigings, E., Marshall, R., Elliot, B. and Jennings, L. (1992) The effectiveness of upper limb rotations in producing racket-head speed in racket sports. *Proceedings of NACOB II - The Second North American Congress on Biomechanics,* 51-52.

Stockill, N.P. and Bartlett, R.M. (1993) A temporal and kinematic comparison of junior and senior international cricket bowlers. *Proceedings of the XIVth International Congress on Biomechanics*, 1290-1291.

Tupling, S.J. and Pierrynowski, M.R. (1987) Use of cardan angles to locate rigid bodies in three dimensional space. *Med. & Biol. Eng. Comput.* 25, 527-532.

Whiting, W.C., Gregor, R.J. and Halushka, M. (1991) Body segment and release parameter contributions to new-rules javelin throwing. *Int. J. Sport Biomechanics,* 7(2), 111-124.

Winter, D.A. (1990) Biomechanics and Motor Control of Human Movement (2nd ed.) John Wiley & Sons, Inc., USA.

Woltring, H.J. (1991) Representation and calculation of 3-D joint movement. *Hum. Mov. Sci.* 10, 603-616.

Wood, G.A. and Marshall, R.N. (1986) The accuracy of DLT extrapolation in three-dimensional film analysis. *J. Biomechanics* 19(9), 781-785.

# APPENDIX A
# CALIBRATION COMPARISON

The 11 DLT calibration coefficients provide the relationship between the 3D real space and 2D image space required for the 3D data reconstruction. The accuracy of this reconstruction is expressed in terms of an RMS error in estimating the 3D coordinates of the control points using the estimated DLT coefficients. A lower RMS error indicates a more accurate estimation of the location of the control points in 3D real space.

When all 40 control points were used for the calibration, a relatively high RMS error of 3.81 cm resulted. Attempts were made to reduce this error by removing individual control points yielding high errors regardless of their locations. A control point was removed if it had an error above an arbitrary value in either the X, Y or Z direction. The removal of any control points required a re-calibration whereby new DLT coefficients were estimated and a new RMS error was calculated.

The first cut deleted control points possessing errors above 20 cm leaving 29 points (CALIB29). A RMS error of 2.06 cm was associated with CALIB29. Subsequently, control points from CALIB29 yielding errors above 10 cm were removed leaving 21 control points. CALIB21 had a RMS error of 1.67 cm. The next calibration was performed after removing control points with errors above 5 cm resulting in 9 control points. CALIB9 produced a RMS error of 1.09 cm. Although CALIB9 yielded the least amount of error, most of these remaining control points were located in the left back region of the calibration frame where the stroke did not enter. The general trend showed a lower RMS error being associated with a lower number of control points. However, the

location of the remaining control points did not satisfy the criterion of having an evenly, well distributed set of control points encompassing the testing volume.

The importance of the number and distribution of the control points in estimating the location of an unknown point has been well documented (eg. Wood and Marshall, 1986; Challis and Kerwin, 1992). However, it was uncertain as to the effect that the various calibrations performed in this study would have on the results in terms of the anatomical joint angular velocity profiles.

An investigation was conducted to determine if any substantial differences were apparent in the anatomical joint angular velocity profiles of Stroke #2 between the various calibrations: CALIB40, CALIB29, CALIB21, and CALIB9. The angular velocity profiles were quite similar, in particular during the period of the peak velocities and impact. Only selected angular velocity profiles are shown in Figure A.1a-c, but the similarity in the results obtained from the various calibrations was typical of all angular velocities.

Based on the above results, CALIB21 was chosen as the appropriate calibration since it satisfied both DLT criteria of having a low RMS error and even distribution of the control points and regardless, the anatomical joint angular velocities would have been similar.

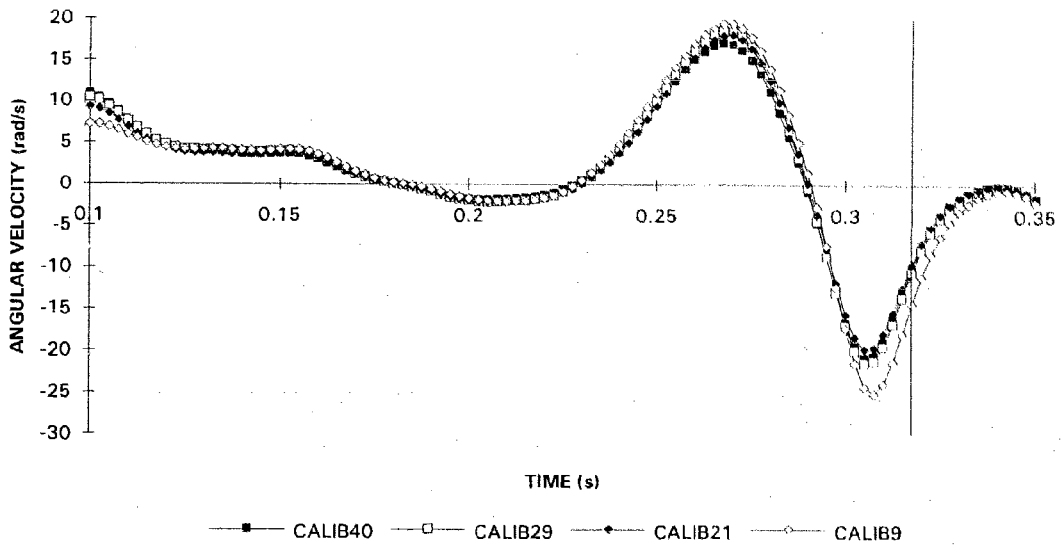


Figure A.1a Calibration comparison: shoulder outward rotation angular velocity

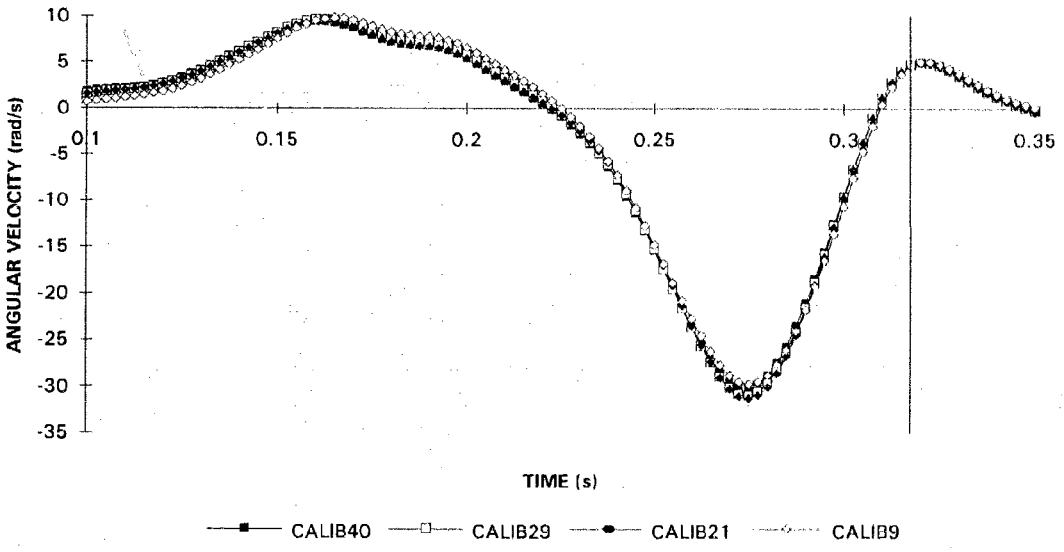


Figure A.1b Calibration comparison: elbow flexion angular velocity

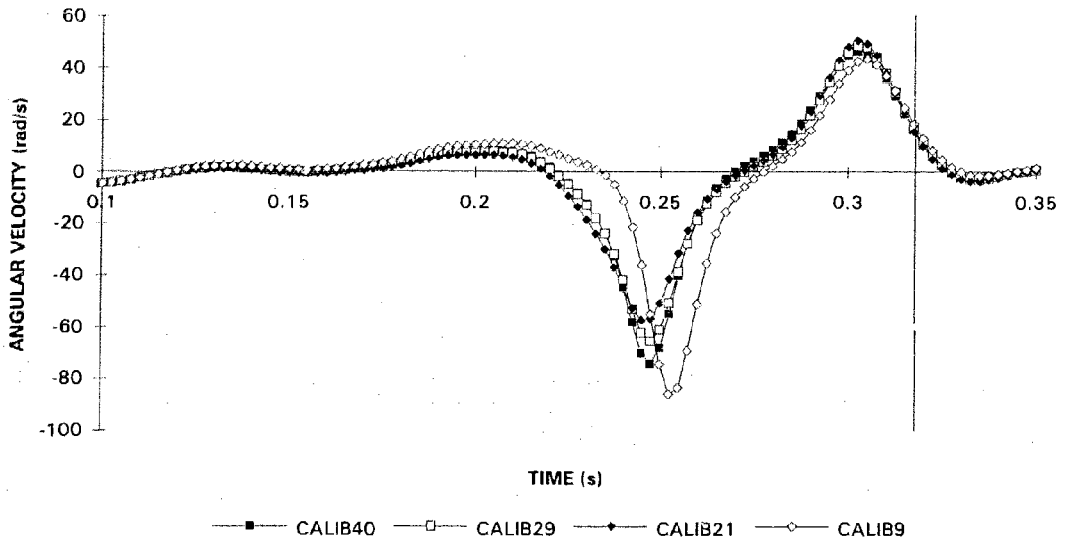


Figure A.1c Calibration comparison: wrist flexion angular velocity

# APPENDIX B

# XYZ COORDINATES OF THE SQUASH BALL AS A CONSEQUENCE OF USING VERSUS NOT USING A FIXED REFERENCE POINT

A comparison was made between XYZ coordinates reconstructed from 2D (U,V) image coordinates of the squash ball from which the image coordinates of the reference point were subtracted and when the image coordinates were not subtracted. The reference point and the centre of the squash ball were digitized in 29 frames beginning at the time when the ball was barely released from the subject's hand until the ball went out of view which was just prior to hitting the floor. When the reference point was used, its 2D (U,V) image coordinates were subtracted from those of the ball and the control points prior to 3D data reconstruction. On the other hand, the data were reconstructed directly when the reference point was excluded from the analysis. The reconstructed XYZ coordinates of the squash ball during free fall from both conditions are presented in Tables B.1 and B.2.

When the image coordinates of the reference point were not subtracted, more reasonable results were produced. This was not only true of the absolute XYZ coordinates, but also the excursions in the all three directions from the first to the last frame. Therefore, the image coordinates of the reference point were not subtracted from those of subsequent points. Any random errors due to misalignment of the film were removed by filtering.

Table B.1 The XYZ coordinates of the centre of the squash ball when not subtracting the reference point.

| FRAME | X (cm) | Y (cm) | Z (cm) |
|---|---|---|---|
| 1 | 127.47 | 150.48 | 129.41 |
| 2 | 126.83 | 150.46 | 127.35 |
| 3 | 125.68 | 150.56 | 125.33 |
| 4 | 124.27 | 150.38 | 122.69 |
| 5 | 123.87 | 150.81 | 119.81 |
| 6 | 122.15 | 150.94 | 117.01 |
| 7 | 121.49 | 150.96 | 114.09 |
| 8 | 120.51 | 151.20 | 110.87 |
| 9 | 118.67 | 151.37 | 107.63 |
| 10 | 117.45 | 151.17 | 104.04 |
| 11 | 116.65 | 151.60 | 100.32 |
| 12 | 115.01 | 151.77 | 96.84 |
| 13 | 114.02 | 152.05 | 93.17 |
| 14 | 112.98 | 152.25 | 89.47 |
| 15 | 111.59 | 152.44 | 85.67 |
| 16 | 109.65 | 153.11 | 81.31 |
| 17 | 109.38 | 152.72 | 78.71 |
| 18 | 108.11 | 153.27 | 73.02 |
| 19 | 106.44 | 153.61 | 68.04 |
| 20 | 105.22 | 153.81 | 64.07 |
| 21 | 103.93 | 154.06 | 59.45 |
| 22 | 103.13 | 154.17 | 55.06 |
| 23 | 101.34 | 154.35 | 50.55 |
| 24 | 100.03 | 154.81 | 46.05 |
| 25 | 99.02 | 155.07 | 41.08 |
| 26 | 97.84 | 155.01 | 36.88 |
| 27 | 96.41 | 155.83 | 31.79 |
| 28 | 95.59 | 155.80 | 27.02 |
| 29 | 94.09 | 156.02 | 21.85 |

Table B.2 The XYZ coordinates of the centre of the squash ball when subtracting the reference point.

| FRAME | X (cm) | Y (cm) | Z (cm) |
|---|---|---|---|
| 1 | 139.08 | 332.71 | 125.61 |
| 2 | 139.97 | 333.04 | 124.31 |
| 3 | 140.60 | 333.70 | 122.90 |
| 4 | 141.51 | 334.14 | 121.15 |
| 5 | 143.05 | 335.04 | 119.11 |
| 6 | 143.68 | 335.85 | 117.31 |
| 7 | 145.16 | 336.34 | 115.27 |
| 8 | 146.51 | 337.13 | 113.09 |
| 9 | 147.36 | 338.08 | 110.86 |
| 10 | 148.91 | 338.46 | 108.38 |
| 11 | 150.65 | 339.46 | 105.73 |
| 12 | 151.77 | 340.38 | 103.22 |
| 13 | 153.36 | 341.23 | 100.59 |
| 14 | 155.07 | 342.06 | 97.78 |
| 15 | 156.49 | 342.91 | 95.01 |
| 16 | 157.72 | 344.48 | 91.82 |
| 17 | 158.82 | 344.10 | 90.35 |
| 18 | 161.90 | 345.66 | 85.49 |
| 19 | 163.93 | 346.86 | 81.52 |
| 20 | 165.50 | 347.67 | 78.46 |
| 21 | 167.52 | 348.60 | 74.75 |
| 22 | 169.68 | 349.20 | 71.27 |
| 23 | 171.10 | 350.13 | 67.74 |
| 24 | 172.96 | 351.32 | 64.02 |
| 25 | 175.25 | 352.21 | 60.01 |
| 26 | 177.07 | 352.68 | 56.53 |
| 27 | 179.22 | 354.45 | 52.13 |
| 28 | 181.67 | 354.92 | 48.14 |
| 29 | 183.83 | 355.94 | 43.79 |

# APPENDIX C
# FILTER SEQUENCE

The filter sequence was investigated to determine whether it was appropriate to filter either the 2D (U,V) image coordinates, the 3D (X,Y,Z) real coordinates, or the angular positional data. The resulting anatomical joint angular velocity profiles were used as criteria in deciding which filter sequence was appropriate. Figure C.1 illustrates the flow diagram used to compare the profiles obtained from either raw data (RAW), filtered 2D (U,V) image coordinates (FILTUV), filtered 3D (X,Y,Z) real coordinates (FILTXYZ) and filtered anatomical joint angles (FILTANG). Raw joint angular velocities were omitted from this comparison because they were too noisy to be meaningful.

Comparable angular velocity profiles were produced from either filtering XYZ and angular displacement data (Figures C.2a-j). There were discrepancies in the shoulder angular velocity profiles using filtered 2D (U,V) image coordinates possibly due to data distortion prior to data reconstruction. It was decided from these results and the nature of the anatomical joint angle calculations that filtering XYZ coordinate data was most appropriate for this study. The wrist joint angle calculations were based on forearm angles, therefore filtering the XYZ coordinates ensured that the data would be filtered once and at the same time.

The comparison used data filtered at a cutoff frequency of 12 and 20 Hz. These cutoff frequencies were chosen based on preliminary analyses. However, a residual analysis was performed later on the XYZ coordinates and found that the optimal cutoff frequency was only 8 Hz (Appendix D). Nonetheless, the main purpose of the filter

sequence investigation was to compare the angular velocity profiles as a result of various filter sequences.

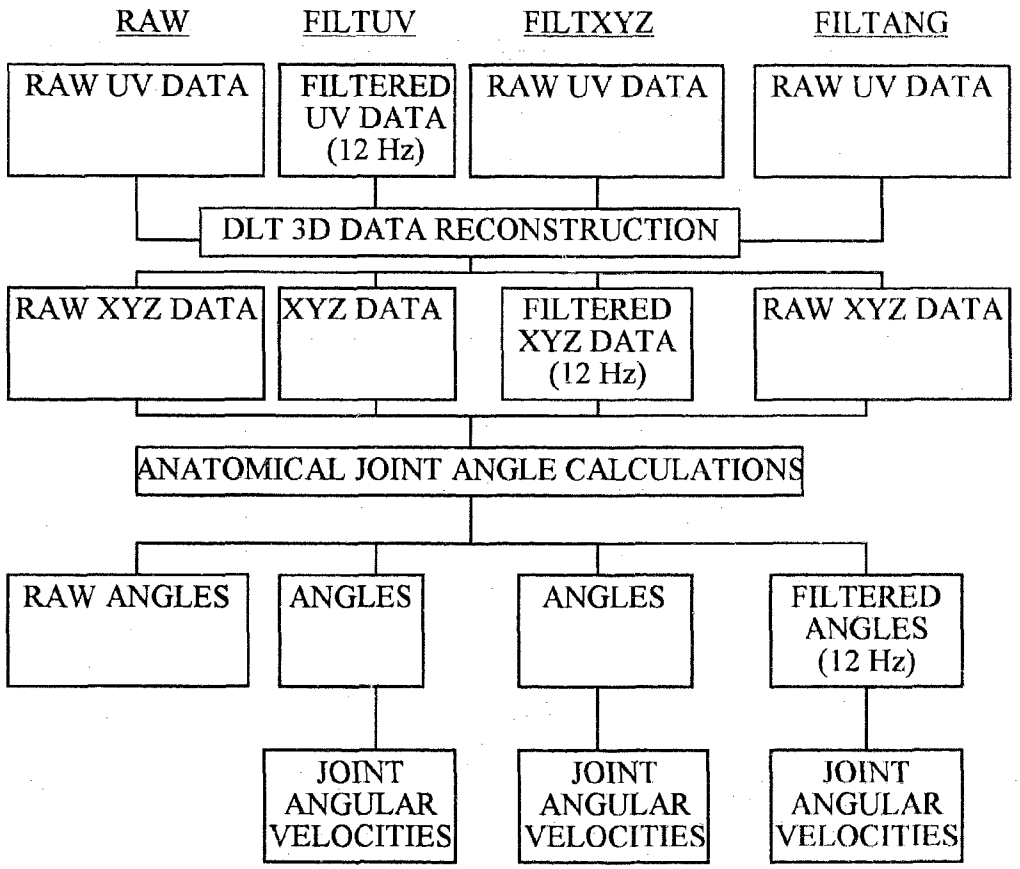


Figure C.1 Flow diagram of filter sequence comparison.

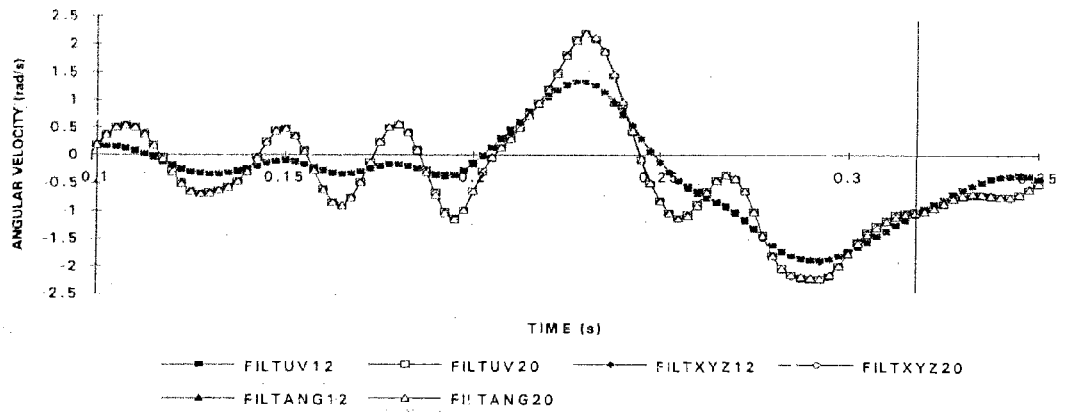


Figure C.2a Filter sequence: trunk flexion angular velocity profiles.

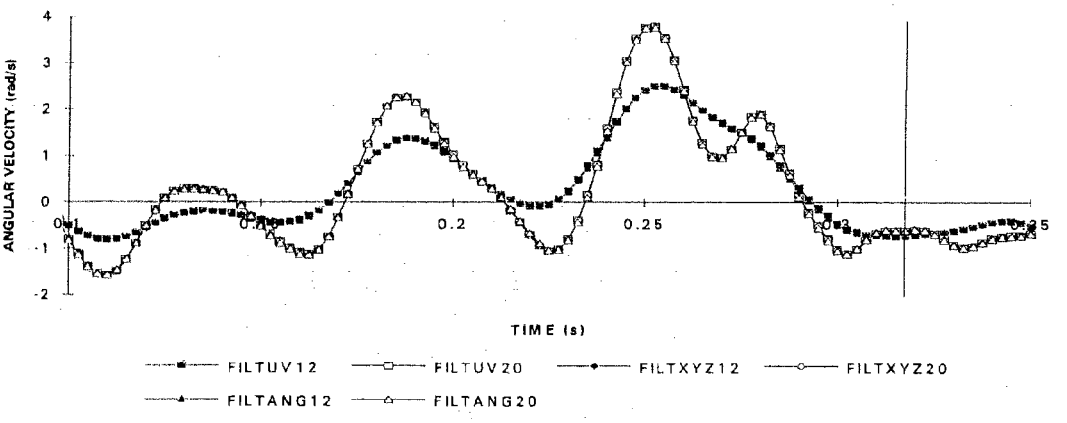


Figure C.2b Filter sequence: trunk right lateral flexion angular velocity profiles.

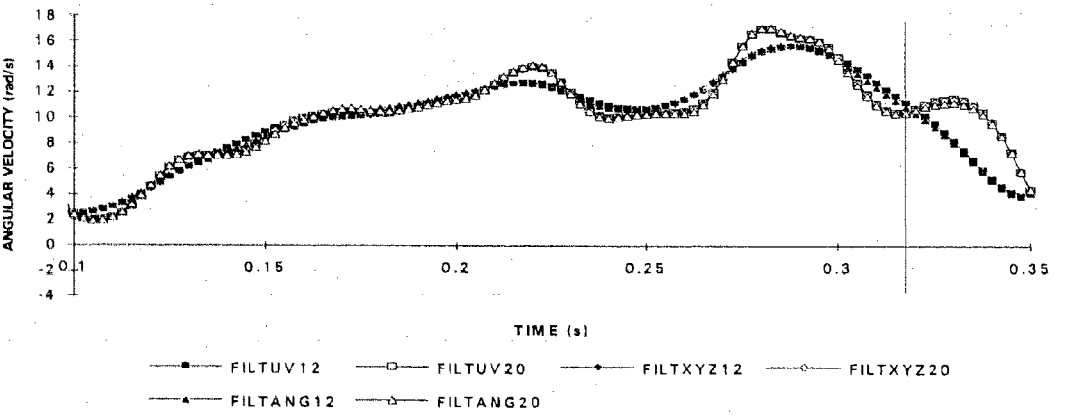


Figure C.2c Filter sequence: trunk left rotation angular velocity profiles.

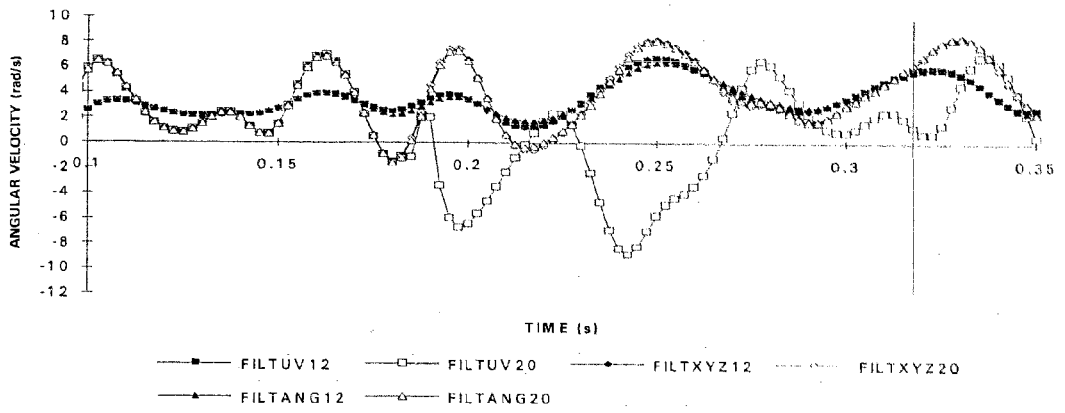


Figure C.2d Filter sequence: shoulder adduction angular velocity profiles.

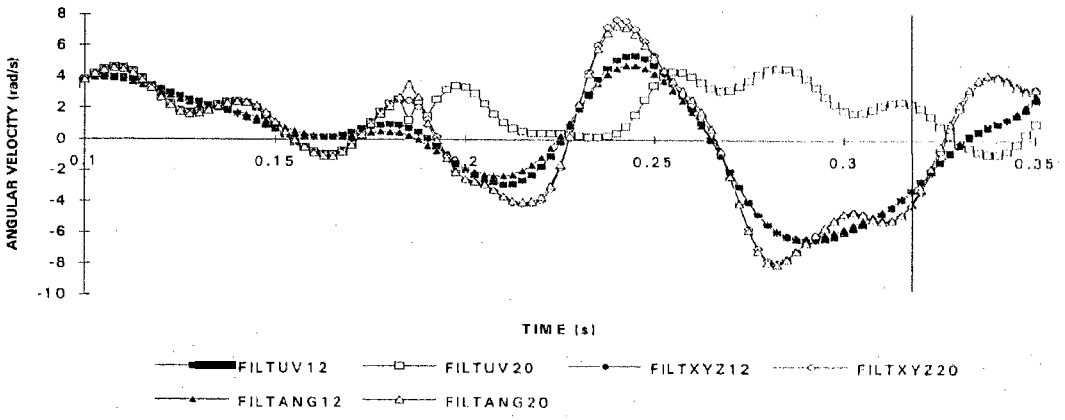


Figure C.2e Filter sequence: shoulder horizontal adduction angular velocity profiles.

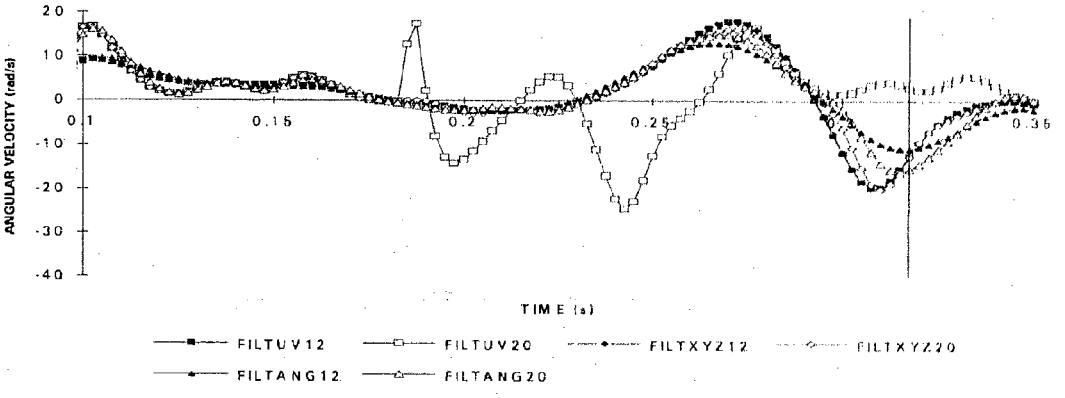


Figure C.2f Filter sequence: shoulder outward rotation angular velocity profiles.

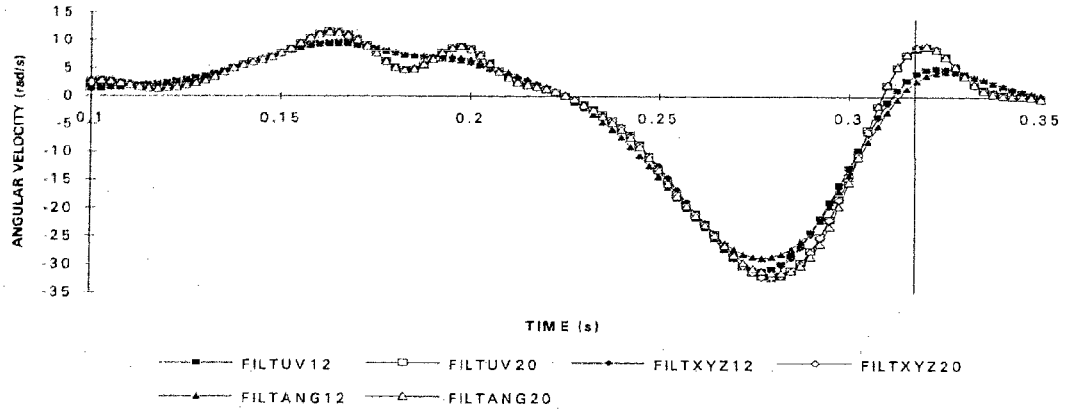


Figure C.2g Filter sequence: elbow flexion angular velocity profiles.

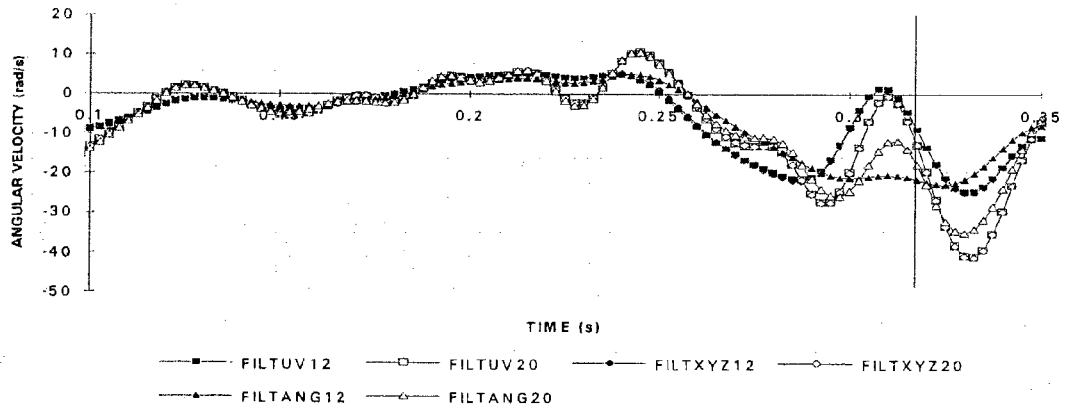


Figure C.2h Filter sequence: forearm supination angular velocity profiles.

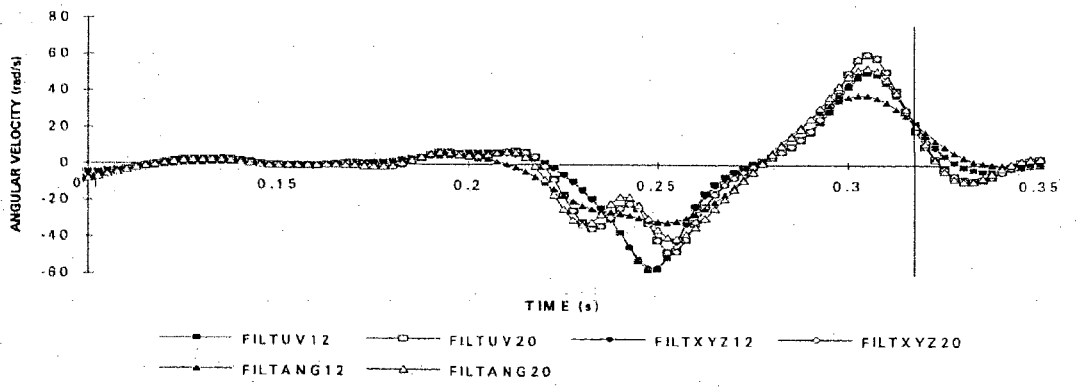


Figure C.2i Filter sequence: wrist flexion angular velocity profiles.

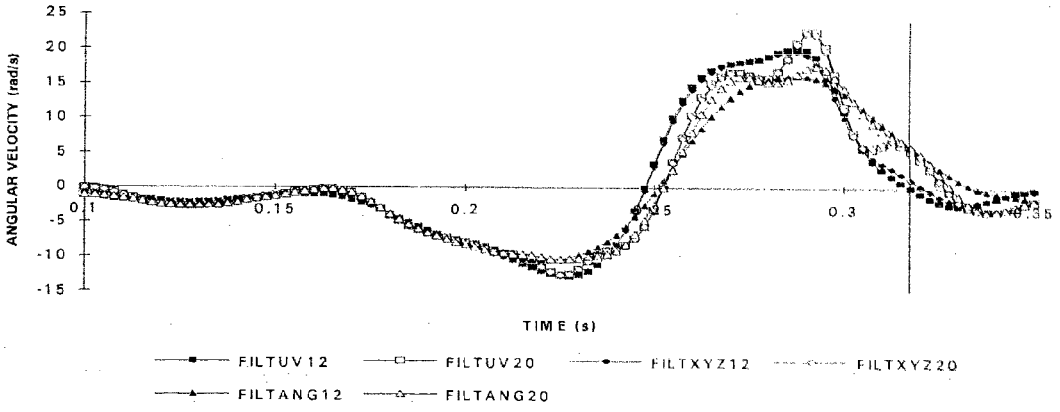


Figure C.2j Filter sequence: wrist adduction angular velocity profiles.

# APPENDIX D

# RESIDUAL ANALYSIS OF THE XYZ COORDINATE DATA

The optimal cutoff frequency at which to filter the XYZ coordinate data was determined by performing a residual analysis of the differences between filtered and raw data over a wide range of cutoff frequencies. The residual at any cutoff frequency was calculated using the following equation:

$$R(fc) = \sqrt{\frac{1}{N}\sum_{i=1}^{N}(Xi - \overline{X}i)^2}$$

where $R$ = residual
$fc$ = cutoff frequency
$N$ = number of sample points
$Xi$ = raw data at the ith sample
$\overline{X}i$ = filtered data at the ith sample.

Figure D.1 is a typical residual plot with the residuals plotted against the cutoff frequencies. If the signal contained only random noise, the plot would be a straight line decreasing from an intercept at 0 Hz to an intercept on the abscissa at the Nyquist frequency (0.5 *fs*). In this case, the y-intercept represents the RMS value of the noise. However, if the data contained true signal and noise, the signal would become distorted indicated by a dramatic rise above the straight line **de** as the cutoff frequency is reduced.

The cutoff frequency is chosen by extending the straight line **de** to the ordinate. Then, projecting a horizontal line from the y-intercept to the residual line, the cutoff frequency is the frequency representing this intersection point. At this frequency, the

amount of signal distortion and noise passed through are equal which is a suitable compromise.

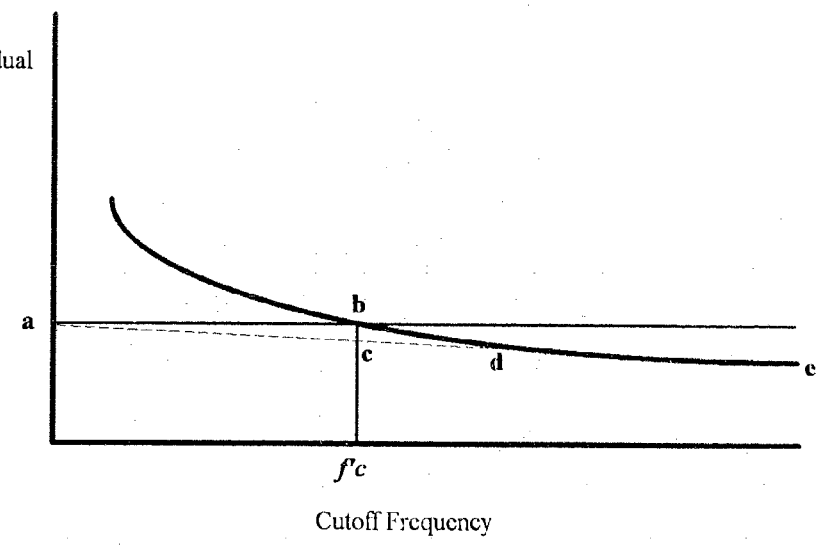


Figure D.1 A typical residual plot.

A residual analysis using cutoff frequencies of 6, 8, 10 ,12, 16, and 20 Hz was conducted on the XYZ coordinates of each of the markers to determine appropriate cutoff frequencies. The cutoff frequencies ranged from 5 to 10 Hz with a mean of 8.17 Hz. There was no trend suggesting that the more distal markers had a higher frequency component, thus requiring a higher cutoff frequency. The optimal cutoff frequency chosen was 8 Hz which was representative of the value for all the marker coordinates. Table D.1 summarizes the cutoff frequencies for the X, Y and Z coordinate data of the body markers as obtained from Stroke #2. Not all the residual plots are shown in Figure D.2. As an indication of the the range of cutoff frequencies pertinent to this study, the residual plots of the XYZ coordinates of the mid-hip (MHIP) and racquet tip (RTIP) markers are illustrated.

Table D.1 The optimal cutoff frequencies of the XYZ coordinate data of all the markers based on a residual analysis.

| MARKER | X (Hz) | Y (Hz) | Z (Hz) |
|---|---|---|---|
| MHIP | 7 | 9 | 5 |
| STRN | 8 | 9 | 10 |
| SHLD | 9 | 9 | 9 |
| ELB | 7 | 9 | 9 |
| WRST | 8 | 8 | 8 |
| FORE | 8 | 9 | 9 |
| RCM | 7 | 10 | 9 |
| RTIP | 8 | 10 | 6 |

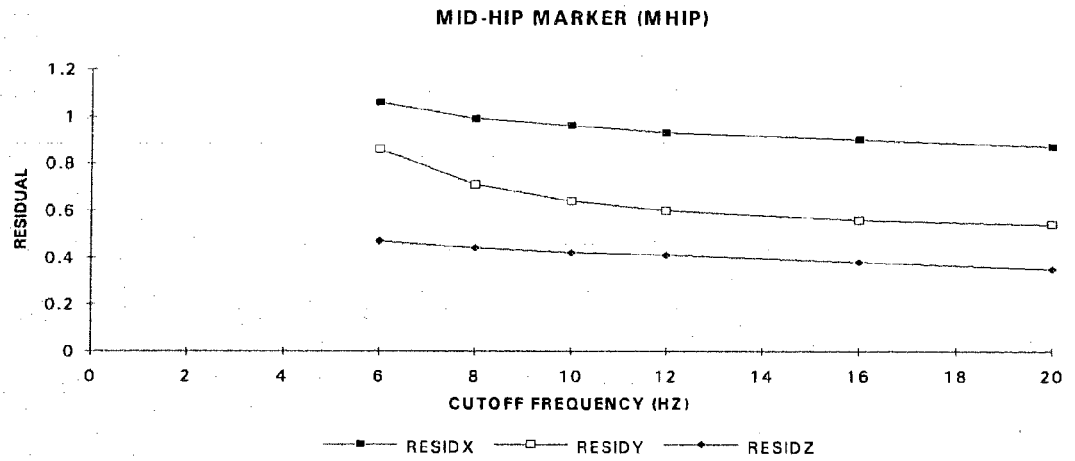


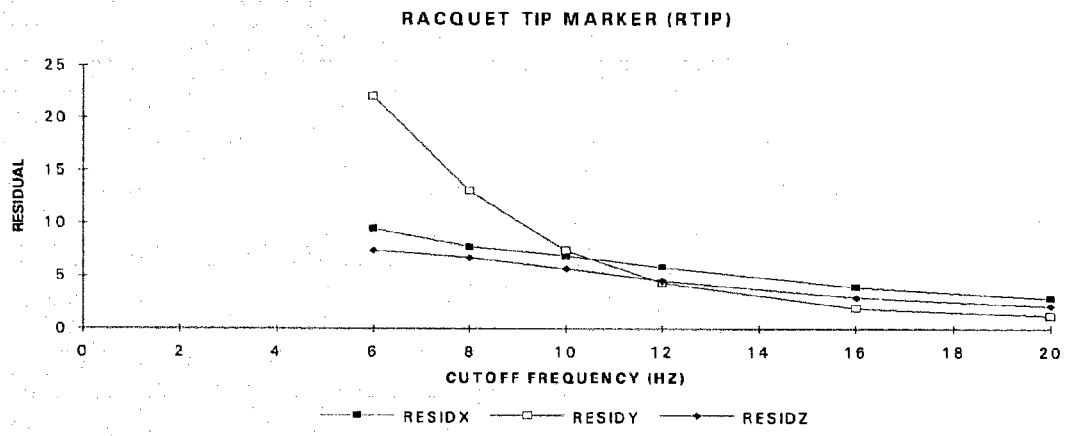


Figure D.2 The residual plots of the XYZ coordinates of the mid-hip (MHIP) and racquet tip (RTIP) markers.

# APPENDIX E
# CALCULATION OF THE ANATOMICAL JOINT ANGLES

## *E.1 General Mathematical Background*

The anatomical joint angles were calculated using Cardan angles such that the joint angles were defined with respect to the orientation of its adjacent proximal neighbour. An orthogonal reference frame embedded in the proximal segment A with its origin located at the proximal joint centre defined the orientation of the segment. It was considered the fixed frame of reference (FFR) having axes X, Y and Z with unit vectors **I**, **J** and **K**. Another orthogonal frame of reference (MFR) with axes x, y, and z with unit vectors **i**, **j** and **k** was embedded in the 'moving' distal segment B. Its origin was at the proximal joint centre. Both the FFR and MFR were known in terms of the inertial, global frame of reference ($R_1$). Its axes were labelled $X_G$, $Y_G$ and $Z_G$ with unit vectors $\mathbf{I}_G$, $\mathbf{J}_G$ and $\mathbf{K}_G$.

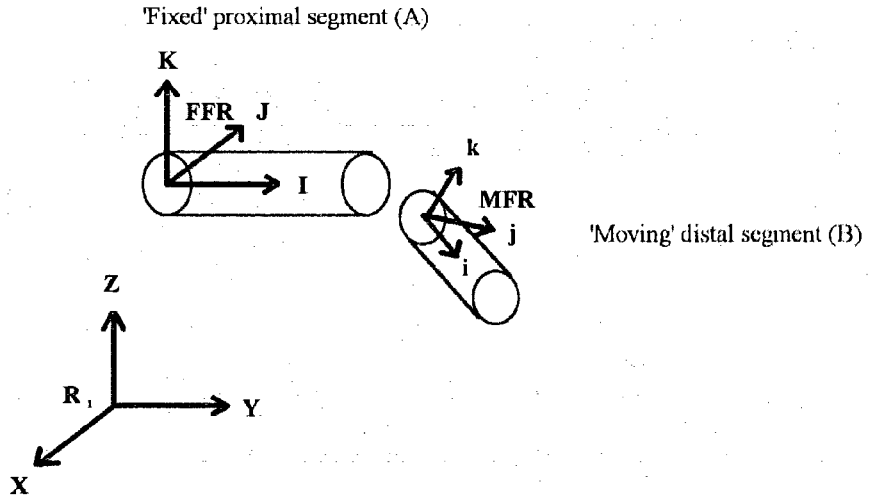


Figure E.1 A schematic diagram illustrating the relative orientation between the FFR and MFR in the proximal (A) and distal (B) segments, respectively.

## *E.2 Mathematical Description of the Kinematic Model*

The rigid-body model comprised five segments connected by ideal joints. The segment lengths were assumed to be constant throughout the stroke. The following table indicates the labels and mathematical definitions used in the analysis.

Table E.1 The labels and vectorial definitions of the body segments in the mathematical model.

| SEGMENT | LABEL | VECTOR |
|---|---|---|
| TRUNK | T | $r_1 = (X_{STRN} - X_{MHIP})\mathbf{I}_G + (Y_{STRN} - Y_{MHIP})\mathbf{J}_G + (Z_{STRN} - Z_{MHIP})\mathbf{K}_G$ |
| CLAVICULAR | C | $r_2 = (X_{SHLD} - X_{STRN})\mathbf{I}_G + (Y_{SHLD} - Y_{STRN})\mathbf{J}_G + (Z_{SHLD} - Z_{STRN})\mathbf{K}_G$ |
| UPPER ARM | U | $r_3 = (X_{ELB} - X_{SHLD})\mathbf{I}_G + (Y_{ELB} - Y_{SHLD})\mathbf{J}_G + (Z_{ELB} - Z_{SHLD})\mathbf{K}_G$ |
| FOREARM | F | $r_4 = (X_{WRST} - X_{ELB})\mathbf{I}_G + (Y_{WRST} - Y_{ELB})\mathbf{J}_G + (Z_{WRST} - Z_{ELB})\mathbf{K}_G$ |
| HAND/RACQUET | H | $r_5 = (X_{RCM} - X_{WRST})\mathbf{I}_G + (Y_{RCM} - Y_{WRST})\mathbf{J}_G + (Z_{RCM} - Z_{WRST})\mathbf{K}_G$ |

All coordinate systems were embedded at the proximal joint centres of the segments. The unit vectors of the coordinate systems were written in bold letters labelled with subscripts identifying the segments in which they were embedded. Capital letters were used to refer to the unit vectors of the FFR. Small letters corresponded to unit vectors of the MFR. Consistently, the **i** unit vector was directed along the longitudinal axis towards the distal endpoint of the segment. The second unit vector, **j**, was calculated as the cross product of the two adjacent segments at a given joint. Lastly, the third unit vector, **k**, was the cross product of the two known unit vectors.

### *E.2.1 TRUNK SEGMENT*

The trunk segment was the first segment in the kinematic chain. Although, the spine consists of many intervertebral joints, it was simplified as a single rigid body. Its proximal endpoint was located at MHIP and its distal endpoint located at STRN. The orientation of the trunk segment was defined by three angles as shown in Figure E.2:

i) trunk flexion/extension,

ii) trunk right/left lateral flexion, and

iii) trunk right/left rotation.

The FFR was embedded at MHIP with unit vectors of $\mathbf{I}_{pv}$, $\mathbf{J}_{pv}$ and $\mathbf{K}_{pv}$ representing the orientation of the pelvis. The MFR was also embedded at MHIP, but its orientation was defined by the orientation of the trunk segment with the x axis along the longitudinal axis of the trunk. The corresponding units vectors describing the two sets of axes, FFR and MFR, are summarized in the tables below.

Table E.2a The unit vectors of the FFR at the hip joint.

| Unit vectors in the FFR (pelvis) | Unit vectors defined with respect to GFR |
|---|---|
| $\mathbf{I}_{pv}$ | $\mathbf{J}_{pv} \times \mathbf{K}_G$ |
| $\mathbf{J}_{pv}$ | $(X_{MHIP} - X_{RHIP})\mathbf{I}_G + (Y_{MHIP} - Y_{RHIP})\mathbf{J}_G + (Z_{MHIP} - Z_{RHIP})\mathbf{K}_G$ |
| $\mathbf{K}_{pv}$ | $\mathbf{K}_G$ |

Table E.2b The unit vectors of the MFR at the hip joint.

| Unit vectors in the MFR (trunk) | Unit vectors defined with respect to GFR |
|---|---|
| $\mathbf{i}_T$ | $(X_{STRN} - X_{MHIP})\mathbf{I}_G + (Y_{STRN} - Y_{MHIP})\mathbf{J}_G + (Z_{STRN} - Z_{MHIP})\mathbf{K}_G$ |
| $\mathbf{j}_T$ | $-r_1 \times r_2$ |
| $\mathbf{k}_T$ | $\mathbf{i}_T \times \mathbf{j}_T$ |

The individual trunk angles were calculated as follows.

Trunk flexion/extension:

$$\theta_{tr} = \sin^{-1}(-\mathbf{i}_T \bullet \mathbf{K}_G) \quad \text{where} \quad -\frac{\pi}{2} \le \theta_{tr} \le \frac{\pi}{2} \tag{E.1}$$

This was the angle between the unit vector along the longitudinal axis of the trunk segment, $\mathbf{i}_T$, and the unit vector $\mathbf{K}_G$. A positive angle referred to trunk flexion.

Trunk right/left lateral flexion:

$$\phi_{tr} = \cos^{-1}(r_1 \bullet V_R) \quad \text{where} \quad -\frac{\pi}{2} \le \phi_{tr} \le \frac{\pi}{2} \tag{E.2}$$

The vector $V_R$ was the projection of the trunk segment, $r_1$, on the plane defined by unit vectors $\mathbf{I}_{pv}$ and $\mathbf{K}_{pv}$. The vector $V_R$ was calculated as follows.

$$V_R = (X_{STRN} - X_{MHIP})\mathbf{I}_G + (Z_{STRN} - Z_{MHIP})\mathbf{K}_G \tag{E.2a}$$

Right lateral flexion was defined as a positive angle.

Trunk right/left rotation:

The trunk rotation angle was calculated as the rotation about $\mathbf{K}_{pv}$.

$$\psi_{tr} = \sin^{-1}(\mathbf{j}_T \bullet \mathbf{K}_G / \cos\theta_{tr}) \quad \text{where} \quad -\pi \leq \psi_{tr} \leq \pi \tag{E.3}$$

A positive angle would reflect longitudinal rotation of trunk segment towards the left.

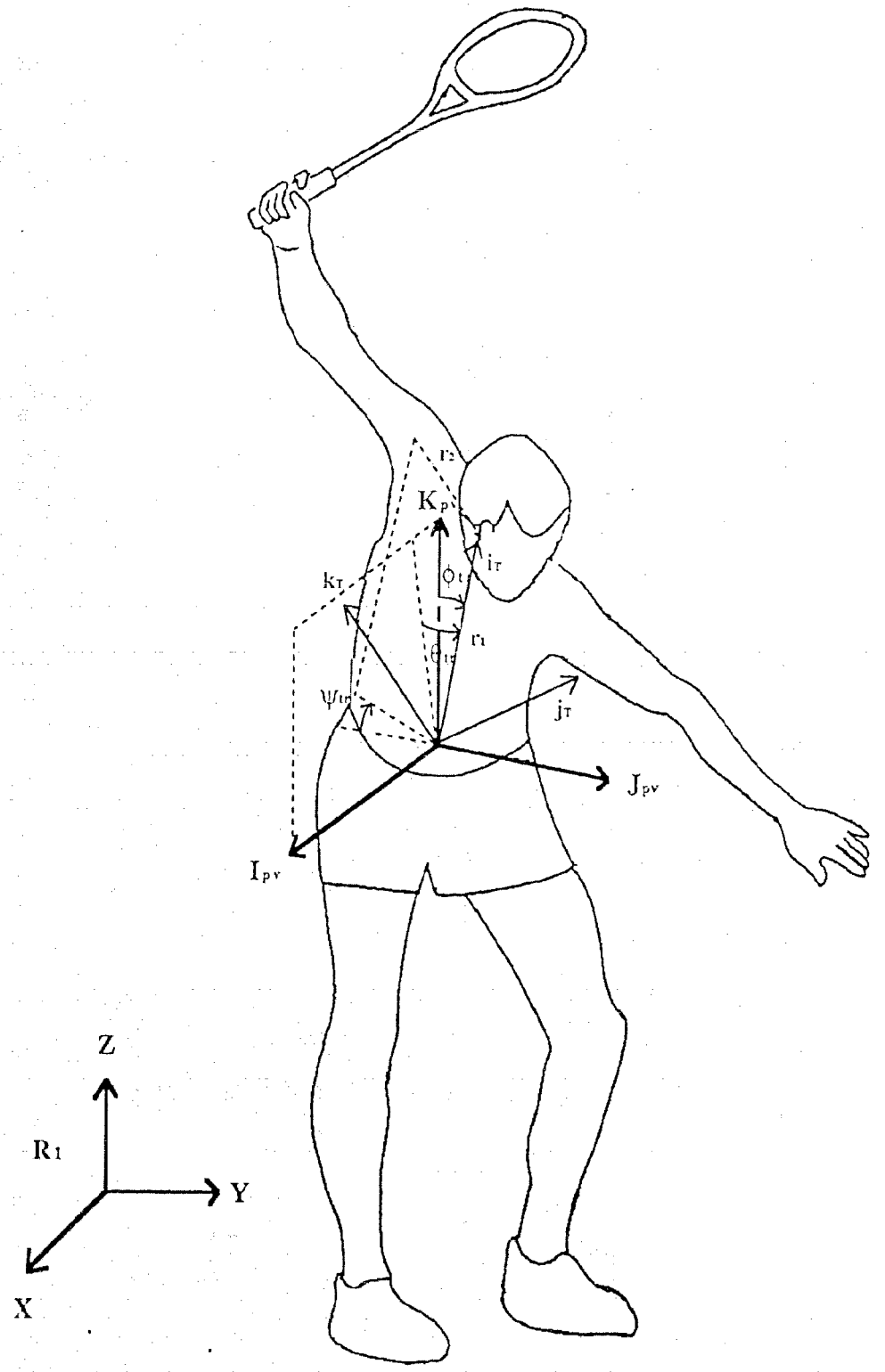


Figure E.2 The anatomical joint angles of the trunk.

### *E.2.2 SHOULDER JOINT*

The shoulder joint angles were abduction/adduction, horizontal abduction/adduction, and internal/external rotation as illustrated in Figure E.3. The relative orientation between the upper arm and the clavicular segments described the abduction/adduction and horizontal abduction/adduction angles. Therefore, these angles described the position of the upper arm relative to the trunk. The FFR was embedded at the STRN point with its unit vector $\mathbf{I}_C$ coincident with the longitudinal axis of the clavicular segment pointing towards the shoulder joint centre. The cross product of the trunk ($r_1$) and clavicular ($r_2$) segments defined the unit vector $\mathbf{J}_C$. Consequently, $\mathbf{K}_C$ was the cross product of $\mathbf{I}_C$ and $\mathbf{J}_C$. In the MFR, the $\mathbf{i}_U$ unit vector was along the longitudinal axis of the upper arm, $\mathbf{j}_U$ was the cross product of the clavicular ($r_2$) and upper arm ($r_3$) segments, and $\mathbf{k}_U$ was the cross product of these known unit vectors. The unit vectors are summarized in the Tables below.

Table E.3a The unit vectors of the FFR at the sternal point.

| Unit vectors in the FFR (clavicular) | Unit vectors defined with respect to GFR |
|---|---|
| $\mathbf{I}_C$ | $(X_{SHLD} - X_{STRN})\mathbf{I}_G + (Y_{SHLD} - Y_{STRN})\mathbf{J}_G + (Z_{SHLD} - Z_{STRN})\mathbf{K}_G$ |
| $\mathbf{J}_C$ | $r_2 \times -r_1$ |
| $\mathbf{K}_C$ | $\mathbf{I}_C \times \mathbf{J}_C$ |

Table E.3b The unit vectors of the MFR at the shoulder joint.

| Unit vectors in the MFR (upper arm) | Unit vectors defined with respect to GFR |
|---|---|
| $\mathbf{i}_U$ | $(X_{ELB} - X_{SHLD})\mathbf{I}_G + (Y_{ELB} - Y_{SHLD})\mathbf{J}_G + (Z_{ELB} - Z_{SHLD})\mathbf{K}_G$ |
| $\mathbf{j}_U$ | $r_3 \times -r_2$ |
| $\mathbf{k}_U$ | $\mathbf{i}_U \times \mathbf{j}_U$ |

Shoulder abduction/adduction:

$$\theta_{sh} = \sin^{-1}(-\mathbf{i}_U \bullet \mathbf{K}_C) \qquad \text{where } -\pi \le \theta_{sh} \le \pi \tag{E.4}$$

A positive angle indicated shoulder adduction.

Shoulder horizontal abduction/adduction:

$$\phi_{sh} = \sin^{-1}(\mathbf{i}_U \bullet \mathbf{J}_C / \cos\theta_{sh}) \quad \text{where } -\pi \le \phi_{sh} \le \pi \tag{E.5}$$

A positive angle represented shoulder horizontal adduction.

Shoulder inward/outward rotation:

Unlike the above angles, the calculation for the rotation of the upper arm about its longitudinal axis was based on the relative orientations of the coordinate axes of the upper arm and the forearm. Therefore, the FFR was located in the upper arm segment as indicated in Table E.3b and the MFR was situated in the forearm segment originating at the elbow joint (Table E.3c).

Table E.3c. The unit vectors of the MFR at the elbow joint.

| Unit vectors in the MFR (forearm) | Unit vectors defined with respect to GFR |
|---|---|
| $\mathbf{i}_F$ | $(X_{WRST} - X_{ELB})\mathbf{I}_G + (Y_{WRST} - Y_{ELB})\mathbf{J}_G + (Z_{WRST} - Z_{ELB})\mathbf{K}_G$ |
| $\mathbf{j}_F$ | $r_4 \times -r_3$ |
| $\mathbf{k}_F$ | $\mathbf{i}_F \times \mathbf{j}_F$ |

Therefore, the angle of shoulder internal/outward rotation was

$$\psi_U = \sin^{-1}(\mathbf{j}_F \bullet \mathbf{K}_U / \cos\theta_U) \quad \text{where } -\pi \le \psi_U \le \pi \tag{E.6}$$

The second rotation, $\theta_U$, about the y'axis of the FFR being

$$\theta_U = \sin^{-1}(-\mathbf{i}_F \bullet \mathbf{K}_U) \tag{E.6a}$$

Outward rotation at the shoulder was defined as a positive angle.

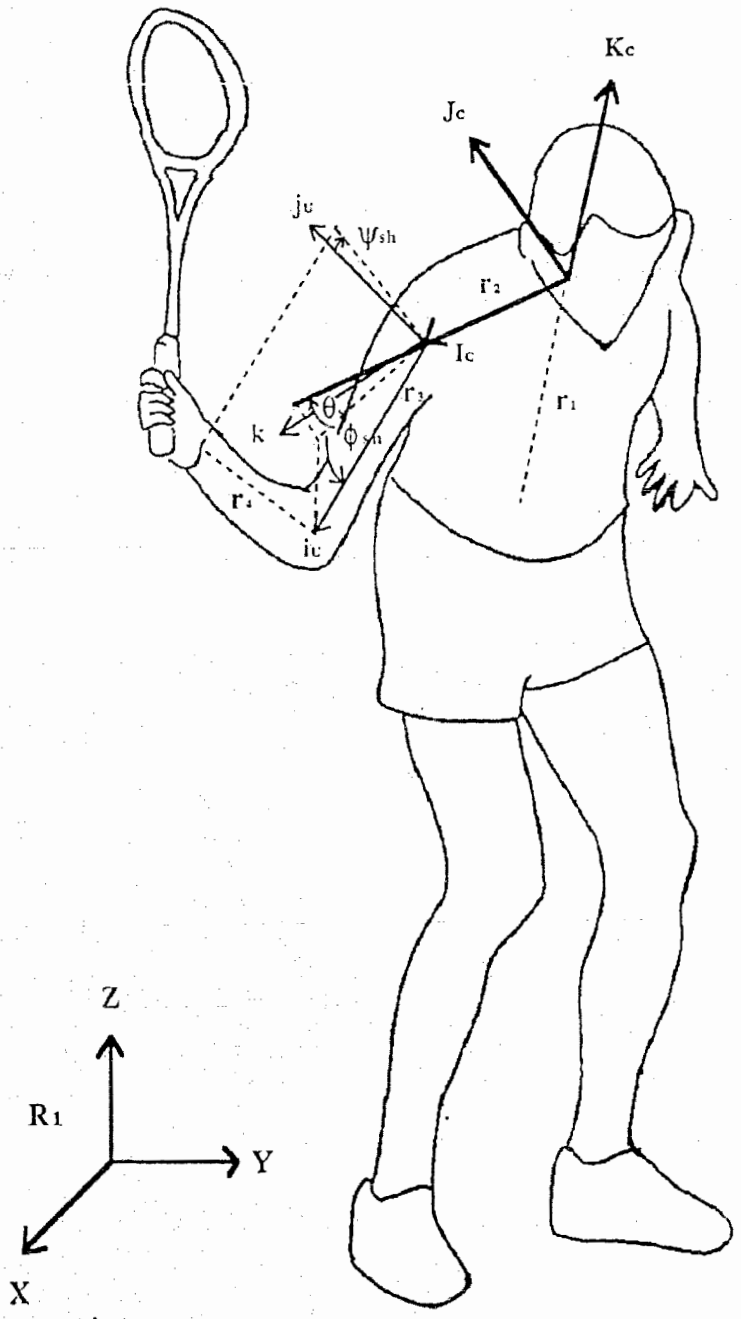


Figure E.3 The anatomical joint angles of the shoulder.

### *E.2.3 ELBOW JOINT*

The elbow joint was classified as a uniaxial, hinge joint, therefore having only one angle. Elbow flexion/extension was the angle between the upper arm and forearm segments. Full elbow extension would be - $\pi$ radian. This angle is shown in Figure E.4.

$$\theta_{elb} = -\cos^{-1}((-r_3 \bullet r_4)/(|r_3||r_4|)) \qquad \text{where } -\pi \le \theta_{elb} \le 0 \qquad \text{(E.7)}$$

### *E.2.4 RADIO-ULNAR JOINT*

The rotation about the radio-ulnar joint, otherwise known as forearm supination/pronation, was the angle of rotation about the x axis ($\mathbf{I}_F$) of the forearm reference frame ($RF_F$) to align its axes with those of the forearm marker reference frame ($RF_M$). The unit vectors $\mathbf{I}_F$, $\mathbf{J}_F$ and $\mathbf{K}_F$ of FFR remain as those described in Table E.3c. The origin of the MFR was also located at the elbow joint centre, but its orientation was defined by the location of the forearm marker (FORE) and the elbow (ELB) and wrist (WRST) joints (Table E.4). The forearm angle is illustrated in Figure E.4.

Table E.4 The unit vectors of the MFR at the elbow joint.

| Unit vectors of MFR (FORE marker) | Unit vectors defined with respect to GFR |
|---|---|
| $\mathbf{i}_M$ | $(X_{FORE} - X_{ELB})\mathbf{I}_G + (Y_{FORE} - Y_{ELB})\mathbf{J}_G + (Z_{FORE} - Z_{ELB})\mathbf{K}_G$ |
| $\mathbf{j}_M$ | $-r_3 \times \mathbf{i}_M$ |
| $\mathbf{k}_M$ | $\mathbf{i}_M \times \mathbf{j}_M$ |

Therefore, the angle of forearm rotation was the rotation about the $\mathbf{I}_F$ calculated as follows:

$$\psi_{fore} = \sin^{-1}(\mathbf{j}_M \bullet \mathbf{K}_F / \cos\theta_{fore}) - \psi_{refore} \qquad \text{where } -\frac{\pi}{2} \le \psi_{fore} \le \frac{\pi}{2} \qquad \text{(E.8)}$$

$$\text{where} \qquad \theta_{fore} = \sin^{-1}(-\mathbf{i}_M \bullet \mathbf{K}_F) \qquad \text{(E.8a)}$$

Forearm supination was indicated by a positive angle.

It was necessary to subtract the reference angle of the forearm from subsequent calculations of forearm rotation in order to obtain true forearm supination/pronation angles. The forearm marker was located on the anterior radial surface of the forearm to improve its visibility throughout the stroke as the arm swung across the body. Therefore, the marker would have indicated some rotation even though the forearm was not rotated. The reference angle was calculated from coordinate data obtained with the subject in the reference position. In this position, the subject kept the forearm in the neutral position.

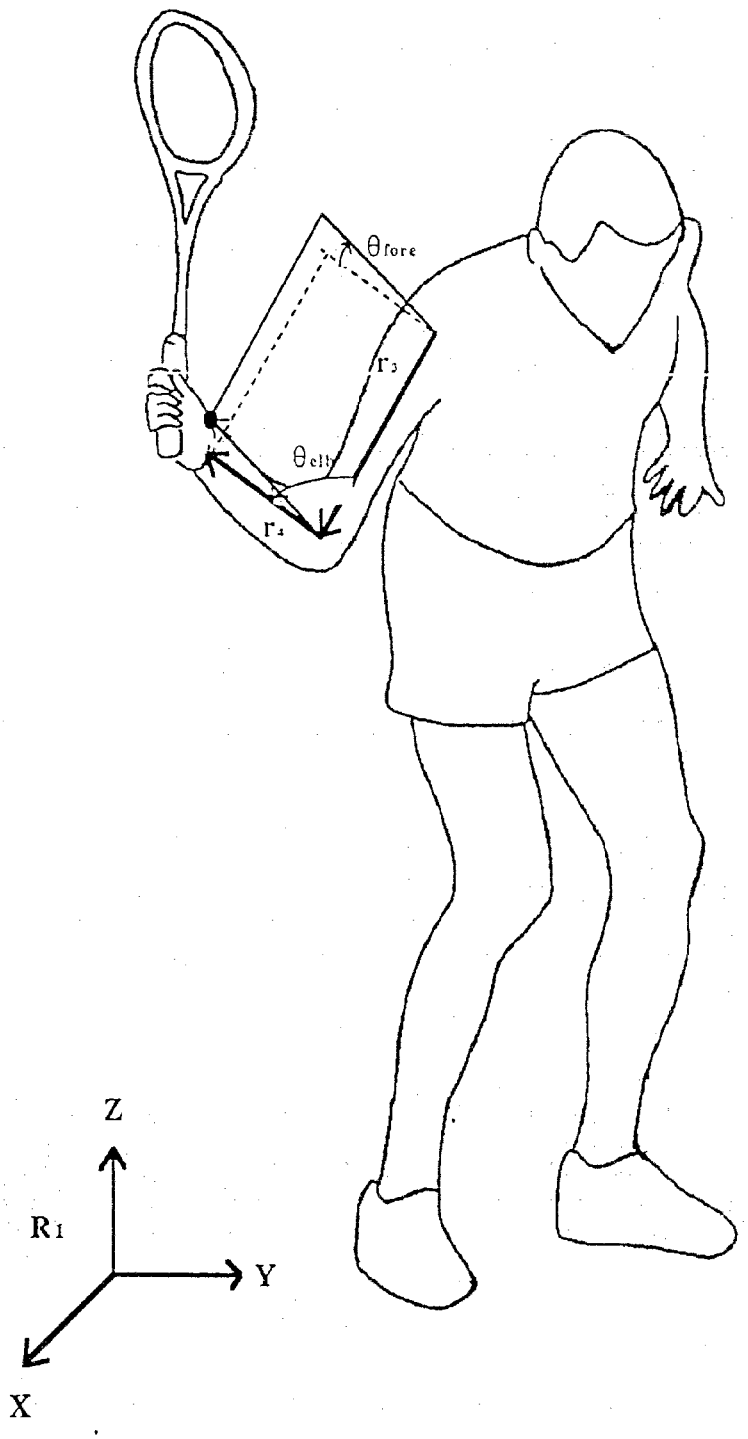


Figure E.4 The anatomical joint angles of the elbow and forearm.

### *E.2.5 WRIST JOINT*

The wrist joint was described as having two motions, wrist abduction/adduction and flexion/extension. These angles were based on the relative orientation of the frames of reference in the forearm (FFR) and hand/racquet segments (MFR). The hand/racquet segment assumed rigid body characteristics from the wrist joint centre to the marker representing the centre of mass of the racquet. Therefore, any relative movement of the racquet in the subject's hand was not considered. Again, the unit vectors of these references frames were defined as follows. The wrist angles are illustrated in Figure E.5.

Table E.5 The unit vectors of the MFR at the wrist joint.

| Unit vectors of MFR (hand/racquet) | Unit vectors defined with respect to GFR |
|---|---|
| $\mathbf{i}_H$ | $(X_{RCM} - X_{WRST})\mathbf{I}_G + (Y_{RCM} - Y_{WRST})\mathbf{J}_G + (Z_{RCM} - Z_{WRST})\mathbf{K}_G$ |
| $\mathbf{j}_H$ | $-r_4 \times r_5$ |
| $\mathbf{k}_H$ | $\mathbf{i}_H \times \mathbf{j}_H$ |

Wrist abduction/adduction:

Wrist abduction/adduction angle represented the rotation about the y' axis of $RF_F$, therefore it was calculated as

$$\theta_{wr} = \sin^{-1}(-\mathbf{i}_H \bullet \mathbf{K}_F) - \theta_{refwr} \qquad \text{where } -\frac{\pi}{2} \le \theta_{wr} \le \frac{\pi}{2} \qquad \text{(E.9)}$$

A positive angle meant wrist adduction.

Wrist flexion/extension:

The rotation about the Z axis of $RF_F$ was the angle of wrist flexion/extension. It was calculated as

$$\phi_{wr} = \sin^{-1}(\mathbf{i}_H \bullet \mathbf{J}_F / \cos\theta_{wr}) - \phi_{refwr} \quad \text{where} \quad -\frac{\pi}{2} \le \phi_{wr} \le \frac{\pi}{2} \qquad \text{(E.10)}$$

Wrist flexion was noted by a positive angle.

As in the case of calculating the forearm rotation, the true wrist angles were obtained after subtracting the corresponding reference angles at the wrist. This was necessary because of the use of the racquet in defining the wrist position. When the subject grasped the racquet in his hand keeping the forearm and wrist joint neutral, the projection of the racquet out of the hand would indicate some deviation of the wrist joint. Therefore, reference angles for wrist abduction/adduction and flexion/extension were calculated from the subject being in the reference position.

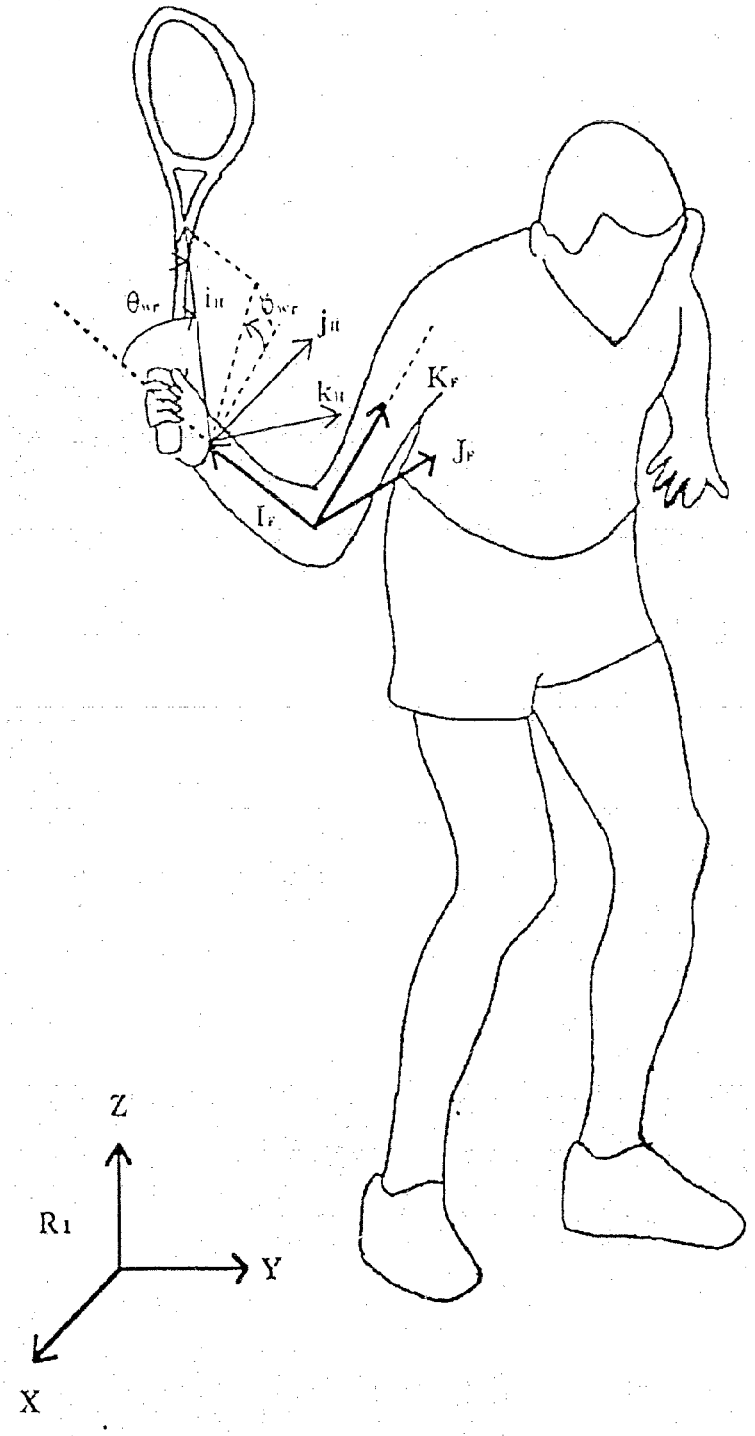


Figure E.5 The anatomical joint angles of the wrist.

Table E.6 A summary of the labels and sign conventions used in describing the various joint angles.

| JOINT | ANGLE | LABEL | POSITIVE ANGLE |
|---|---|---|---|
| TRUNK | flexion/extension | $\theta_{tr}$ | flexion |
| | right/left lateral flexion | $\phi_{tr}$ | right lateral flexion |
| | right/left rotation | $\psi_{tr}$ | left rotation |
| SHOULDER | abduction/adduction | $\theta_{sh}$ | adduction |
| | horizontal abduction/adduction | $\phi_{sh}$ | horizontal adduction |
| | inward/outward rotation | $\psi_{sh}$ | outward rotation |
| ELBOW | flexion | $\theta_{elb}$ | flexion |
| RADIO-ULNAR or FOREARM | pronation/supination | $\psi_{fore}$ | supination |
| WRIST | flexion/extension | $\phi_{wr}$ | flexion |
| | abduction/adduction | $\theta_{wr}$ | adduction |

# APPENDIX F

# ANATOMICAL JOINT ANGLES AND ANGULAR VELOCITIES OF STROKES #1 TO #5 AND THEIR RESPECTIVE VARIABILITIES.

Figures F.1-10a illustrate the anatomical joint angle profiles from all trials (Strokes #1 to #5). Immediately following each of these figures are the respective mean profiles with plus and minus one standard deviation curves as an indication of the variability (Figures F.1-10b). Similarly, the anatomical joint angular velocity profiles are shown in Figures F.11-20a and their variability profiles are presented in Figures F.11-20b. Table F.1 summarizes the peak anatomical joint angular velocities, times of occurrence and the angular velocities at impact for all trial.

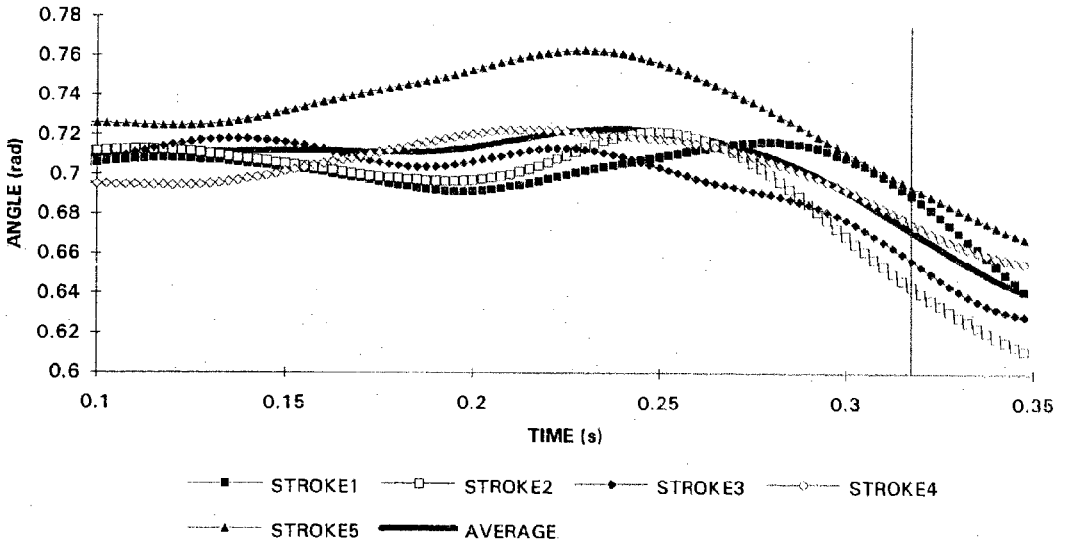


Figure F.1a The trunk flexion angle profiles of Strokes #1 to #5.

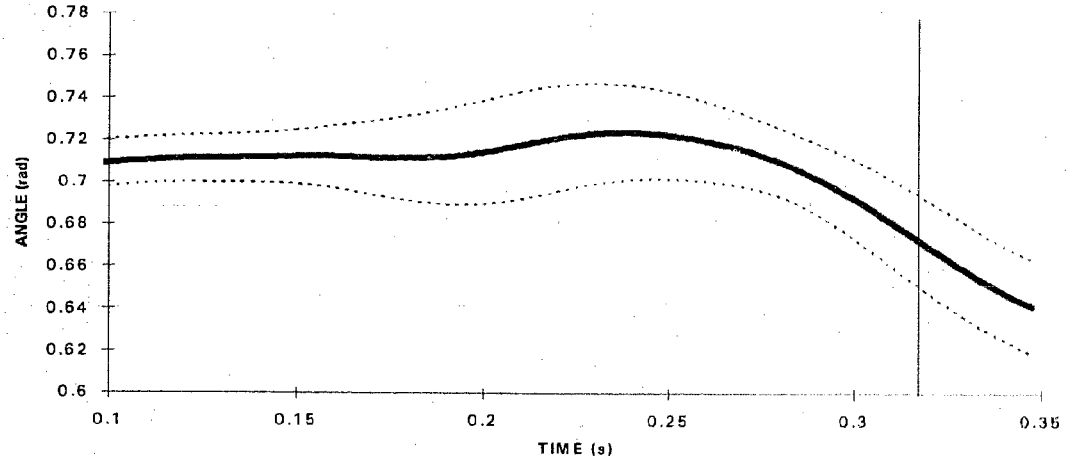


Figure F.1b Variability in the trunk flexion angle profiles.

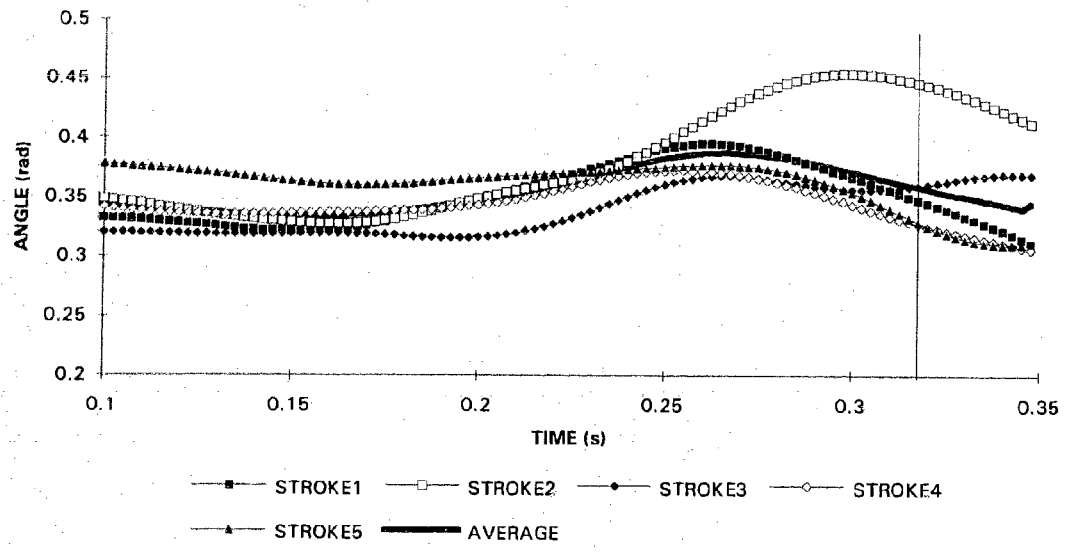


Figure F.2a The trunk right lateral flexion angle profiles of Strokes #1 to #5.

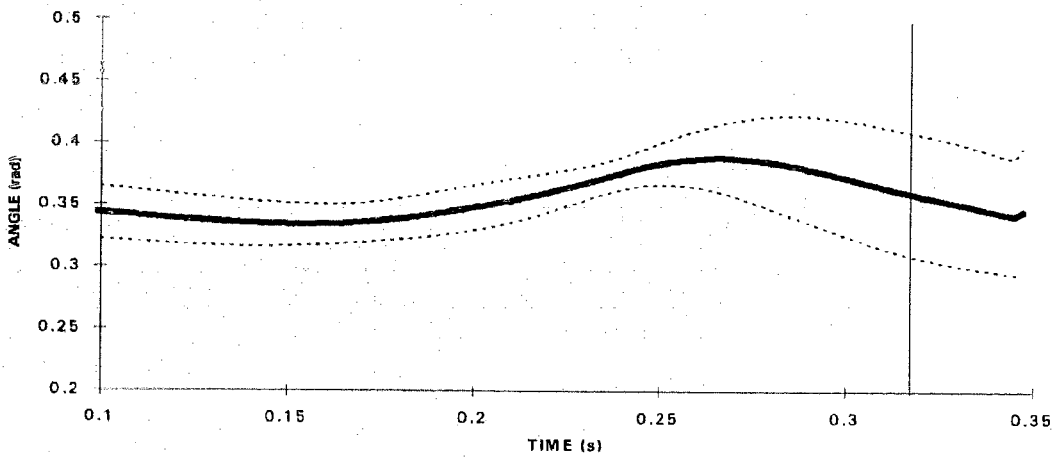


Figure F.2b Variability in the trunk right lateral flexion angle profiles.

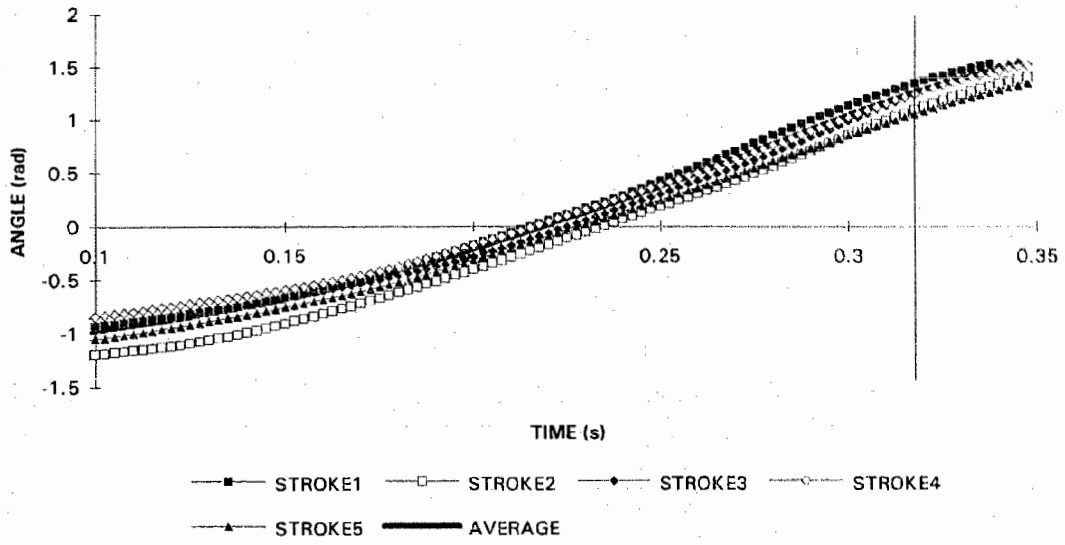


Figure F.3a The trunk left rotation angle profiles of Strokes #1 to #5.

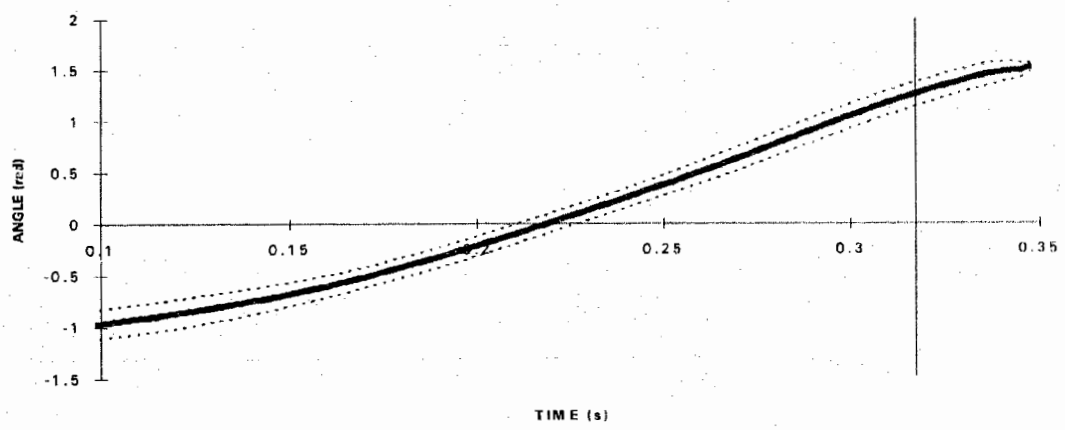


Figure F.3b Variability in the trunk left rotation angle profiles.

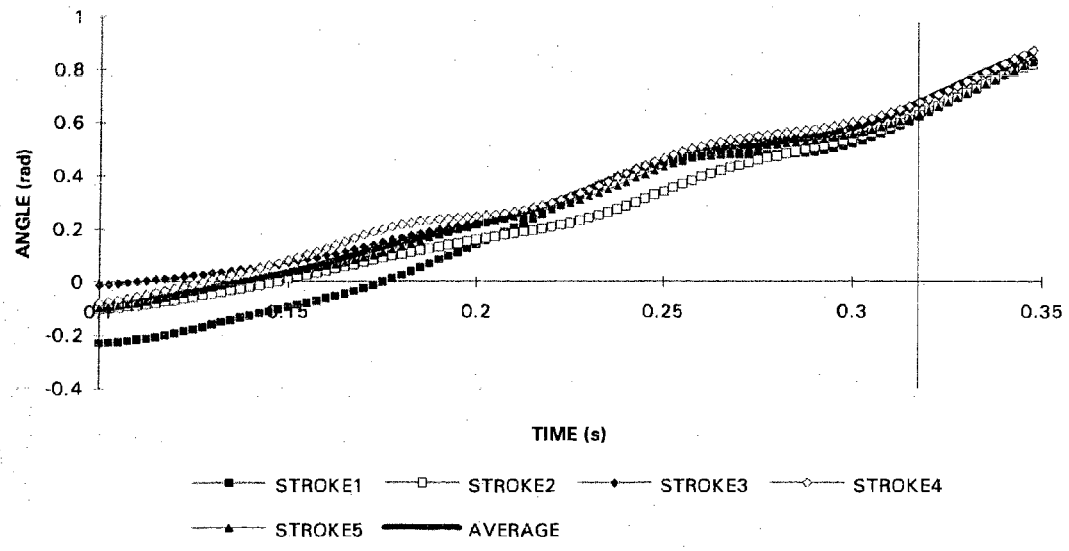


Figure F.4a The shoulder adduction angle profiles of Strokes #1 to #5.

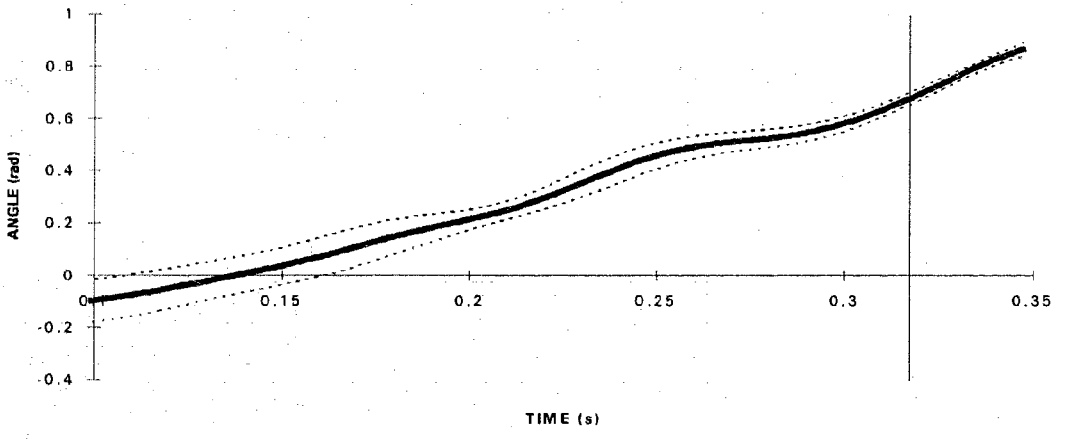


Figure F.4b Variability in the shoulder adduction angle profiles.

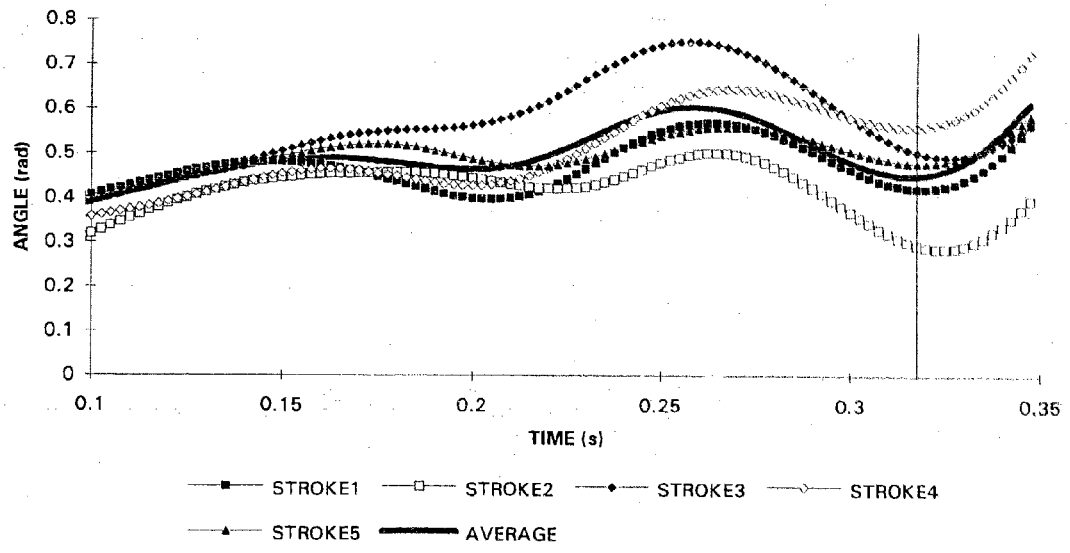


Figure F.5a The shoulder horizontal adduction angle profiles of Strokes #1 to #5.

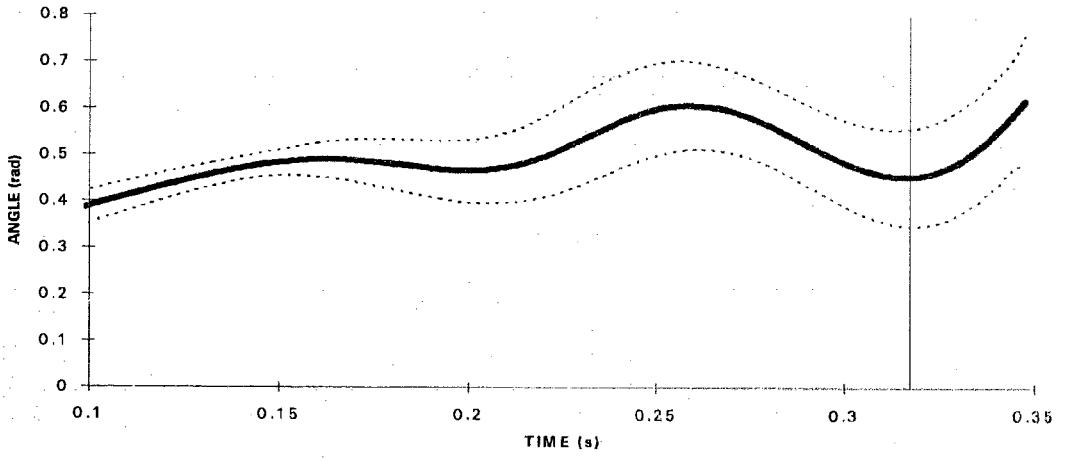


Figure F.5b Variability in the shoulder horizontal adduction angle profiles.

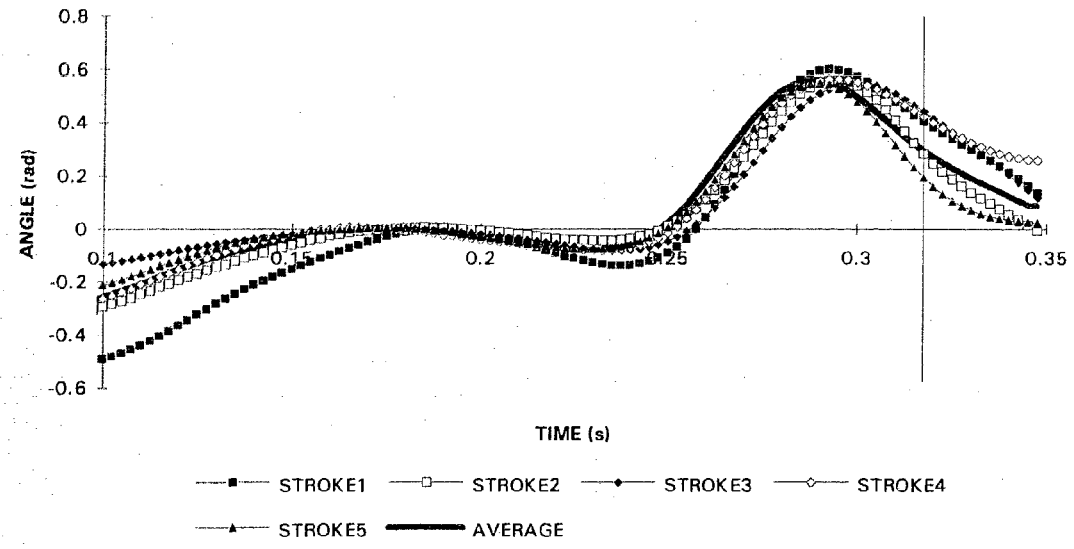


Figure F.6a The shoulder outward rotation angle profiles of Strokes #1 to #5.

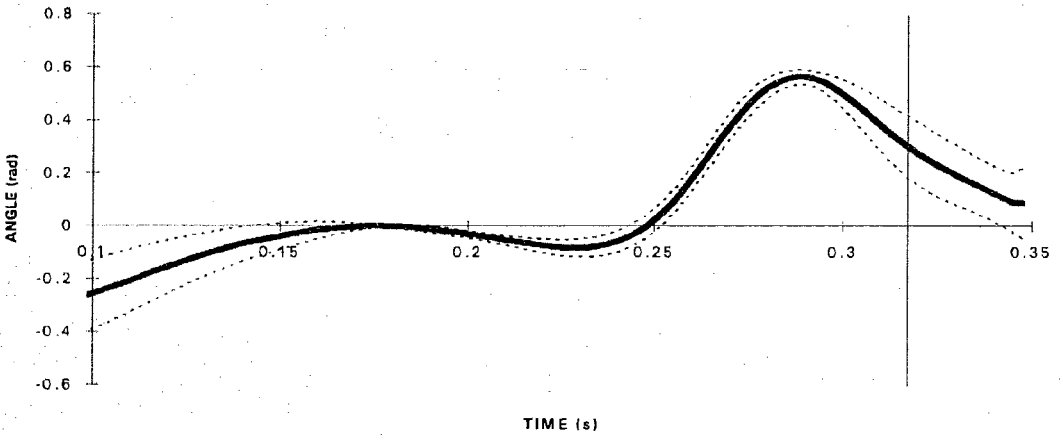


Figure F.6b Variability in the shoulder outward rotation angle profiles.

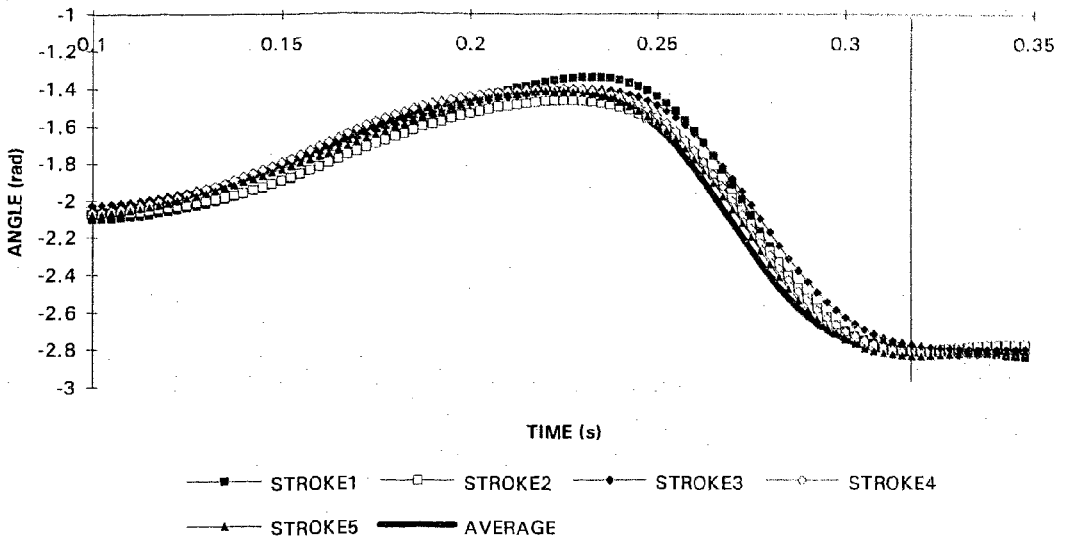


Figure F.7a The elbow flexion angle profiles of Strokes #1 to #5.

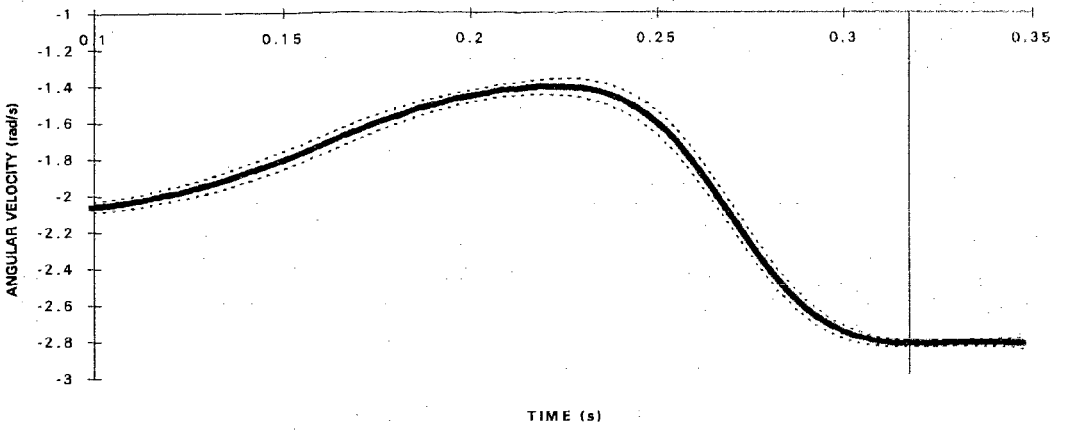


Figure F.7b Variability in the elbow flexion angle profiles.

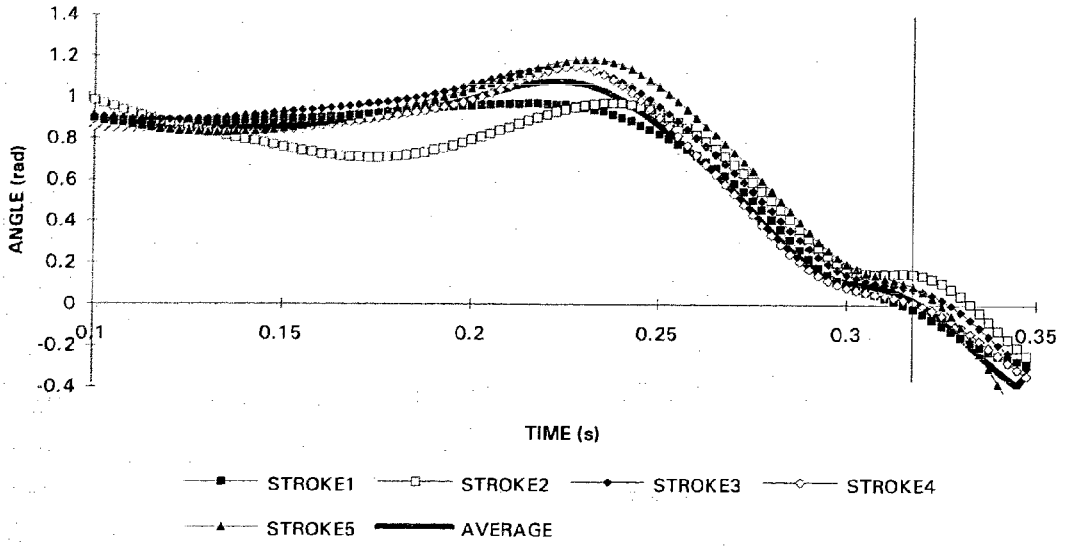


Figure F.8a The forearm supination angle profiles of Strokes #1 to #5.

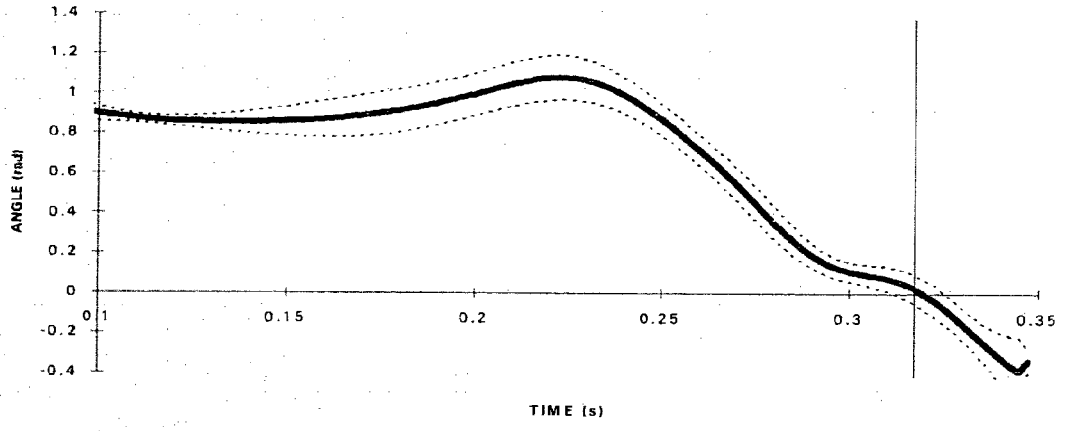


Figure F.8b Variability in the forearm supination angle profiles.

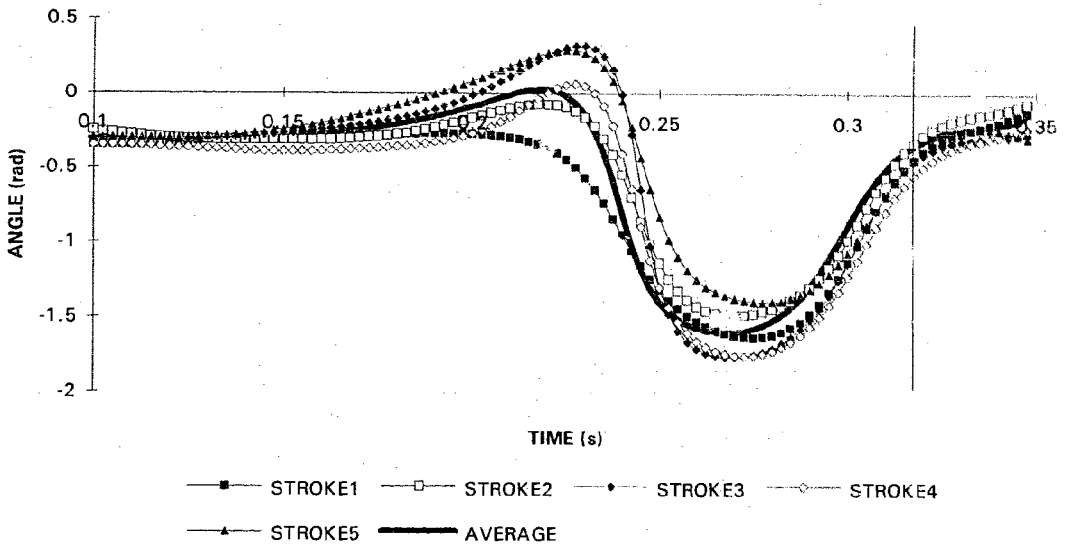


Figure F.9a The wrist flexion angle profiles of Strokes #1 to #5.

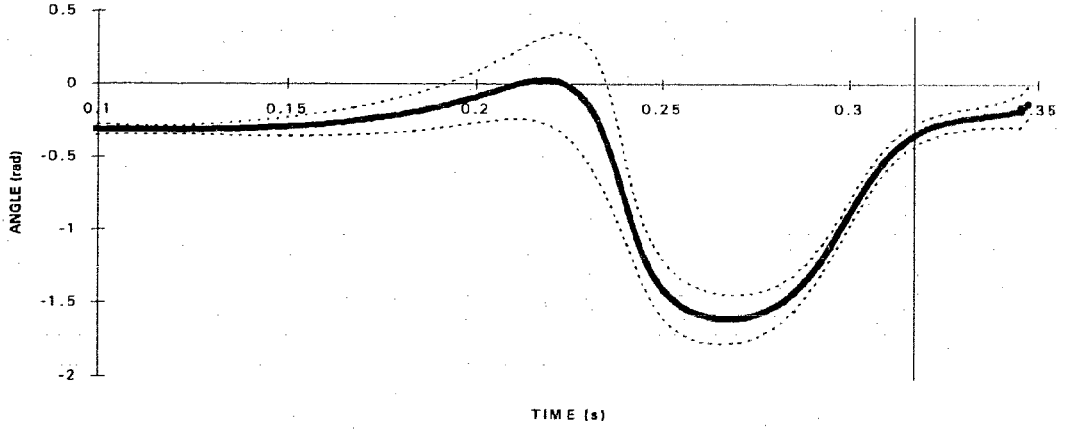


Figure F.9b Variability in the wrist flexion angle profiles.

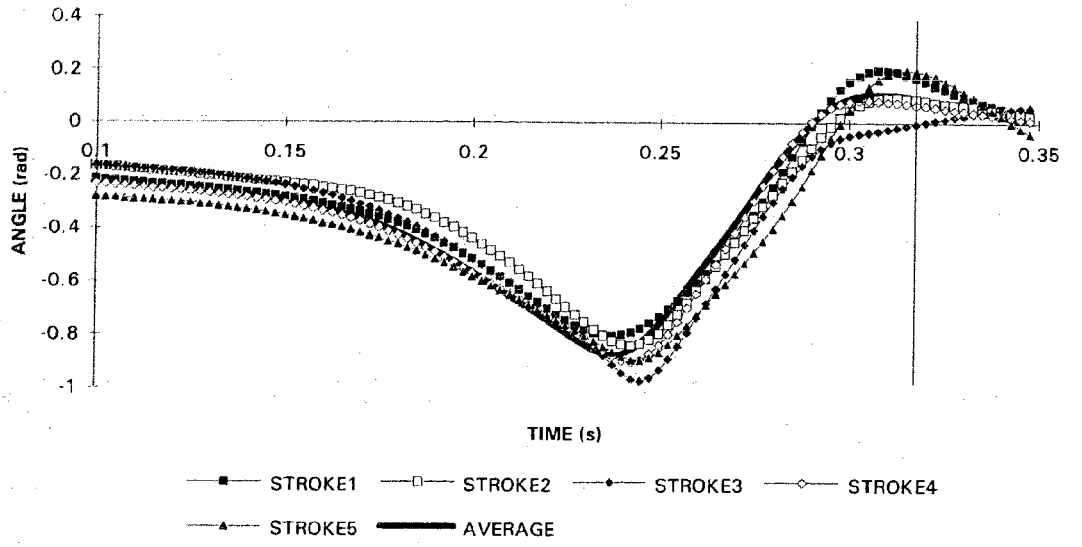


Figure F.10a The wrist adduction angle profiles of Strokes #1 to #5.

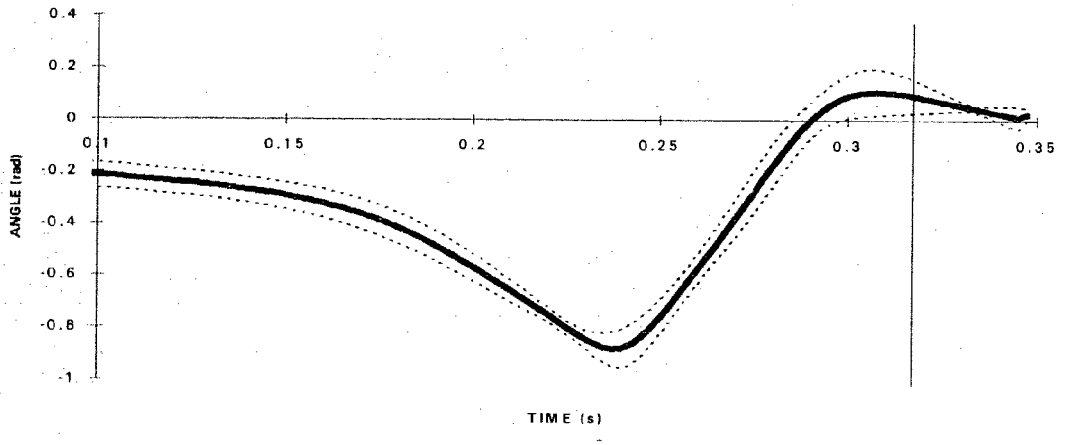


Figure F.10b Variability in the wrist adduction angle profiles.

## *F.2 ANATOMICAL JOINT ANGULAR VELOCITY*

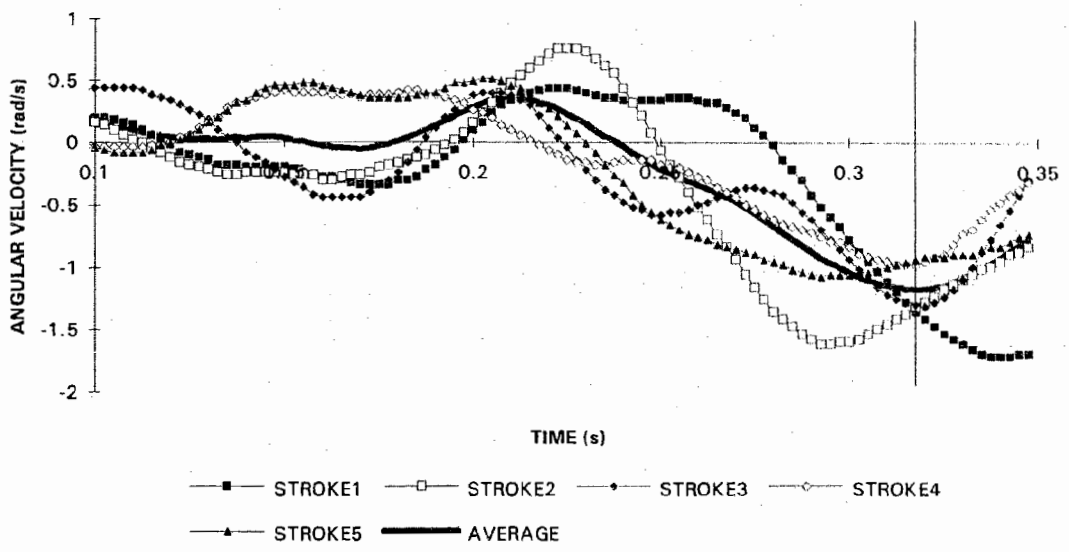


Figure F.11a The trunk flexion angular velocity profiles of Strokes #1 to #5.

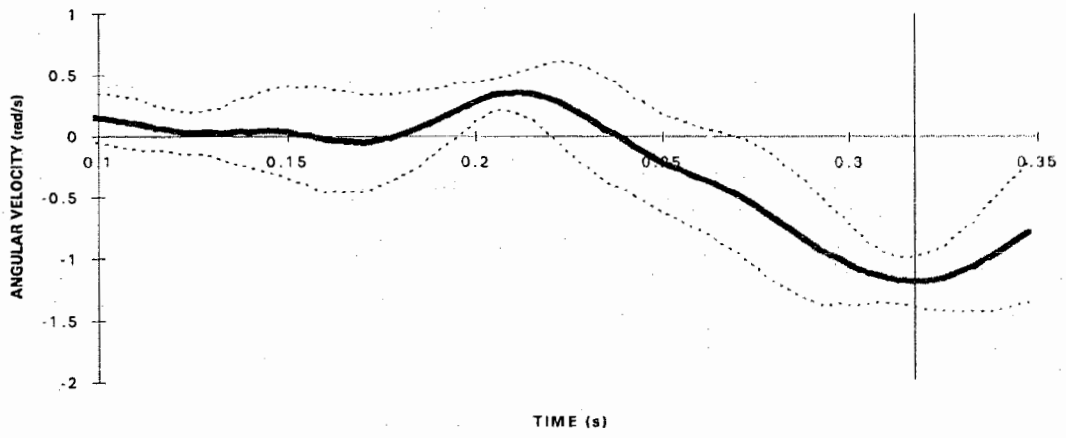


Figure F.11b Variability of the trunk flexion angular velocity profiles.

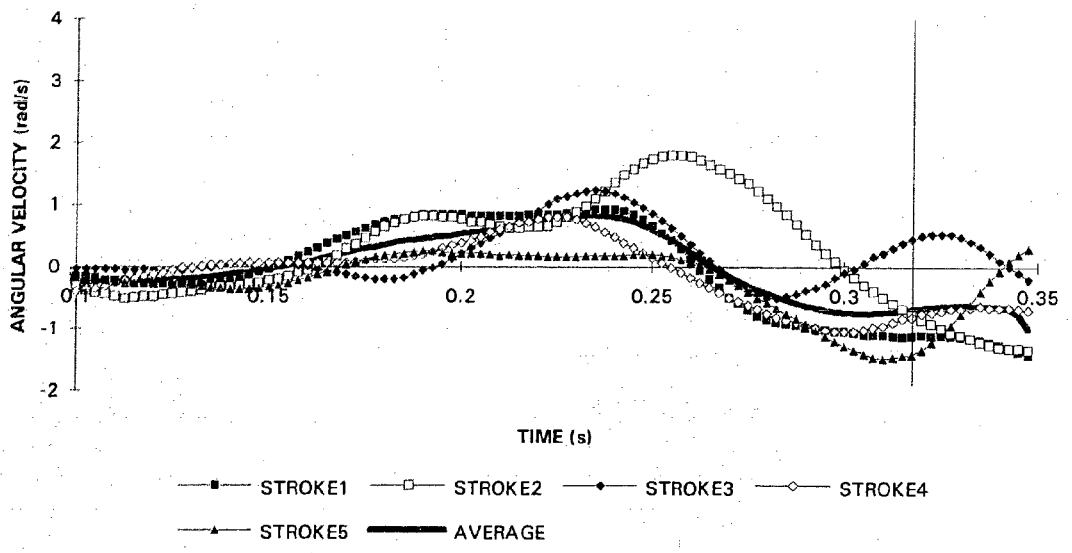


Figure F.12a The trunk right lateral flexion angular velocity profiles of Strokes #1 to #5.

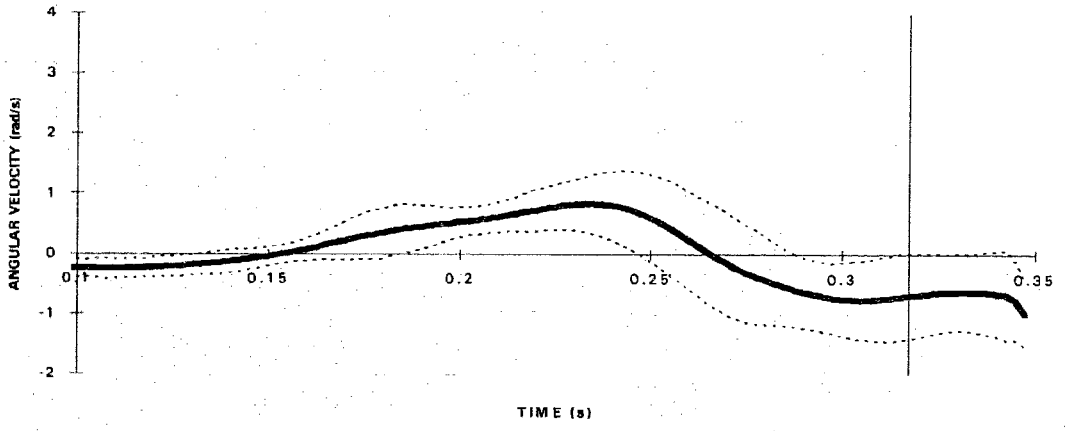


Figure F.12b Variability of the trunk right lateral flexion angular velocity profiles.

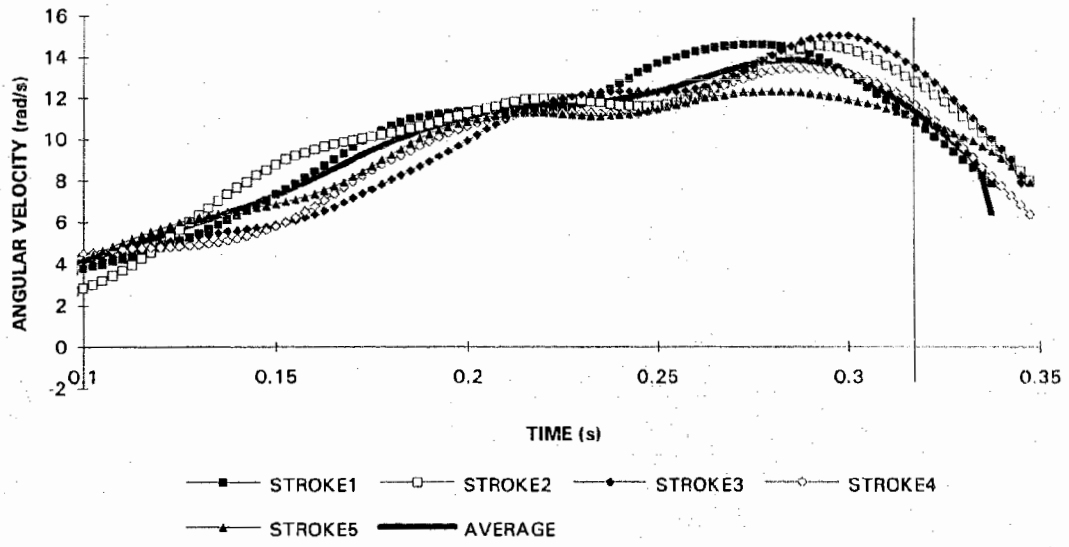


Figure F.13a The trunk left rotation angular velocity profiles of Strokes #1 to #5.

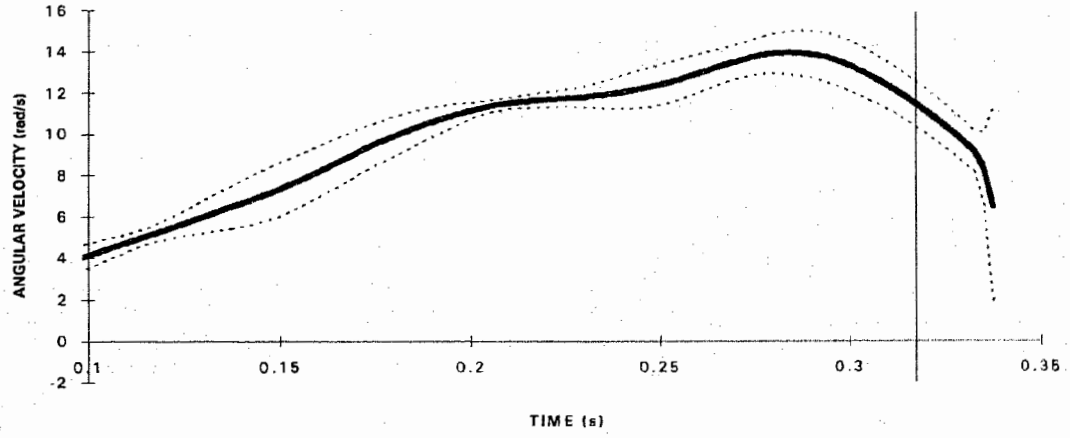


Figure F.13b Variability of the trunk left rotation angular velocity profiles.

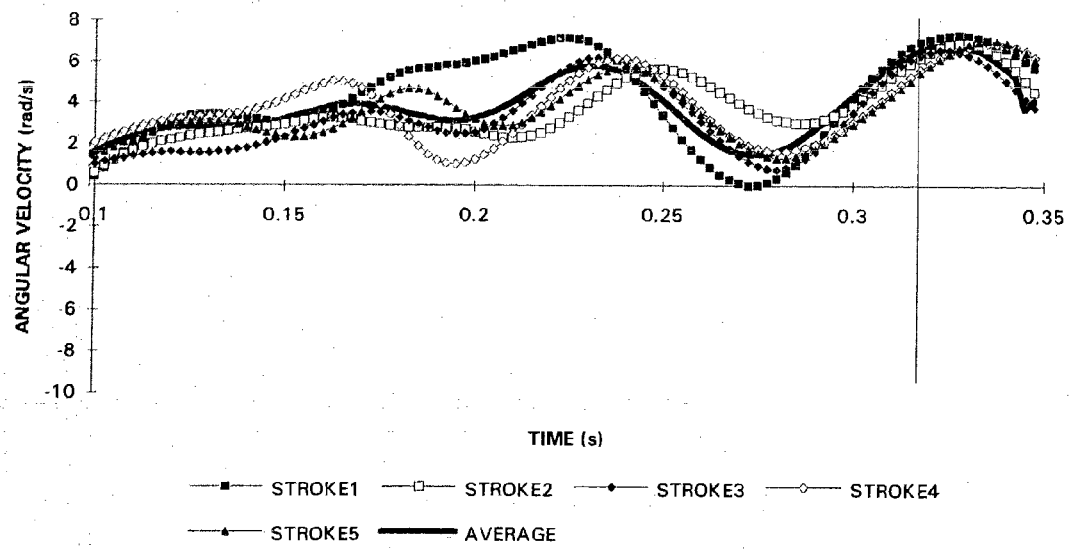


Figure F.14a The shoulder adduction angular velocity profiles of Strokes #1 to #5.

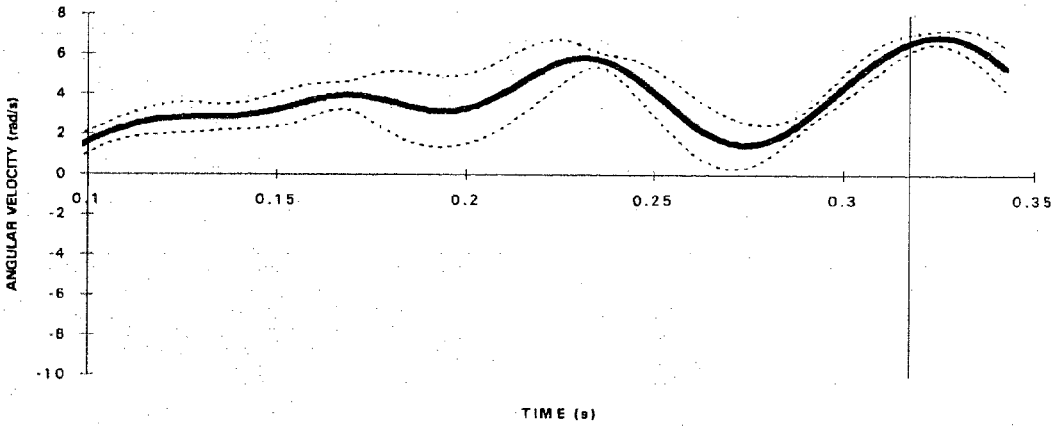


Figure F.14b Variability of the shoulder adduction angular velocity profiles.

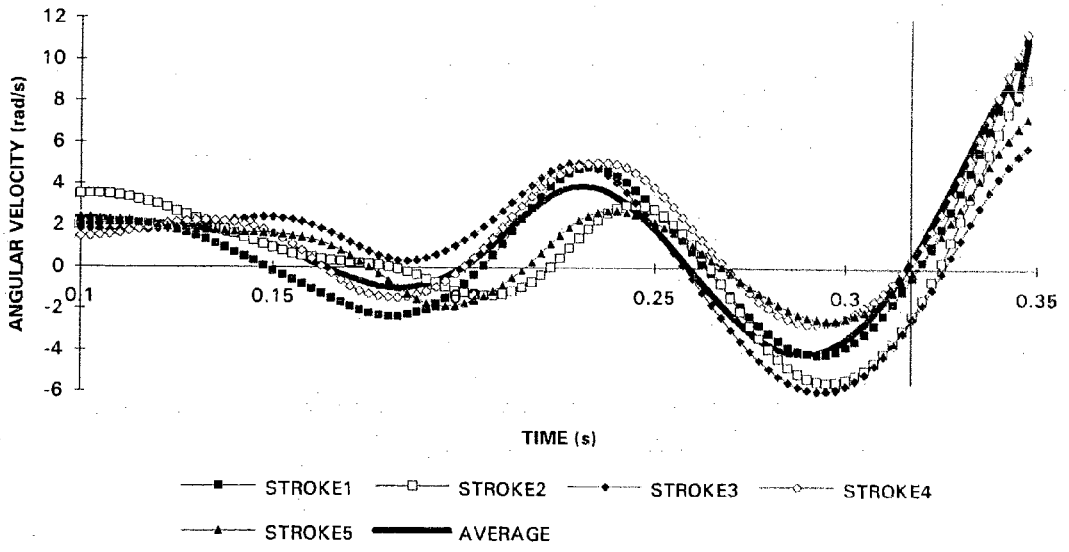


Figure F.15a The shoulder horizontal adduction angular velocity profiles of Strokes #1 to #5.

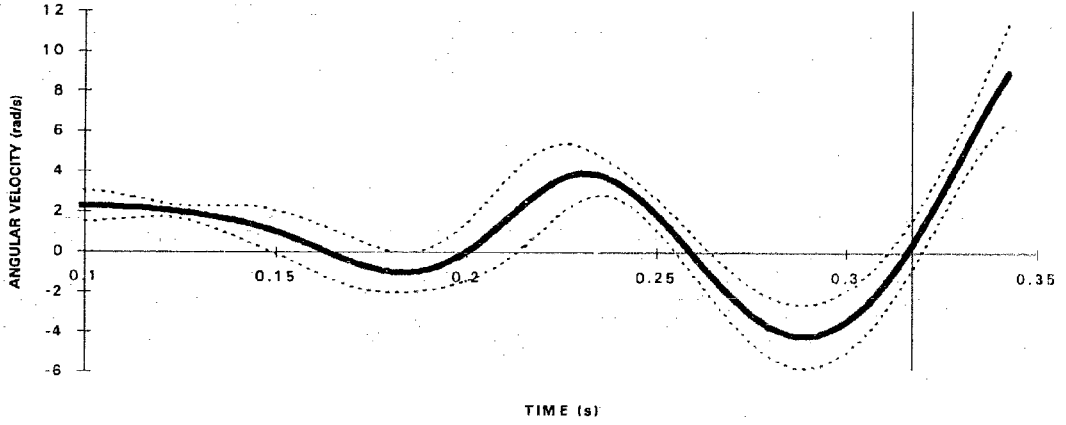


Figure F.15b Variability of the shoulder horizontal adduction angular velocity profiles.

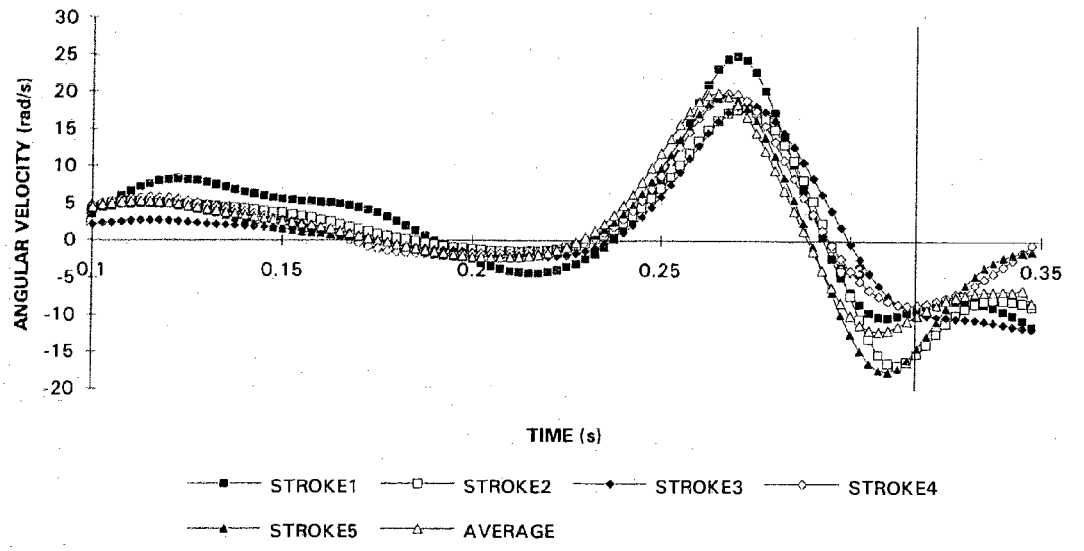


Figure F.16a The shoulder outward rotation angular velocity profiles of Strokes #1 to #5.

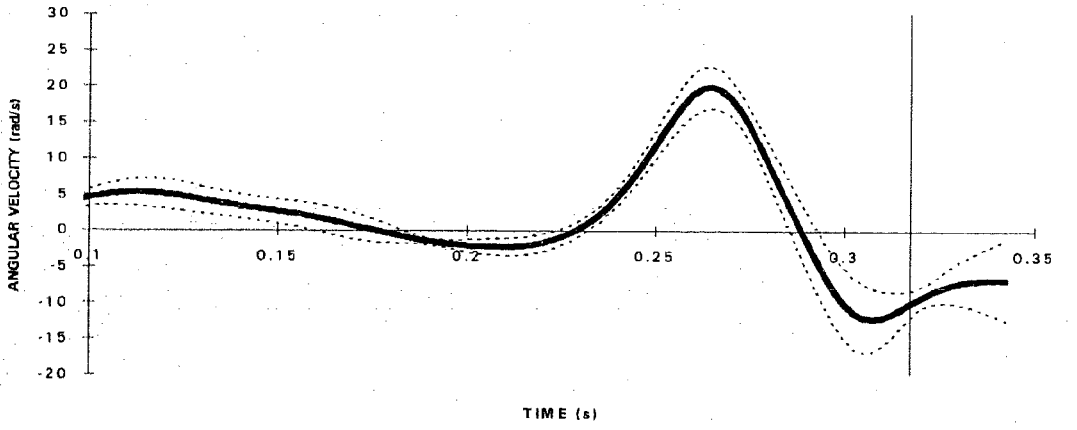


Figure F.16b Variability of the shoulder outward rotation angular velocity profiles.

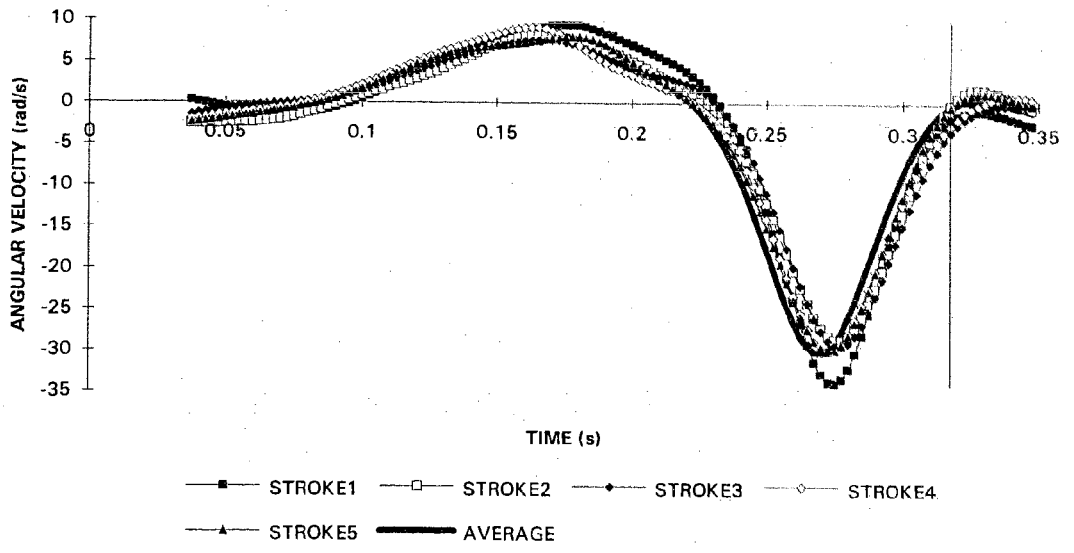


Figure F.17a The elbow flexion angular velocity profiles of Strokes #1 to #5.

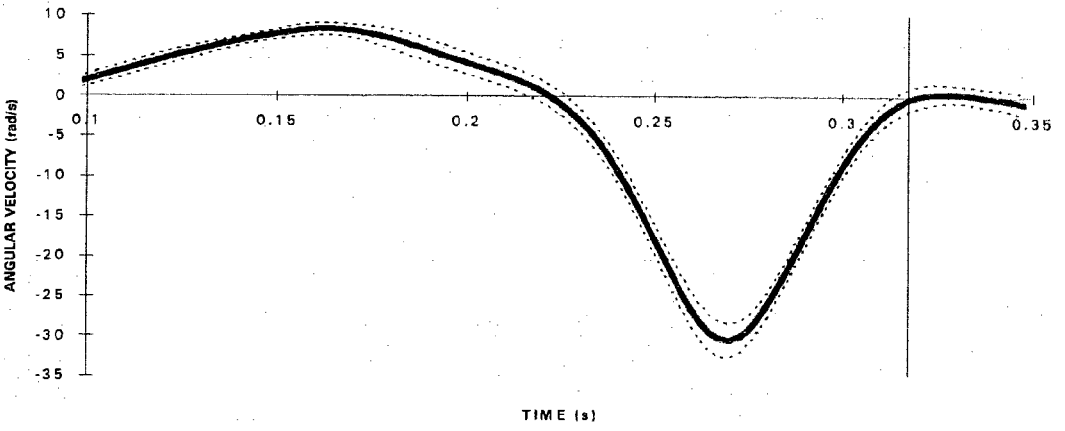


Figure F.17b Variability of the elbow flexion angular velocity profiles.

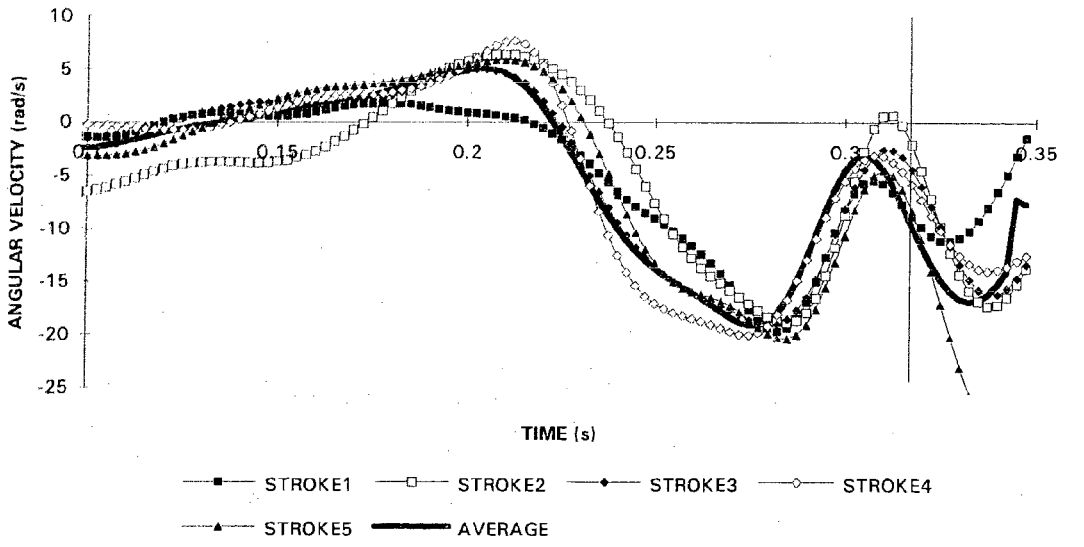


Figure F.18a The forearm supination angular velocity profiles of Strokes #1 to #5.

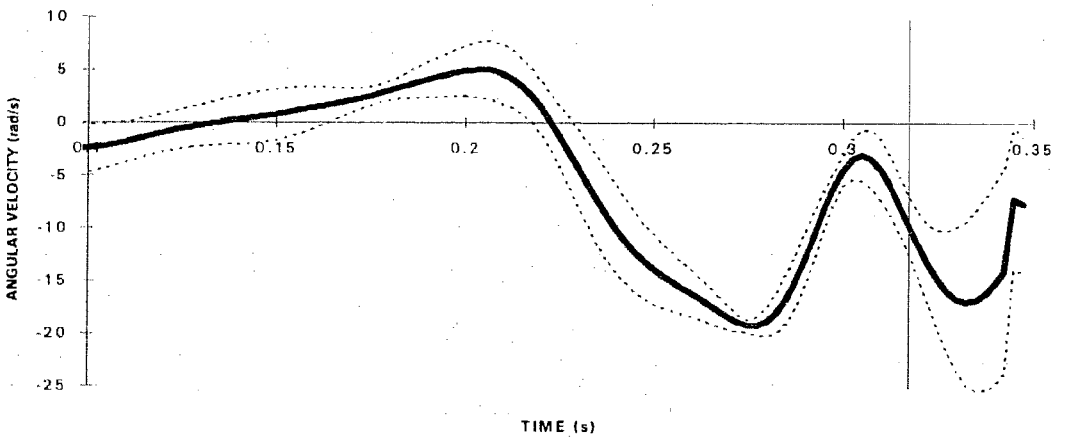


Figure F.18b Variability of the forearm supination angular velocity profiles.

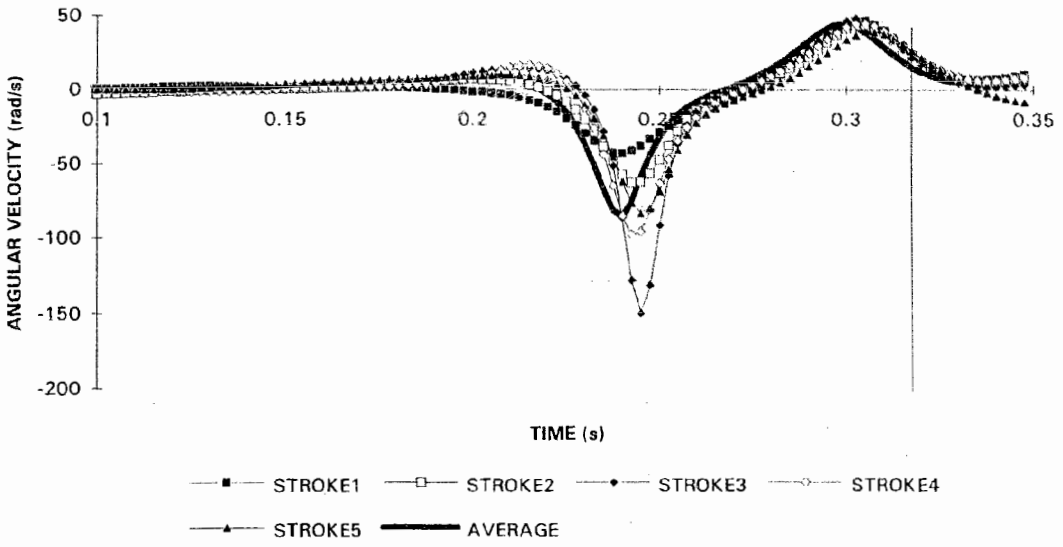


Figure F.19a The wrist flexion angular velocity profiles of Strokes #1 to #5.

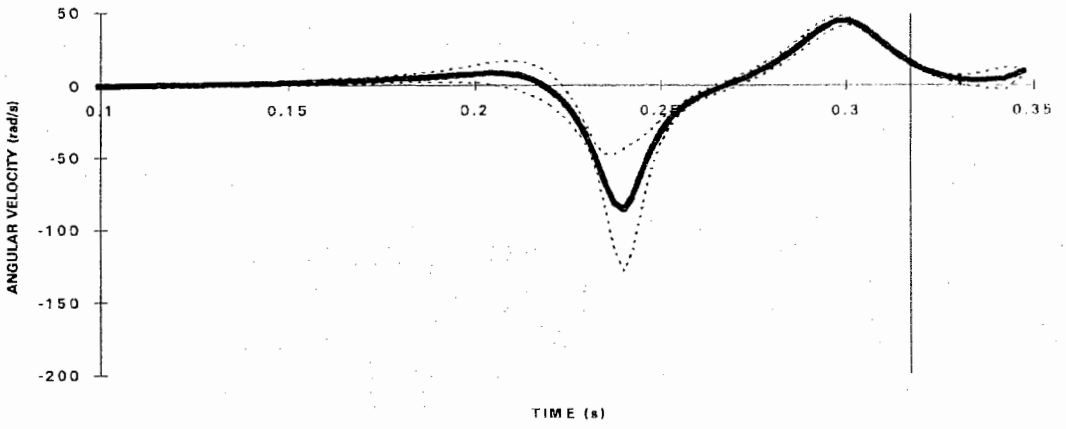


Figure F.19b Variability of the wrist flexion angular velocity profiles.

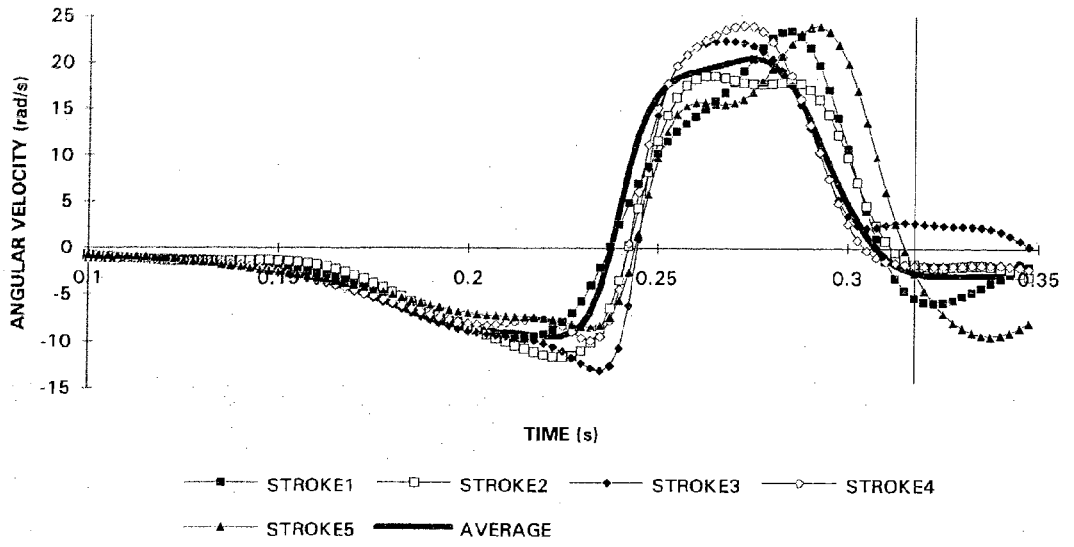


Figure F.20a The wrist adduction angular velocity profiles of Strokes #1 to #5.

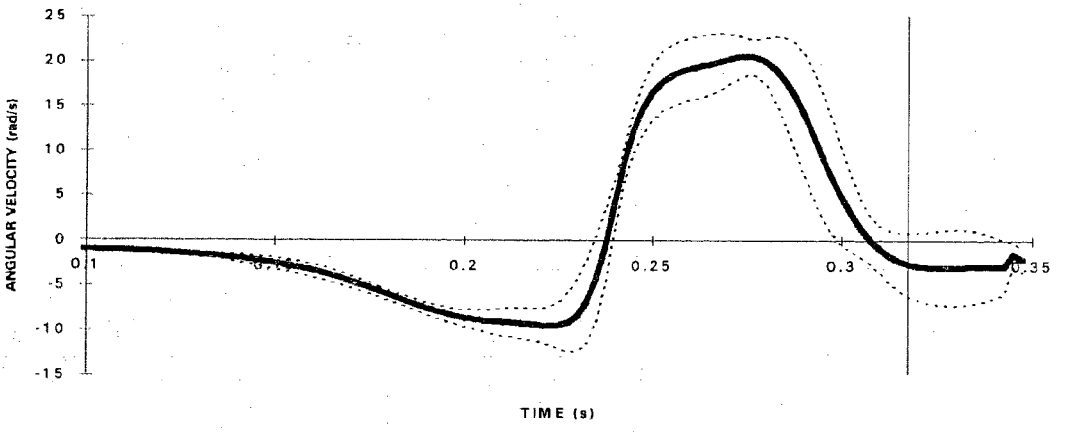


Figure F.20b Variability of the wrist adduction angular velocity profiles.

Table F.1 The peak anatomical joint angular velocities, times of occurrence and the anatomical joint angular velocities at impact of Strokes #1 to #5.

| ANGULAR VELOCITY | STROKE 1 | | | STROKE 2 | | | STROKE 3 | | |
|---|---|---|---|---|---|---|---|---|---|
| | $\dot{\theta}_{peak}$ | $t_{peak}$ | $\dot{\theta}_{impact}$ | $\dot{\theta}_{peak}$ | $t_{peak}$ | $\dot{\theta}_{impact}$ | $\dot{\theta}_{peak}$ | $t_{peak}$ | $\dot{\theta}_{impact}$ |
| TR FLEXION | 0.4 | 0.2250 | -1.4 | 0.8 | 0.2275 | -1.3 | 0.4 | 0.2075 | -1.3 |
| TR RIGHT LATFLEX | -1.1 | 0.3150 | -1.1 | -1.4 | 0.3500 | -0.8 | -0.5 | 0.2825 | 0.4 |
| TR LEFT ROTATION | 14.6 | 0.2775 | 10.9 | 14.6 | 0.2925 | 12.8 | 15.1 | 0.2975 | 13.5 |
| SH ADDUCT | 7.3 | 0.3275 | 6.9 | 6.9 | 0.3300 | 6.2 | 6.6 | 0.3250 | 6.3 |
| SH HORIZ ADDUCT | 4.9 | 0.2325 | -0.4 | 3.1 | 0.2450 | -2.3 | 5.0 | 0.2300 | -2.4 |
| SH OUT ROTATION | -10.3 | 0.3100 | -9.2 | -16.8 | 0.3125 | -15.3 | -11.8 | 0.3500 | -9.7 |
| ELBOW FLEXION | -34.0 | 0.2750 | -1.8 | -28.7 | 0.2775 | -0.1 | -29.4 | 0.2775 | -3.4 |
| FORE SUPINATION | -19.7 | 0.2825 | -8.9 | -18.9 | 0.2850 | -2.1 | -19.1 | 0.2800 | -4.4 |
| WR FLEXION | 46.5 | 0.3025 | 23.9 | 46.8 | 0.3050 | 22.7 | 47.9 | 0.3025 | 21.6 |
| WR ADDUCT | 23.4 | 0.2850 | -5.3 | 18.6 | 0.2650 | -1.7 | 22.4 | 0.2675 | 2.72 |

Table F.1 (con't)

| ANGULAR VELOCITY | STROKE 4 | | | STROKE 5 | | |
|---|---|---|---|---|---|---|
| | $\dot{\theta}_{peak}$ | $t_{peak}$ | $\dot{\theta}_{impact}$ | $\dot{\theta}_{peak}$ | $t_{peak}$ | $\dot{\theta}_{impact}$ |
| TR FLEXION | 0.4 | 0.1850 | -1.0 | 0.5 | 0.2050 | -0.9 |
| TR RIGHT LATFLEX | -1.0 | 0.3025 | -0.8 | -1.5 | 0.3100 | -1.4 |
| TR LEFT ROTATION | 13.5 | 0.2875 | 11.7 | 12.4 | 0.2850 | 11.1 |
| SH ADDUCT | 6.9 | 0.3375 | 5.6 | 7.1 | 0.3350 | 5.5 |
| SH HORIZ ADDUCT | 5.1 | 0.2375 | 0.4 | 2.8 | 0.2400 | -0.2 |
| SH OUT ROTATION | -8.7 | 0.3150 | -8.6 | -17.6 | 0.3100 | -14.5 |
| ELBOW FLEXION | -30.1 | 0.2725 | -2.6 | -30.0 | 0.2725 | -0.3 |
| FORE SUPINATION | -20.1 | 0.2750 | -5.8 | -20.4 | 0.2850 | -8.3 |
| WR FLEXION | 44.4 | 0.3050 | 25.4 | 39.3 | 0.3075 | 26.1 |
| WR ADDUCT | 24.0 | 0.2725 | -1.8 | 24.0 | 0.2925 | -2.6 |

# APPENDIX G
# VARIABILITY IN DIGITIZING

## *G.1. Intra-digitizer Variability*

Intra-digitizer variability was measured by the same individual (Digitizer A) digitizing Stroke #2 three times repeatedly. This was performed during a separate digitizing session, therefore the films required to be re-calibrated. The new DLT calibration used 45 control points yielding an RMS error of 3.67 cm. Reducing the magnitude of the RMS error was not of primary concern in this case. The magnitudes of angular velocities were not important, but rather the shapes of the profiles. As discussed in Appendix A, the shape of the profiles remained essentially intact using calibrations with progressively smaller RMS errors.

In the repeated digitizations, 60 consecutive frames of film, during which all peak velocities occurred, were digitized. Frame #50 was ball contact. However, analyses of these data revealed that this number of frames was insufficient to avoid data distortion due to filtering. From the original set of 60 frames of data, the filtered trunk angles did not fit well with the unfiltered data (Figure G.1). About twenty frames were required for the filtered data to settle. An additional twenty data points were extraplolated at both ends of the original data set prior to filtering by the reflection method resulting in a much closer match of the filtered and unfiltered data.

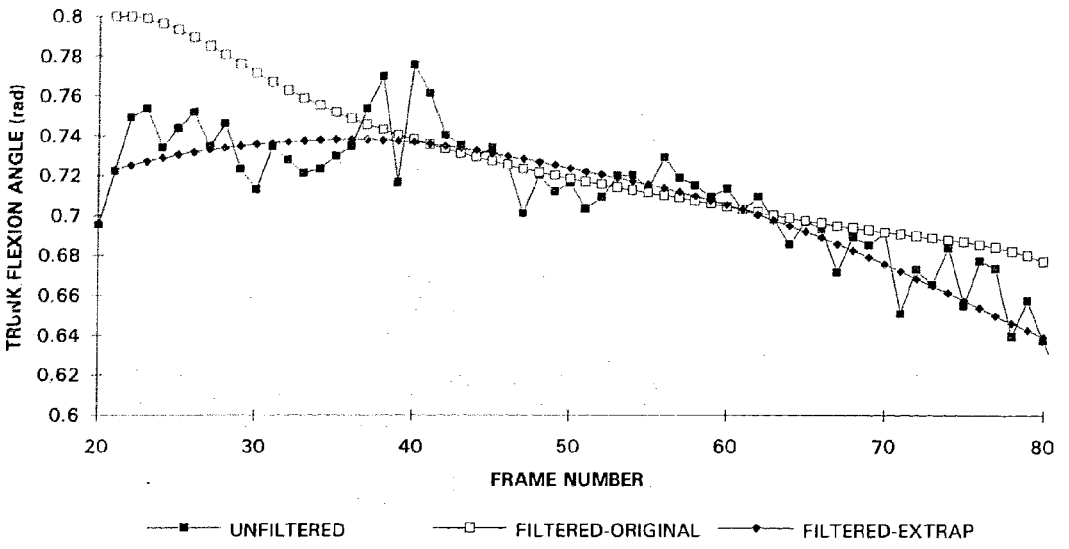


Figure G.1 Comparison of the trunk flexion angle profiles between sets of unfiltered (solid squares), filtered (open squares) and filtered extrapolated data (solid diamonds).

Digitizer A showed good consistency in digitizing as indicated by the low variability in the anatomical joint angular velocity profiles between the three repeated trials (Figures G.2a-j).

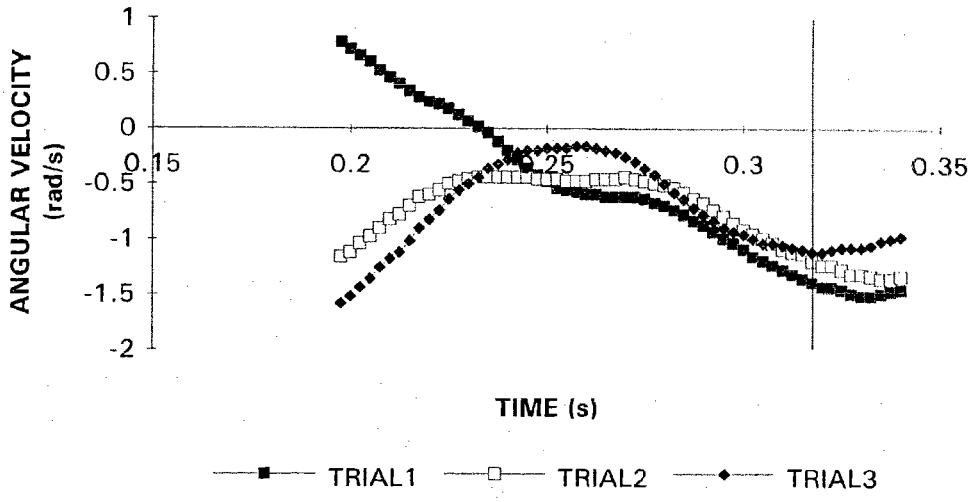


Figure G.2a Intra-digitizer variability: trunk flexion angular velocity profiles.

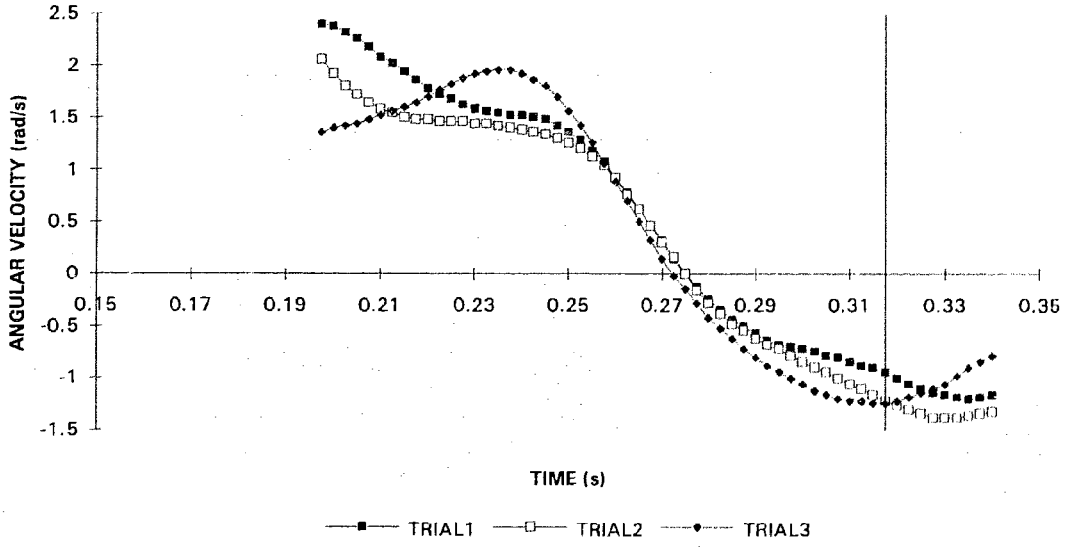


Figure G.2b Intra-digitizer variability: trunk right lateral flexion angular velocity profiles.

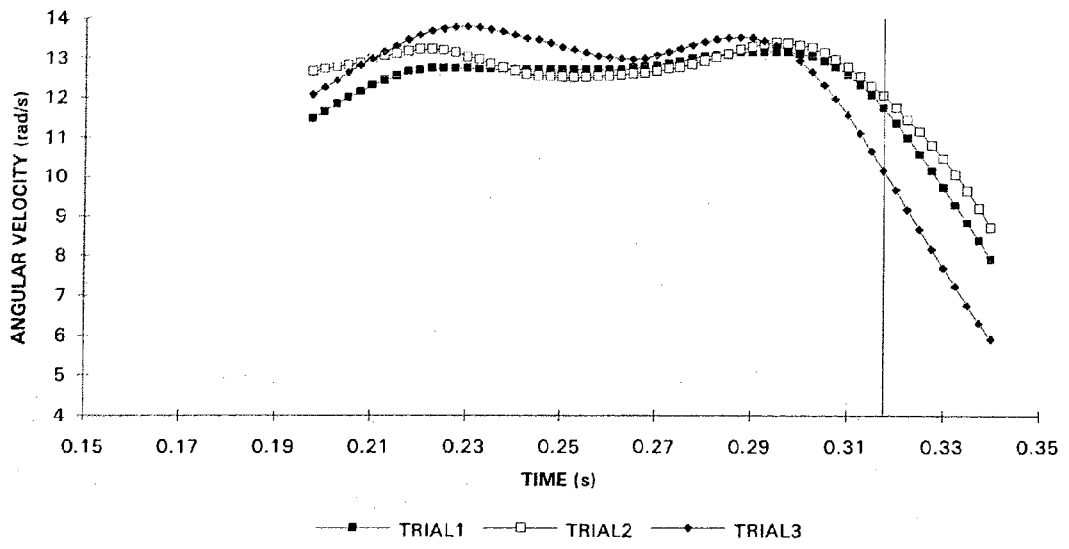


Figure G.2c Intra-digitizer variability: trunk left rotation angular velocity profiles.

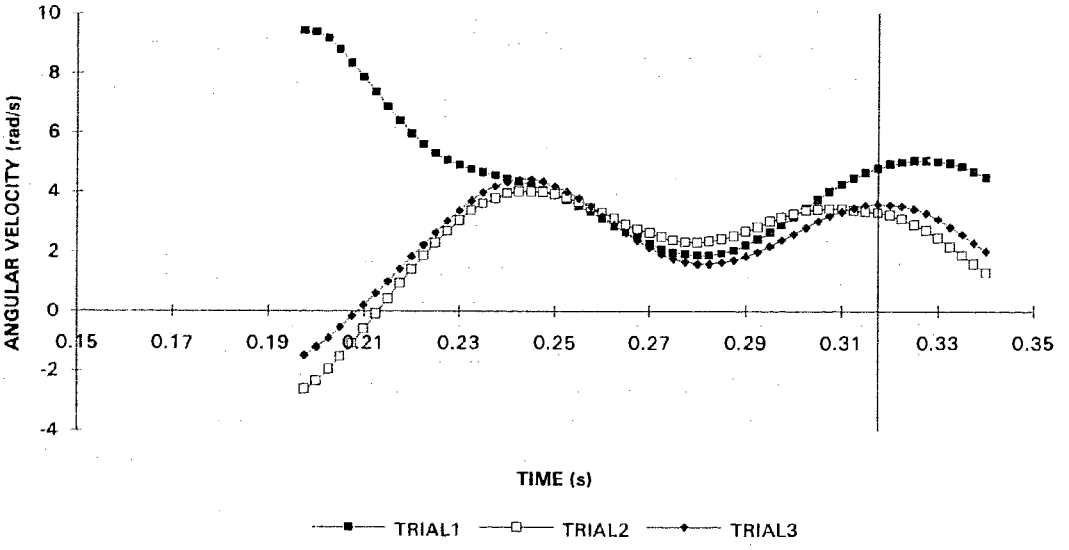


Figure G.2d Intra-digitizer variability: shoulder adduction angular velocity profiles.

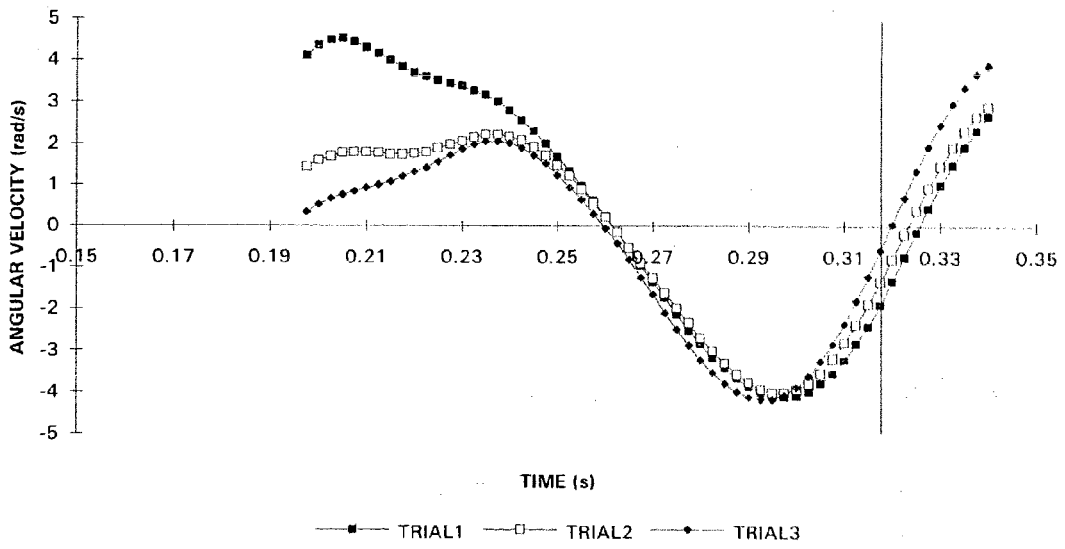


Figure G.2e Intra-digitizer variability: shoulder horizontal adduction angular velocity profiles.

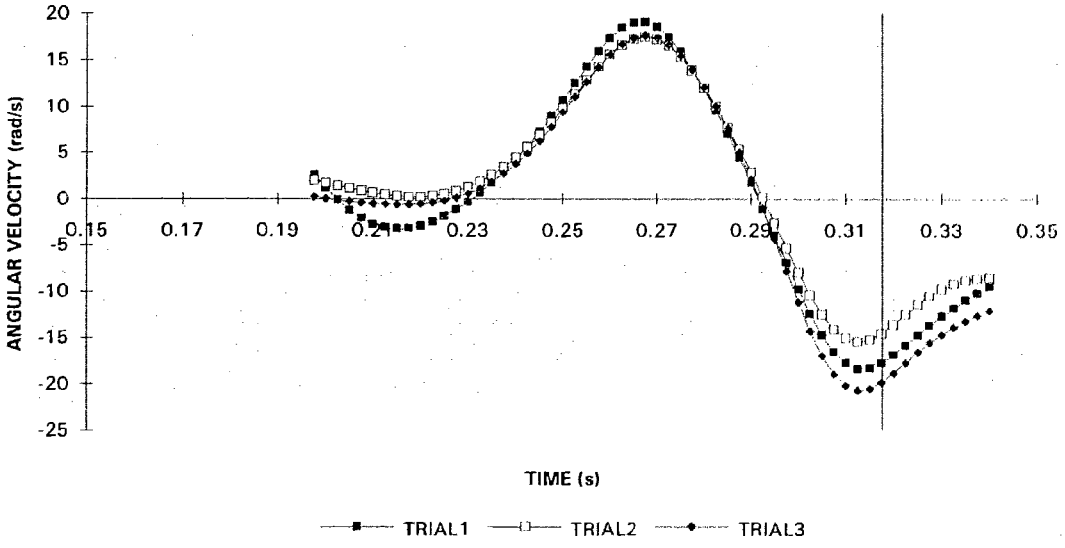


Figure G.2f Intra-digitizer variability: shoulder outward rotation angular velocity profiles.

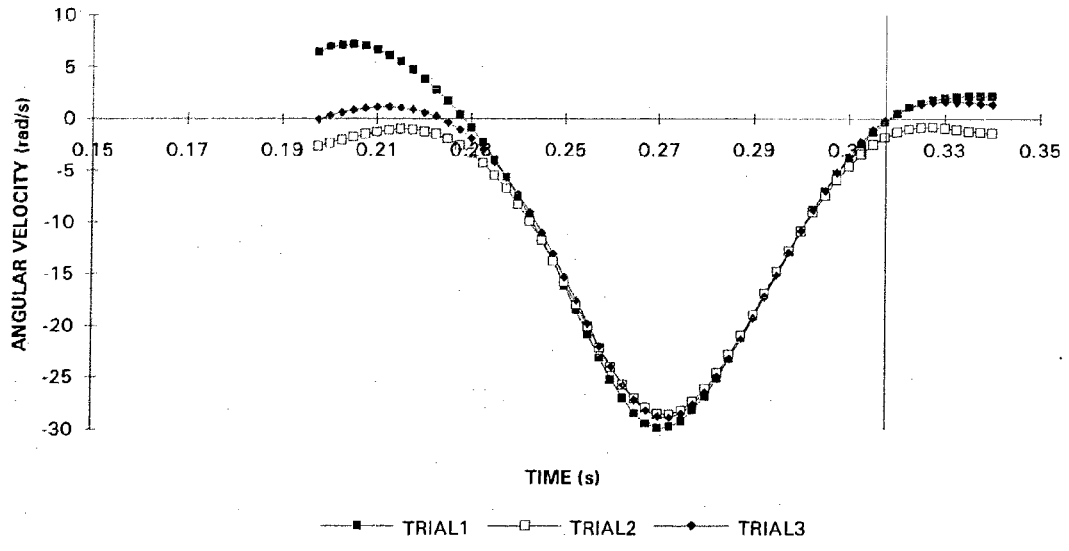


Figure G.2g Intra-digitizer variability: elbow flexion angular velocity profiles.

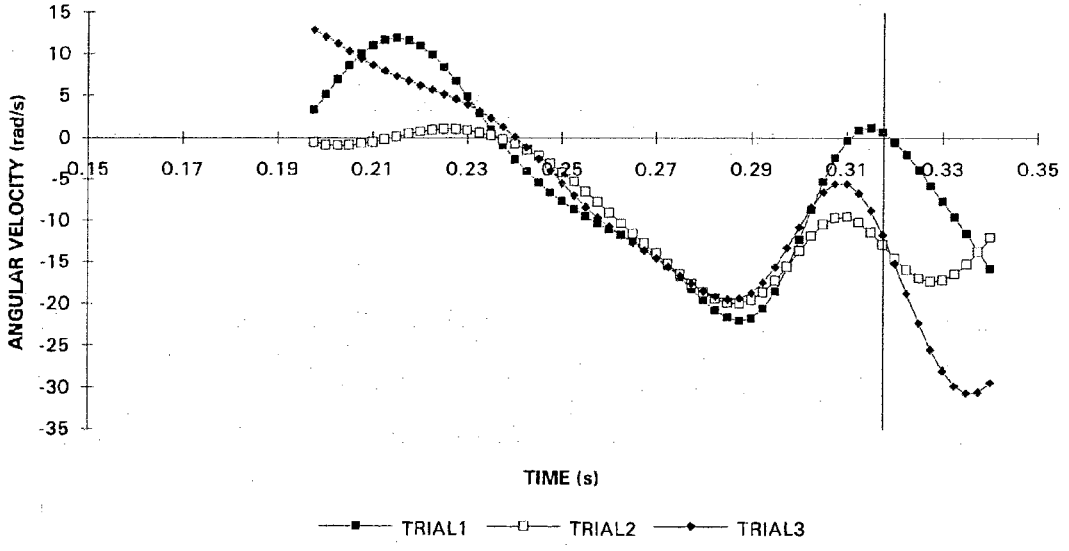


Figure G.2h Intra-digitizer variability: forearm supination angular velocity profiles.

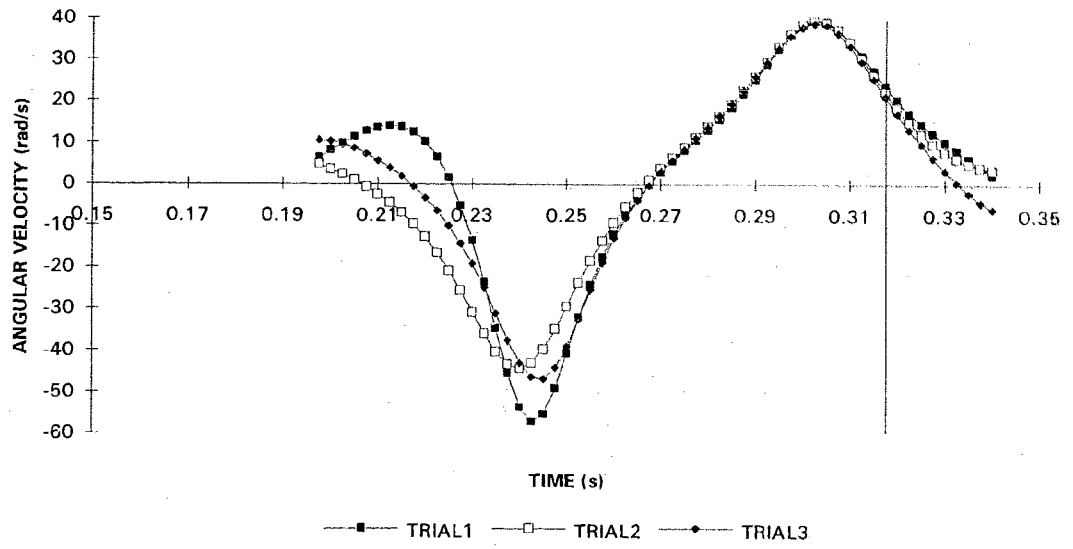


Figure G.2i Intra-digitizer variability: wrist flexion angular velocity profiles.

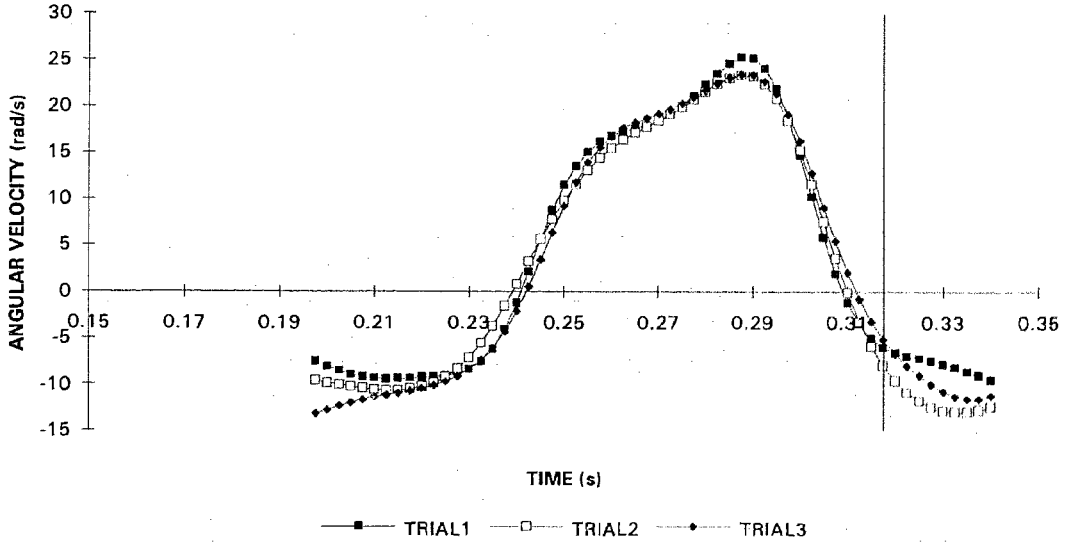


Figure G.2j Intra-digitizer variability: wrist adduction angular velocity profiles.